



รายงานวิจัยฉบับสมบูรณ์

ความสัมพันธ์ของการสั่นสะเทือนของโครงสร้างแผ่นคอมโพสิตที่รับแรงในแนวระนาบ กับค่าภาระการโก่งงอ

The correlations between vibration of in-plane loaded composite plates and their buckling load

ไพโรจน์ สิงหถนัดกิจ

รายงานวิจัยฉบับสมบูรณ์

ความสัมพันธ์ของการสั่นสะเทือนของโครงสร้างแผ่นคอมโพสิตที่รับแรงในแนวระนาบ กับค่าภาระการโก่งงอ

The correlations between vibration of in-plane loaded composite plates and their buckling load

ไพโรจน์ สิงหถนัดกิจ จุฬาลงกรณ์มหาวิทยาลัย

สนับสนุนโดยสำนักงานการอุดมศึกษาและสำนักงานกองทุนสนับสนุนการวิจัย
(ความเห็นในรายงานนี้เป็นของผู้วิจัย สกอ. และ สกว. ไม่จำเป็นต้องเห็นด้วยเสมอไป)

กิตติกรรมประกาศ

งานวิจัยเรื่อง "ความสัมพันธ์ของการสั่นสะเทือนของโครงสร้างแผ่นคอมโพสิตที่รับแรงในแนว ระนาบกับค่าภาระการ โก่งงอ (The correlations between vibration of in-plane loaded composite plates and their buckling load)" เป็นโครงการที่ได้รับการสนับสนุนจากสำนักงานการอุดมศึกษาและสำนักงาน กองทุนสนับสนุนการวิจัย ผู้วิจัยขอขอบพระคุณหน่วยงานทั้งสองที่ให้การสนับสนุนงบประมาณตลอด โครงการวิจัย

ผู้วิจัยขอขอบคุณภาควิชาวิศวกรรมเครื่องกล จุฬาลงกรณ์มหาวิทยาลัยที่ให้การสนับสนุนสถานที่
และเครื่องมือทดลองในการวิจัยพื้นฐาน ขอขอบคุณรองศาสตราจารย์ คร.ฐิติมา จินตนาวัน และ ผู้ช่วย
ศาสตราจารย์ คร.อาณัติ เรื่องรัศมี ที่อนุเคราะห์ชุดวัดการสั่นสะเทือนและชุดประมวลผลข้อมูลการ
สั่นสะเทือน

รองศาสตราจารย์ คร.ไพโรจน์ สิงหถนัคกิจ

มกราคม 2552

บทคัดย่อ

รหัสโครงการ: RMU 4880021

ชื่อโครงการ: ความสัมพันธ์ของการสั่นสะเทือนของโครงสร้างแผ่นคอมโพสิตที่รับแรงในแนว

ระนาบกับค่าภาระการ โก่งงอ

ชื่อนักวิจัย: ไพโรจน์ สิงหถนัดกิจ จุฬาลงกรณ์มหาวิทยาลัย

ระยะเวลาโครงการ: 2548-2551

การ โก่งงอเป็นการเสียหาย โหมดหนึ่งของ โครงสร้างแผ่นบางที่รับภาระกด โดยทั่วไปค่าภาระการ ้ โก่งงอหาได้จากกราฟของภาระในแนวระนาบกับพารามิเตอร์ของการเปลี่ยนรูปเช่น ระยะการเคลื่อนที่ นอกระนาบ การศึกษานี้ใช้เทคนิคความสัมพันธ์ของการสั่นสะเทือนในการหาค่าภาระการโก่งงอของ โครงสร้างแผ่นบางสี่เหลี่ยมผืนผ้าโดยอ้อม จากการเปรียบเทียบสมการครอบคลุมของปัญหาการโก่งงอ และปัญหาการสั่นสะเทือน สามารถแสดงให้เห็นว่าความถี่ธรรมชาติของการสั่นสะเทือนแปรผันตรงกับ ภาระบนระนาบที่ให้ นอกจากนั้นยังพบอีกว่าความถี่ธรรมชาติจะมีค่าเป็นศูนย์เมื่อภาระกคที่ให้มีค่าเข้า ใกล้ภาระการโก่งงอ จากการศึกษาที่ผ่านมาพบว่าทันทีที่มีภาระกดกระทำกับโครงสร้าง โครงสร้างจะมี ระยะการเคลื่อนที่นอกระนาบเนื่องจากความไม่สมบูรณ์ของโครงสร้าง เพื่อที่จะหลีกเลี่ยงผลของการ เคลื่อนที่นอกระนาบก่อนเวลาอันควร การศึกษานี้เสนอให้หาค่าภาระการโก่งงองากความถี่ธรรมชาติของ แผ่นบางที่รับภาระดึง ค่าภาระการโก่งงอสามารถหาได้จากการประมาณค่านอกช่วงของข้อมูลการ สั่นสะเทือนไปยังค่าภาระในระนาบที่ค่ากำลังสองของค่าความถี่ธรรมชาติมีค่าเป็นศูนย์ การทคลองเพื่อ ตรวจสอบความแม่นยำของวิธีที่เสนอในการศึกษานี้ทำโดยใช้ชุดทดลองที่สร้างขึ้นเฉพาะ การทดลองหา ค่าความถี่ธรรมชาติของชิ้นงานภายใต้ภารระแนวเคียวทำโคยวิธีการเคาะ ชิ้นงานที่ใช้ในการทคลองเป็น อะลมินัมและเหล็กกล้าไร้สนิมที่มีการจับยึดแบบ CCCC, CCCF และ CFCF ตามลำดับ ค่าภาระการโก่ง งอหาจากกราฟกำลังสองของความถี่ธรรมชาติที่วัดได้กับภาระในแนวระนาบ ค่าภาระการโก่งงอจาก ข้อมูลการสั่นสะเทือนสอดคล้องกับผลเฉลยเชิงเลขอย่างดี สำหรับชิ้นงานที่มีการจับยึดที่เหมาะสม เปอร์เซ็นต์ความแตกต่างเฉลี่ยของภาระการ โก่งงอจากเทคนิคความสัมพันธ์ของการสั่นสะเทือนกับค่าที่ได้ จากผลเฉลยเชิงเลขมีค่าเท่ากับ -0.18 % และส่วนเบี่ยงแบนมาตรฐานเท่ากับ 5.05 % โดยสรุปแล้ว สามารถ หาค่าภาระการ โก่งงอของแผ่นบางรูปสี่เหลี่ยมผืนผ้าจากข้อมูลการสั่นสะเทือนได้ โดยค่าที่ได้มีความ แม่นยำเป็นที่ยอมรับได้ วิธีการนี้มีประโยชน์โดยเฉพาะกับโครงสร้างที่ไม่ทราบเงื่อนไขขอบเขตหรือมี เงื่อนไขขอบเขตที่ไม่สมบูรณ์ ซึ่งปัญหาเหล่านี้ไม่มีผลเฉลยแม่นตรงหรือผลเฉลยเชิงเลข

Abstract

Project code: RMU 4880021

Project title: The correlations between vibration of in-plane loaded composite

plates and their buckling load

Investigator: Pairod Singhatanadgid Chulalongkorn University

E-mail address: Pairod.S@chula.ac.th

Project period: 2005-2008

Buckling is an important failure mode of thin-walled structures subjected to compressive loading. Usually, plots of an applied compressive load versus a deformation parameter such as out-of-plane displacement or in-plane strains have been employed as a tool to identify the buckling load. In this study, a method utilizing the vibration correlation technique is introduced as an indirect method to determine a buckling load of rectangular thin plates. By comparing the governing equations of buckling and vibration problems, it is theoretically shown that square of the natural frequency of flexural vibration of plate is linearly varied with the applied in-plane load. Moreover, the natural frequency approaches zero when the applied compressive load approaches the buckling load of plate. Due to plate's imperfections, several studies showed that out-of-plane displacement is typically observed as soon as the inplane compressive load is applied. To avoid the effects of premature out-of-plane deformation, it is proposed in this study that the buckling load be identified using the natural frequencies of plates under tensile loading. The buckling load is determined from an extrapolation of the vibration data to the in-plane load at which square of the natural frequency approaches zero. An experimental investigation using a custommade test frame was conducted to verify the accuracy of the proposed method. A set of specimens under a uniaxial loading condition was tested for natural frequencies using an impact test method. Aluminum and stainless steel specimens with CCCC, CCCF and CFCF boundary conditions were included in the experiment. The measured buckling load was determined from the plot of the square of a measured natural frequency versus an in-plane load. The buckling loads from the measured vibration data match the numerical solutions very well. For specimens with well-defined boundary conditions, the average percentage difference between buckling loads from VCT and numerical solutions is -0.18 % with a standard deviation of 5.05 %. In conclusion, buckling load of rectangular thin plates can be experimentally identified with acceptable accuracy using the vibration data in the tensile loading region. This approach is very useful especially for structures with unknown or imperfect boundary conditions where analytical or numerical solutions to the problem are not available.

Executive Summary

Buckling of thin-walled structures is one of the important topics in the field of structural engineering. Buckling problem of thin plates can be investigated using theoretical, numerical or experimental approaches. Usually, experimental study is conducted to validate theoretical or numerical solutions. Several studies reported a moderately high degree of discrepancy of experimental buckling loads compared with theoretical or numerical solutions. Imperfection of plate and boundary condition of the specimens are frequently mentioned as sources of the inconsistency. Additionally, techniques used to identify buckling load are also referred as a candidate source of discrepancy. In the experiment, the buckling load of plates can be identified using various kinds of plots; for example: 1) a plot of in-plane loads vs. out-of-plane displacement; 2) a plot of in-plane loads vs. end-shortening; and 3) a plot of in-plane loads vs. difference of surface strains. These static methods utilize the change of the slope of the curve in pre-buckling and post-buckling regions to identify buckling load. The difficulties of identifying the buckling load using a static test method is that there is a need to draw two lines in the pre-buckling and post-buckling regions to identify the buckling point. The obtained buckling load using these techniques depends on personal judgment, and could be a cause of error. So, there is a requirement to investigate an alternative method. In this study, vibration parameter of thin plate is utilized along with vibration correlation technique to determine buckling load and mode of thin plate. The project classifies into three mains sections; verifying the accuracy of vibration measurement, deriving the relationship between vibration and buckling behaviors, and verifying the derived relationship using experimental method.

In the first part, the similitude theory is employed to vibration of plate problems. This similitude theory is used to derive the scaling law which is used as a tool to verify the accuracy of the measured natural frequency. The scaling law is used because of the difficulty of setting the boundary condition of the test specimens such that they are similar to the theoretical boundary conditions. The experimental results showed that most of the experimental natural frequencies of the prototypes match those of from the scaling law. Uncertainties of the experiments in boundary condition and thickness are believed to be the sources of the discrepancy. Therefore, with a careful experimental setup, the measured natural frequency is efficiently accurate and reliable to use as a data for buckling load identification.

The second part of the project is to derive the relationship between vibration and bucking behavior of plates. By considering the governing equations of the vibration and buckling problems, it is shown that square of the natural frequency of the loaded plate is linearly varied with the applied load. The natural frequency is increased with the tensile load and decrease with the compressive load. This relationship is determined without a need to solve the differential governing equations, so it is applicable for plates with any boundary conditions. It is also shown that the square of the nature frequency approaches zero when the in-plane load approaches the buckling load. The derived relationship is verified by theoretically solving the vibration and buckling problems of specimens with combinations of boundary conditions. The Ritz method is employed to determine natural frequency of the loaded plate and buckling load of plate. In the process, vibration mode shape and buckling mode are also obtained. From the study, the predicted buckling load and mode from the vibration data are corresponded to the theoretical solution very well.

In the final part of the project, experimental verification was performed on a custom-made compression test frame. The test frame is capable of applying a uniform tensile and compressive load to a rectangular specimen, and supporting the specimen with clamped and free boundary conditions. Specimen was loaded and tested for natural frequencies. Both aluminum and stainless steel specimen with CCCC, CCCF and CFCF boundary conditions are included in the specimen. The measured vibration data is plotted against the in-plane load to determine the buckling load and buckling mode. Square of the measured natural frequency is linearly varied with the applied load as expected. The experimental results show that all buckling modes obtained from VCT agree with numerical solutions very well, while most of the measured buckling loads conform to the numerical solutions. Buckling loads of CCCC stainless steel specimens were not well indicated using the proposed technique. The imperfection of boundary conditions of this group of specimens is believed to be a considerable factor in the high percentage difference between the measured and numerical buckling loads. If the experiments of stainless steel specimens with CCCC boundary condition are excluded, the average of the percent difference between measured buckling loads and numerical solutions is -0.18% with the standard deviation of 5.05%. The experimental study demonstrates the accuracy and reliability of using vibration data in the tensile-loading range to determine the buckling load. Boundary conditions of the specimen have a considerable effect on the precision of the measured buckling load. The proposed technique of identifying buckling load of plate has an advantage over the static methods for the fact that this method does not need human's judgment to draw two lines in the pre- and post- buckling regions.

Outputs of this research project are the following:

Manuscript:

 Singhatahadgid, P. and Sukajit, P., "Experimental determination of the buckling load of rectangular plates using vibration correlation technique," submitted to Thin-Walled Structures.

Reprint:

- 1. Singhatanadgid, P. and Na Songkhla, A., "An experimental investigation into the use of scaling laws for predicting vibration responses of rectangular thin plates," Journal of Sound and Vibration 2008;311:314–327.
- Singhatanadgid, P. and Sukajit, P., "Determination of buckling load of rectangular plates using measured vibration data." International Conference on Experimental Mechanics (ICEM2008), Nanjing, China, 8-11 November 2008.
- 3. Sukajit, P. and Singhatanadgid, P. "Identification of buckling load of thin plate using the vibration correlation technique," Proceedings of the 21st Conference of the Mechanical Engineering Network of Thailand (ME-NETT 21), Chonburi, Thailand, 17-19 October 2007, code AMM10.

Contents

Chapter 1 Introduction	1
Chapter 2 Literature review	4
2.1 Buckling of plate	4
2.2 Similitude theory and scaling law	6
2.3 Vibration correlation technique	7
Chapter 3 Mechanics of composite materials	11
3.1 Mechanic of composite plate	11
3.2 The Buckling of Plate Governing Equations	14
3.3 Buckling of a Specially Orthotropic Plate	16
3.4 The Vibration of Plate Governing Equations	18
Chapter 4 Accuracy of vibration measurement	20
4.1 Introduction	20
4.2 Scaling law for vibration of plate	21
4.3 Experimental study	23
4.4 Conclusions	34
Chapter 5 Vibration correlation technique	35
5.1 Relationship between natural frequency and buckling load	35
5.2 Numerical validation	38
Chapter 6 Experimental study	42
6.1 Experiment arrangement	42
6.2 Specimens and boundary conditions	45
6.3 Experiment procedures and data reduction	46
6.4 Experimental result and discussion	50
6.5 Conclusions	62
Chapter 7 Discussions and conclusions	64
References	67
Appendix	71







โครงการความสัมพันธ์ของการสั่นสะเทื่อนของโครงสร้างแผ่นคอมโพสิตที่รับแรงในแนวระนาบกับค่าภาระการโก่งงอ

Chapter 1. Introduction

Buckling load is one of the important parameters which should be considered in the design of thin or slender structures subjected to compressive loading. Buckling behavior of several engineering structures such as columns, plates, frames, and shells has been continuously investigated in the past several decades. Among several types of structure, a thin plate is one of the most important types of structure used in engineering applications. Mainly, the stability problem of plate is investigated using theoretical, numerical and experimental approaches. The theoretical method is applicable to a limited type of problems where a closed-form solution is possible. For more complicated structures, the numerical methods such as a finite element method are required. Solutions from both theoretical and numerical methods are generally verified with the experimental results. Experimental method involves in a number of costly and time consuming processes, however, imperfections and complicated effects of the problem are naturally included. For an experimental study of buckling of plate, identification of the buckling point is an important process, since it directly affects the accuracy of the measurement. In the experiment, the buckling load of plates can be identified using various kinds of plots; for example: 1) a plot of in-plane loads vs. out-of-plane displacement; 2) a plot of inplane loads vs. end-shortening; and 3) a plot of in-plane loads vs. difference of surface strains. These methods which may be classified as static methods utilize the change of the slope of the curve in pre-buckling and post-buckling regions to identify buckling load. However, these approaches have a drawback for the fact that it is required to draw two lines in the pre- and post- buckling regions to get the buckling load. Drawing these lines might be a cause of error due to human bias. So, there is a need to explore an alternative method of buckling load identification.

In this study, the relationship between buckling and vibration behavior of thin plates is investigated. The relationship between applied in-plane load and the natural frequency of plates is derived from the differential governing equations of both problems. The derived relationship, which is applicable to thin plates with any boundary conditions, is numerically verified by simulating a plot of the derived relationship. Because of the premature curvature, which is usually detected even before the specimen has buckled, it is proposed in this study that the buckling load be determined from the vibration data of a plate subjected to tensile loading. A test frame, capable of applying tensile and compressive loading to a specimen, was prepared. A series of vibration tests was performed to determine the natural frequencies of the plates. The vibration data, along with the derived relationship, are used to predict the buckling load. Experimental buckling loads are compared to the numerical solutions to verify the proposed technique. In this study, numerical solutions is served as benchmark solutions, and determined using the Ritz method using beam functions as basis function.

In summary, objectives of this study may be itemized as follows:

- 1. To derive the relationship between vibration and buckling of plate in order to use the vibration data to identify the buckling load
- 2. To verify the accuracy of vibration measurement and determine the cause of error that might encounter during the experiment
- 3. To determine the buckling load of plate using vibration correlation technique using vibration data in the tensile loading range.

In this report, literature reviews concerning buckling and vibration of thin plate, similitude concept, and vibration correlation technique used to identify buckling load are presented in chapter 2. The fundamental concepts of mechanics of composite plates are outlined in the next chapter. Chapter 4 presents a study on an accuracy of the vibration

measurement. Scaling law for vibration a thin plate problem used as a concept for vibration experiment is described. The experiment demonstrated accuracy of vibration measurement is outlined in the second half of the chapter. The next chapter presents the vibration correlation technique used to identify buckling load of plates. The relationship between vibration parameter and buckling parameter is derived and verified with the known solutions. This technique is employed in chapter 6 where experimental study is explained. Experimental setup, specimens and experimental procedures are described along with extensive experimental result. This report concludes in chapter 7 with some discussions and conclusions of the present study. The outputs of the project are also presented in the Appendix at the end of this report.

Chapter 2. Literature Review

This chapter gives a review of previous studies on some topics related to this research project. The general buckling behaviors of thin plate are described in the first part of this chapter, including reviews of the studies available in the literature. Then, the similitude theory and scaling law for vibration problem are presented. Finally, the vibration correlation technique used in bucking problem is outlined and reviewed.

2.1 Buckling of plate

Besides tensile or compression failures, buckling is another mode of failure that involves stability of structures. It usually happens in slender elements such as beams, columns, or plates. This study focuses on buckling of plates; so only plate structures are of interest herein. A panel subjected to uniaxial or biaxial compressive loading will buckle if compressive stress at any point is sufficiently high. A plate under compression-tension biaxial loading may also buckle. Buckling phenomenon may even arise from more complicated loading conditions such as non-uniform tensile loading, shear loading, moisture, or exposure to elevated temperatures.

The buckling phenomenon can be described from a plot of the out-of-plane displacement at a specific point, usually at the point of maximum out-of-plane displacement, against in-plane load. In classical linear buckling theory, when in-plane load increases from zero, out-of-plane displacements are assured to remain zero until the critical load is reached. Buckling of plates can be investigated using analytical and numerical analysis. Analytical solution of the buckling of composite plates requires a solution of the governing equations. These equations are only solvable in a few simple

cases, such as a specially orthotropic rectangular plate with simply supported boundary conditions. A closed-form solution for a specially orthotropic plate, i.e. either unidirectional or a symmetric cross-ply panels, is thoroughly derived by Whitney [1]. Mode shape transitions are also graphically presented. Several studies on buckling of composite plates using the Ritz method are available. In 1986, Lagace et al. [2] employed the Ritz method to study the effect of mechanical couplings on buckling behavior. They concluded that those mechanical couplings, especially stretching-bending couplings, cause out-of-plane displacement prior to buckling in unsymmetric laminates. This phenomenon significantly reduces the critical buckling load. An experimental verification was also performed. The Ritz method was demonstrated, by Narita and Leissa [3], to be accurate for symmetric laminates if enough number of terms (more than 100 terms) were used. A double sine series was used to approximate the out-of-plane displacement. Convergence studies and contour plots of buckling mode shape were also presented. However, the in-plane displacements were ignored in the strain energy function. Similar approximate function and analysis method were used by Chai and Hoon [4] to study the buckling of generally laminated plates. The results agreed with the exact solution for symmetric crossply, antisymmetric crossply, and antisymmetric angle-ply. The effect of mechanical couplings, D_{16} and D_{26} , on buckling load was shown to be an important factor in the analysis.

There have been several experimental studies on buckling of composite plates using different measurement techniques appeared during the past two decades. Chai, Hoon, and Chin [5] experimentally confirmed the buckling behavior determined from the Ritz method using laser-based holography and strain gauges. Chai, Banks, and Rhodes [6] used a linear variable differential transformer (LVDT) to measure the out-of-plane deflection to study the buckling of simply supported plates under uniaxial loading. The

results correlated well with finite element solutions and other available studies [7, 8]. Discrepancies between -7% and 11% of experimentally determined buckling loads were reported. Another experimental method for monitoring out-of-plane displacement is the shadow moiré technique. This experiment method was used by Tuttle, Singhatanadgid, and Hinds [9] to observe the whole-field out-of-plane deflections of composite plates under tension-compression biaxial loading. Experimental buckling modes were well compared with predictions obtained numerically based on the Galerkin method. As expected, buckling loads increased as the transverse tensile loads were increased. Almost all of the previous studies indicated several difficulties in setting up the experimental conditions, such as loading conditions and boundary conditions, which are comparable to the conditions assumed in the analysis. These factors are the common sources of discrepancy between measurement and prediction.

2.2 Similitude theory and scaling law

The similitude theory has been applied to many problems in the field of structural engineering, including vibration and buckling problems of plates. Simitses [10] applied similitude transformation to the bending, buckling, and vibration of laminated plates. The derived scaling laws were successfully employed to the problem with appropriate similarity requirements between model and prototype systems. Rezaeepazhand et al. [11] demonstrated a procedure for deriving a scaling law for the frequency response of laminated plates. Both Simitses and Rezaeepazhand derived scaling laws from the closed-form solutions of the problems. Alternatively, scaling laws can be derived directly from the governing equation of the problems. In references [12-14], the authors derived the scaling laws for the vibration and buckling behaviour of laminated rectangular plates. In those studies, similitude transformation was applied to the governing equations of the

problems directly. Besides the scaling law, the similarity requirements were also obtained. An advantage of this approach is that a solution of the governing equations is not required. The obtained scaling laws were verified with the theoretical solution and found to be exact for complete similitude cases. Partial similitude cases were also investigated and recommended. It was also found that the scaling laws were independent of boundary conditions. This implies that, for a problem with complicated boundary conditions, the behavior of the prototype can be predicted from the experimental results of the corresponding scaled model given that the boundary conditions of both systems are identical. This concept is especially beneficial for problems where the boundary conditions cannot be numerically modeled in the numerical solutions but can be built in the scaled model.

In addition to a simple-supported rectangular thin plate, the similitude theory was moreover applied to the elastically restrained flat plates subjected to dynamic loads by Wu [15]. The author showed that the geometric, kinematic and dynamic similarities must be satisfied to assure the complete similitude. A similar concept was also applied to the dynamic analysis of rectangular plates under a moving load line [16]. Both complete and partial similitude cases were presented. An agreement between the theoretical vibration response of the full-scale prototype and the prediction from the solution of the scale model was obtained. Wu et al. [17] employed the similitude concept with a more complex structure where a scale model and the scaling law were utilized to determine the vibration characteristics of a full-size crane structure.

2.3 Vibration correlation technique

Buckling load is one of the important parameters which should be considered in the design of thin or slender structures subjected to compressive loading. Buckling behavior of several engineering structures such as columns, plates, frames, and shells has been continuously investigated in the past several decades. Among several types of structure, a thin plate is one of the most important types of structure used in engineering applications. Mainly, the stability problem of plate is investigated using theoretical, numerical and experimental approaches. The theoretical method is applicable to a limited type of problems where a closed-form solution is possible. For more complicated structures, the numerical methods such as a finite element method are required. Solutions from both theoretical and numerical methods are generally verified with the experimental results. Experimental method involves in a number of costly and time consuming processes, however, imperfections and complicated effects of the problem are naturally included. For an experimental study of buckling of plate, identification of the buckling point is an important process, since it directly affects the accuracy of the measurement. In the experiment, the buckling load of plates can be identified using various kinds of plots; for example: 1) a plot of in-plane loads vs. out-ofplane displacement; 2) a plot of in-plane loads vs. end-shortening; and 3) a plot of inplane loads vs. difference of surface strains. These methods which may be classified as static methods utilize the change of the slope of the curve in pre-buckling and postbuckling regions to identify buckling load. The plots mentioned above and other static methods are properly summarized in Ref. [18]. There are several studies employed the static methods to identify the buckling load of plates. Chai et al.[19] verified the theoretical buckling load of composite plates using the experimental method. Buckling load was determined from the intersection of the tangents drawn in the pre-buckling and post-buckling slopes of the load versus membrane strain curve. The discrepancies between the experimental and theoretical solutions between -7 % and +11 % were reported. Tuttle et al. [20] determined buckling loads of composite panels from the plots of applied in-plane load vs. out-of-plane displacement, and compared the experimental

results to numerical predictions obtained using a Galerkin method. Although the average percentage error between the measured and predicted buckling loads is low, the standard deviation of the percentage error is as high as 15%. The difficulties of identifying the buckling load using a static test method were documented. In particular, drawing two lines in the pre-buckling and post-buckling regions to identify the buckling point depended on personal judgment, and could be a cause of error. To use the experimental result as a benchmark solution, the method used to identify buckling load must be accurate and reliable.

There is a need for an alternative approach to experimentally identify the buckling load of a plate. In this paper, the vibration correlation technique (VCT) is explored and modified to determine buckling load of a plate. The VCT is a nondestructive testing utilizing the measured vibration data. This concept has been applied to buckling problems in the past with a variety of amount of success. Lurie and Monica [21] showed that the square of the frequency of the lateral vibration of a thin plate with simple supports on all edges is linearly related to the end load. They also conducted some experiments on elastically restrained columns, rigid-joint trusses, and thin flat plates. The authors reported that VCT was successfully employed to predict the buckling load of only columns and trusses. For flat plates, because of the initial curvature, the buckling load cannot be predicted by the proposed method. However, Chailleux et al. [22] later showed that with a carefully designed experimental setting, VCT can be used to determine the buckling load with satisfactory accuracy. The experimental dynamical curved is linear in the low load region, such that it is possible to extrapolate the data to obtain the buckling load. Segall and Springer [23] proposed a dynamic method to determine linear buckling loads of elastic rectangular plates. With an integral equation representation of the elastic stability, the proposed technique does not require the application of an in-plane load. A

few studies [24-26] concerning the use of vibration data to investigate buckling behavior can be found in the literature.

Chapter 3. Mechanics of composite material

In this chapter, fundamental principles of mechanics of composite materials are summarized. The basic equations of theory of composite plate are reviewed. Then, the governing equations of buckling and vibration problems are derived.

3.1 Mechanic of composite plate

- Fig. 3.1 shows the x-y-z coordinate system used in developing the laminates anisotropic plate. The midplane of the plate lies on the x-y plane of the coordinate system. The displacements at any points in x, y, and z directions, are u, v, w respectively. The following assumptions are made:
- 1) The plate is composed of orthotropic laminae bonded together with arbitrary directions of orthotropic axes measured with respect to *x-y* plane.
- 2) The thickness of the plate, h is much smaller than the length and width of the plate.
- 3) The displacements u, v, and w are small compared to the thickness.
- 4) The in-plane strains ε_x , ε_y , and γ_{xy} are small compared to unity.
- 5) The transverse normal strain, ε_z is negligible.
- 6) The transverse shear strains γ_{xz} , and γ_{yz} are negligible.
- 7) Tangential displacements u, and v are linear function of z.
- 8) Each orthotropic lamina obeys Hooke's law.
- 9) The plate thickness is constant.
- 10) There is no shear stress, τ_{xz} , and τ_{yz} on the surface $z = \pm h/2$

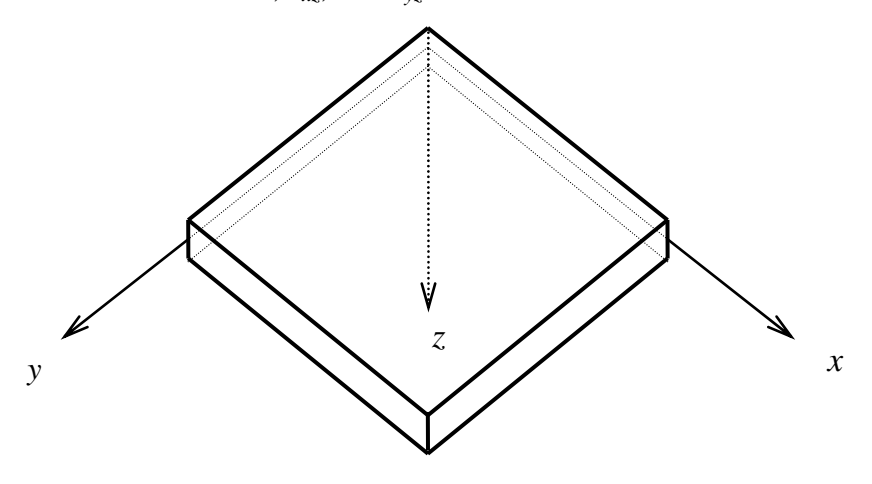


Fig 3.1 Coordinate system for laminated plate.

According to assumption 5 and 7, the displacements at an arbitrary point are described as

$$u(x,y,z) = u^{\circ}(x,y) + zF_{1}(x,y)$$

$$v(x,y,z) = v^{\circ}(x,y) + zF_{2}(x,y)$$

$$w(x,y,z) = w^{\circ}(x,y)$$
(3.1)

where u^o and v^o are the in-plane displacements of the mid-plane in x and y direction, respectively. w^o is the transverse displacement of the mid-plane which is independent of coordinate z, as assumed in assumption 5.

Using strain-displacement relationship, it can be shown that;

$$\varepsilon_{x} = \frac{\partial u}{\partial x} = \varepsilon_{x}^{o} + z\kappa_{x}$$

$$\varepsilon_{y} = \frac{\partial v}{\partial y} = \varepsilon_{y}^{o} + z\kappa_{y}$$

$$\gamma_{xy} = \frac{\partial u}{\partial y} + \frac{\partial v}{\partial x} = \gamma_{xy}^{o} + z\kappa_{xy}$$
(3.2)

where \mathcal{E}_{x}^{o} , \mathcal{E}_{y}^{o} and γ_{xy}^{o} are the strains at the mid-plane which can be written as;

$$\varepsilon_{x}^{o} = \frac{\partial u^{o}}{\partial x}$$

$$\varepsilon_{y}^{o} = \frac{\partial v^{o}}{\partial y}$$

$$\gamma_{xy}^{o} = \frac{\partial u^{o}}{\partial y} + \frac{\partial v^{o}}{\partial x}$$
(3.3)

 κ_x, κ_y , and κ_{xy} are the curvatures of the mid-plane surface which can be written as;

$$\kappa_{x} = -\frac{\partial^{2} w}{\partial x^{2}}$$

$$\kappa_{y} = -\frac{\partial^{2} w}{\partial y^{2}}$$

$$\kappa_{xy} = -2\frac{\partial^{2} w}{\partial x \partial y}$$
(3.4)

From Eq.(3.2) and the lamina stress-strain relationship, stresses in the laminated plate can be written as

$$\begin{cases}
\sigma_{x} \\
\sigma_{y} \\
\tau_{xy}
\end{cases}_{k} = \begin{bmatrix}
\overline{Q}_{11} \ \overline{Q}_{12} \ \overline{Q}_{16} \\
\overline{Q}_{12} \ \overline{Q}_{22} \ \overline{Q}_{26} \\
\overline{Q}_{16} \ \overline{Q}_{26} \ \overline{Q}_{66}
\end{bmatrix}_{k} \begin{cases}
\varepsilon_{x}^{o} + z\kappa_{x} \\
\varepsilon_{y}^{o} + z\kappa_{y} \\
\gamma_{xy}^{o} + z\kappa_{xy}
\end{cases}$$
(3.5)

where $[\overline{Q}]_k$ is the property of the *k*th lamina which is depended on the orientation of the orthotropic axes of each ply.

The stresses in laminated plate are related to the applied forces and moments as;

$$(N_x, N_y, N_{xy}) = \int_{\frac{-h}{2}}^{\frac{h}{2}} (\sigma_x, \sigma_y, \tau_{xy})_k dz$$

$$(M_x, M_y, M_{xy}) = \int_{\frac{-h}{2}}^{\frac{h}{2}} (\sigma_x, \sigma_y, \tau_{xy})_k z dz$$

$$(3.6)$$

where $(\sigma_x, \sigma_y, \sigma_{xy})_k$ = stresses in the *k*th lamina

 (N_x, N_y, N_{xy}) = applied forces per unit length.

 (M_x, M_y, M_{xy}) = applied moments per unit length.

h = laminate thickness

Substitute stresses from Eq.(3.5) into Eq.(3.6), perform the integration and rewrite in form of matrix,

$$\begin{bmatrix}
N_{x} \\
N_{y} \\
N_{xy} \\
M_{x} \\
M_{y} \\
M_{xy}
\end{bmatrix} =
\begin{bmatrix}
A_{11} A_{12} A_{16} B_{11} B_{12} B_{16} \\
A_{12} A_{22} A_{16} B_{12} B_{22} B_{26} \\
A_{16} A_{26} A_{66} B_{16} B_{26} B_{66} \\
B_{11} B_{12} B_{16} D_{11} D_{12} D_{16} \\
B_{12} B_{22} B_{26} D_{12} D_{22} D_{26} \\
B_{16} B_{26} B_{66} D_{16} D_{26} D_{66}
\end{bmatrix}
\begin{bmatrix}
\mathcal{E}_{x}^{o} \\
\mathcal{E}_{y}^{o} \\
\gamma_{x}^{o} \\
\kappa_{x} \\
\kappa_{y} \\
\kappa_{xy}
\end{bmatrix}$$
(3.7)

where
$$(A_{ij}, B_{ij}, D_{ij}) = \int_{\frac{-h}{2}}^{\frac{h}{2}} (\overline{Q}_{ij})_k (1, z, z^2) dz$$

Eq.(3.7), a so-called "constitutive equation" relates the applied forces and moments to the strains and curvatures of laminated plate.

3.2 The Buckling of Plate Governing Equations

The governing equations for buckling of a plate under in-plane loading can be derived by considering the infinitesimal element of plate as shown in Fig. 3.2. Fig. 3.2(a) shows the in-plane stress resultants, and the moment resultants. The transverse shear stress resultants are shown in Fig. 3.2(b). Since the buckled plate is under a static condition, the summation of forces along x and y direction must be equal to zero and can be written as;

$$\frac{\partial N_x}{\partial x} + \frac{\partial N_{xy}}{\partial y} = 0 \tag{3.8}$$

$$\frac{\partial N_{y}}{\partial y} + \frac{\partial N_{xy}}{\partial x} = 0 \tag{3.9}$$

Under buckling conditions, the in-plane stress resultants, N_x , N_y , and N_{xy} , will not lie on the x-y plane as shown in Fig. 3.2(a). Thus, the summation of forces in the z direction has to include the effects of these in-plane stress rotations. By summing of forces in the z direction and summing moments about the x and y axes, it can be shown that;

$$\frac{\partial^2 M_x}{\partial x^2} + 2 \frac{\partial^2 M_{xy}}{\partial x \partial y} + \frac{\partial^2 M_y}{\partial y^2} + N_x \frac{\partial^2 w}{\partial x^2} + 2N_{xy} \frac{\partial^2 w}{\partial x \partial y} + N_y \frac{\partial^2 w}{\partial y^2} + q(x, y) = 0$$
(3.10)

Eqs.(3.8)-(3.10) are the equations of motion in term of stress and moment resultants. The equations of motion in term of displacements which are more convenient to implement in further derivation can be determined by substituting the constitutive equation, Eq.(3.7), and strain displacement relations, Eq.(3.3), into the equations of motion in term of stress and moment resultants. Eq.(3.8)-(3.10) become;

$$A_{11} \frac{\partial^{2} u^{o}}{\partial x^{2}} + 2A_{16} \frac{\partial^{2} u^{o}}{\partial x \partial y} + A_{66} \frac{\partial^{2} u^{o}}{\partial y^{2}} + A_{16} \frac{\partial^{2} v^{o}}{\partial x^{2}} + (A_{12} + A_{66}) \frac{\partial^{2} v^{o}}{\partial x \partial y} + A_{26} \frac{\partial^{2} v^{o}}{\partial y^{2}}$$

$$-B_{11} \frac{\partial^{3} w}{\partial x^{3}} - 3B_{16} \frac{\partial^{3} w}{\partial x^{2} \partial y} - (B_{12} + 2B_{66}) \frac{\partial^{3} w}{\partial x \partial y^{2}} - B_{26} \frac{\partial^{3} w}{\partial y^{3}} = 0$$
(3.11)

$$A_{16} \frac{\partial^{2} u^{o}}{\partial x^{2}} + (A_{12} + A_{66}) \frac{\partial^{2} u^{o}}{\partial x \partial y} + A_{26} \frac{\partial^{2} u^{o}}{\partial y^{2}} + A_{66} \frac{\partial^{2} v^{o}}{\partial x^{2}} + 2A_{26} \frac{\partial^{2} v^{o}}{\partial x \partial y} + A_{22} \frac{\partial^{2} v^{o}}{\partial y^{2}}$$

$$-B_{16} \frac{\partial^{3} w}{\partial x^{3}} - (B_{12} + 2B_{66}) \frac{\partial^{3} w}{\partial x^{2} \partial y} - 3B_{26} \frac{\partial^{3} w}{\partial x \partial y^{2}} - B_{22} \frac{\partial^{3} w}{\partial y^{3}} = 0$$
(3.12)

$$D_{11} \frac{\partial^{4} w}{\partial x^{4}} + 4D_{16} \frac{\partial^{4} w}{\partial x^{3} \partial y} + 2(D_{12} + 2D_{66}) \frac{\partial^{4} w}{\partial x^{2} \partial y^{2}} + 4D_{26} \frac{\partial^{2} w}{\partial x \partial y^{3}} + D_{22} \frac{\partial^{4} w}{\partial y^{4}}$$

$$-B_{11} \frac{\partial^{3} u^{o}}{\partial x^{3}} - 3B_{16} \frac{\partial^{3} u^{o}}{\partial x^{2} \partial y} - (B_{12} + 2B_{66}) \frac{\partial^{3} u^{o}}{\partial x \partial y^{2}} - B_{26} \frac{\partial^{3} u^{o}}{\partial y^{3}} - B_{16} \frac{\partial^{3} v^{o}}{\partial x^{3}}$$

$$-(B_{12} + 2B_{66}) \frac{\partial^{3} v^{o}}{\partial x^{2} \partial y} - 3B_{26} \frac{\partial^{3} v^{o}}{\partial x \partial y^{2}} - B_{22} \frac{\partial^{3} v^{o}}{\partial y^{3}} = q(x, y) + N_{x} \frac{\partial^{2} w}{\partial x^{2}} +$$

$$2N_{xy} \frac{\partial^{2} w}{\partial x \partial y} + N_{y} \frac{\partial^{2} w}{\partial y^{2}}$$

$$(3.13)$$

In the case of a simply supported, symmetric laminate ($B_{ij} = 0$) plate, the out-ofplane displacement, w disappears in the first two equations of motion. Only the last equation which contains the w term will be considered in the buckling analysis. If only inplane loads, N_x and N_y , are applied, Eq.(3.13) becomes;

$$D_{11} \frac{\partial^4 w}{\partial x^4} + 4D_{16} \frac{\partial^4 w}{\partial x^3 \partial y} + 2(D_{12} + 2D_{66}) \frac{\partial^4 w}{\partial x^2 \partial y^2} + 4D_{26} \frac{\partial^2 w}{\partial x \partial y^3}$$

$$+ D_{22} \frac{\partial^4 w}{\partial y^4} = N_x \frac{\partial^2 w}{\partial x^2} + N_y \frac{\partial^2 w}{\partial y^2}$$

$$(3.14)$$

More specifically, the D_{16} and term D_{26} terms are zero for a specially orthotropic plate. The governing equation reduces to;

$$D_{11} \frac{\partial^4 w}{\partial x^4} + 2(D_{12} + 2D_{66}) \frac{\partial^4 w}{\partial x^2 \partial y^2} + D_{22} \frac{\partial^4 w}{\partial y^4} = N_x \frac{\partial^2 w}{\partial x^2} + N_y \frac{\partial^2 w}{\partial y^2}$$
(3.15)

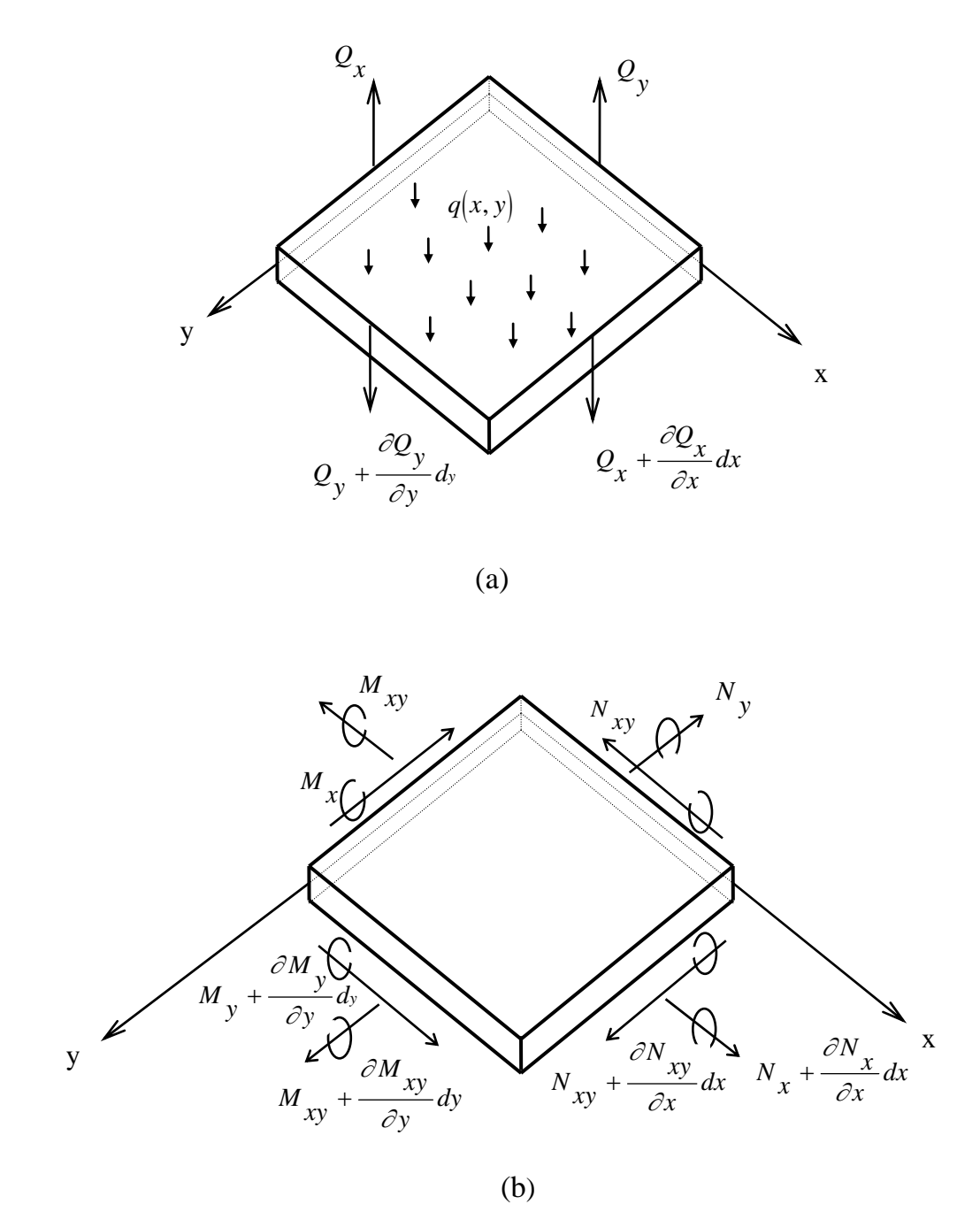


Fig 3.2 Stress and moment resultants on the edges of the rectangular plate.

3.3 Buckling of a Specially Orthotropic Plate

Buckling of a specially orthotropic plate is the simplest case compared to other kinds of composite plates. Uniform tension N_y and compression N_x are applied to a specially orthotropic plate as shown in Fig. 3.3. The behavior of this plate is governed by Eq. (3.15). For a simply supported plate, the boundary conditions can be written as;

$$w = M_x = -D_{11} \frac{\partial^2 w}{\partial x^2} - D_{12} \frac{\partial^2 w}{\partial y^2} = 0$$
 On $x = 0$ or $x = a$

$$w = M_y = -D_{12} \frac{\partial^2 w}{\partial x^2} - D_{22} \frac{\partial^2 w}{\partial y^2} = 0$$
 On $y = 0$ or $y = b$

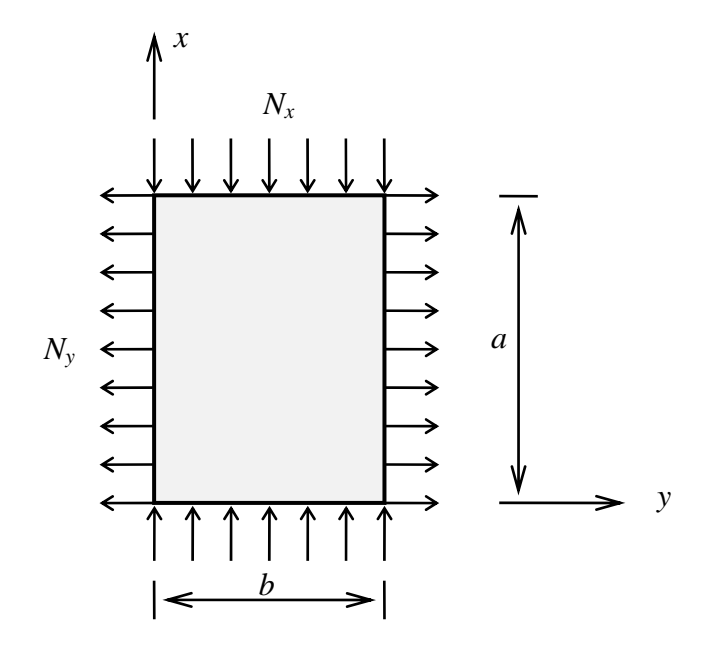


Fig. 3.3 Uniform compression, N_x , and tension, N_y , loads

To solve Equation (3.15), it is assumed that the solution satisfies all boundary conditions such that;

$$w(x,y) = A_{mn} \sin \frac{m\pi x}{a} \sin \frac{n\pi y}{b}$$
(3.16)

where ; A_{mn} is the maximum out-of-plane displacement of plate.

m, n are positive integer number which represent the mode shapes exhibited by the buckled plate.

Substituting the assumed solution, Eq.(3.16), into the governing equation (3.15) and making some simplifications, the buckling load N_x can be related to the transverse tension loading, N_y as follows;

$$N_{x} = \frac{-\pi^{2} \left[D_{11} \left(\frac{m}{a} \right)^{2} + 2 \left(D_{12} + 2 D_{66} \right) \left(\frac{n}{b} \right)^{2} + D_{22} \left(\frac{n}{b} \right)^{4} \left(\frac{a}{m} \right)^{2} \right]}{1 + R \left(\frac{an}{bm} \right)^{2}}$$
(3.17)

where the load ratio, $R = \frac{N_y}{N_x}$

The load ratio is negative for tension-compression biaxial loading and equals to zero for uniaxial loading. For a given value of N_y , there are infinite values of N_x which satisfy Eq.(3.17). The critical buckling load is the lowest value of N_x . The mode shape is determined from the corresponding values of m and n.

In the case of uniaxial or tension-compression biaxial loading, the buckling load always corresponds to n=1 since there are second and fourth orders of n in the numerator but only second orders in the denominator. This leads to the conclusion that the mode shape in the direction along y-axis is a half sine curve. In contrast, m is not necessarily equal to 1 for the lowest value of N_x . It depends on the value of D_{ij} and load ratio R.

3.4 The Vibration of Plate Governing Equations

Using the equilibrium equations similar to the buckling problem, the governing equation for free transverse vibration of specially orthotropic plate can be written as [27];

$$D_{11} \frac{\partial^4 W}{\partial x^4} + 2(D_{12} + 2D_{66}) \frac{\partial^4 W}{\partial x^2 \partial y^2} + D_{22} \frac{\partial^4 W}{\partial y^4} + \rho_0 \frac{\partial^2 W}{\partial t^2} = 0$$
(3.18)

where W is the displacement in the out-of-plane direction, ρ_0 is the mass density of the specimen, and D is the plate bending stiffness.

Assuming that the out-of-plane displacement is separable as a function of position and time, the governing equation is reduced to

$$D_{11} \frac{\partial^4 w}{\partial x^4} + 2(D_{12} + 2D_{66}) \frac{\partial^4 w}{\partial x^2 \partial y^2} + D_{22} \frac{\partial^4 w}{\partial y^4} - \rho_0 \omega^2 w = 0$$
(3.19)

where w is function of x and y only, i.e. w = w(x,y), and ω is the frequency of the vibration.

The vibration equation, Eq. (3.19), can be solved if the boundary conditions of the plate are known. For simple-supported plates, the analytical closed form solution is

$$\omega_{mn}^{2} = \frac{\pi^{4}}{\rho_{0}a^{4}} \left(D_{11}m^{4} + 2(D_{12} + 2D_{66}) \left(\frac{mna}{b} \right)^{2} + D_{22} \left(\frac{na}{b} \right)^{4} \right)$$
(3.20)

where ω_{mn} are natural frequency of the plate in Hz, a and b are plate width and length, respectively, h is specimen thickness, m and n are positive integer.

Chapter 4. Accuracy of vibration measurement

This chapter focuses on the accuracy of vibration measurement. To use the vibration data to identify the bucking load, it must be certain that the measured vibration parameters are reliable and accurate.

4.1 Introduction

The vibration parameter requires to used in the buckling load identification is the natural frequency of the structure. This parameter can be measured using an impact testing. The objective of this chapter is to determine the accuracy of vibration measurement. Instead of comparing the measured natural frequency with the theoretical solution, this study utilizes the scaling law as a tool in the experimental study because it is very difficult to setup the experiment such that the boundary condition is similar to the theoretical one. By using the scaling law, it is certain that the boundary conditions of the model and prototype are very similar, if not identical.

The scaling law has been utilized in many engineering applications. The principle provides a powerful tool for engineers and scientists to replicate the behavior of the prototype using an appropriate scaled model. Similitude theory can be stated as [28]; "the sufficient and necessary condition of similitude between two systems is that the mathematical model of the one be related by a bi-unique transformation to that of the other." For a prototype of interest, a scaled replica can be built to duplicate the behavior of the full-scale system. The experimental results on the model can be utilized to predict the behavior of the prototype. The similitude concept is thus very useful, especially, for problems with either a complex domain or complicated boundary conditions for which numerical solutions are not sufficiently accurate, if possible. If the prototype is perfectly replicated, the experiment result on the model can be scaled to predict the behavior of the

prototype with sufficient accuracy.

In this study, the scaling law for vibration problem is employed to predict the natural frequency of the prototype. This natural frequency is then compared with the experimental measurement. With this approach, the accuracy and reliability of the vibration measurement is determined.

4.2 Scaling law for vibration of plate

Although the natural frequencies of thin plates with combinations of simple support, clamped support or free boundary conditions are available, they may not be practically appropriate for engineering structures which accurate natural frequencies are required. The boundary conditions of practical structures are usually non-classical ones such as elastically restrained or imperfect boundary conditions which are not easily modeled because the level of restraining is unknown. This is where the scaling law can be utilized to determine the vibration behavior of the structure or prototype of interest using the experimental results of the scaled model. The scaled model is either a scaled-down or scaled-up test specimen having complete similarity with the real structure. Although the boundary conditions of the prototype are not exactly known, they can be modeled in the scaled model using similar supports. Thus, the experimental results from the corresponding test specimen along with the scaling law can be used to predict the vibration behavior of the prototype. The derivation of the scaling law for vibration behavior is briefly derived in this section.

The scaling law for the vibration of rectangular isotropic plates is derived from the governing equation by comparing the governing equations of the model with that of the prototype. From both equations, the similitude invariant term, which leads to the scaling

law, is obtained. Let the variables of the prototype and their corresponding model variables be related to each other as follows:

$$x_p = C_x x_m$$
, $y_p = C_y y_m$, $w_p = C_w w_m$, $D_p = C_D D_m$, $\omega_p = C_\omega \omega_m$, and $\rho_p = C_\rho \rho_m$,

where subscripted p refers to the prototype system and subscripted m refers to the model system, and C_i are the scaling factors of the i parameters. To derive the similitude invariant, the governing equations of the model and prototype are written as the following:

$$\frac{\partial^4 w_m}{\partial x_m^4} + 2 \frac{\partial^4 w_m}{\partial x_m^2 \partial y_m^2} + \frac{\partial^4 w_m}{\partial y_m^4} - \frac{\omega_m^2 \rho_m}{\partial y_m} w_m = 0, \qquad (4.1)$$

$$\frac{C_w}{C_x^4} \frac{\partial^4 w_m}{\partial x_m^4} + 2 \frac{C_w}{C_x^2 C_y^2} \frac{\partial^4 w_m}{\partial x_m^2 \partial y_m^2} + \frac{C_w}{C_y^4} \frac{\partial^4 w_m}{\partial y_m^4} - \frac{C_\omega^2 C_\rho C_w}{C_D} \frac{\omega_m^2 \rho_m}{D_m} w_m = 0.$$

$$(4.2)$$

It should be noted that Eq.(4.2) can be written in the same form as Eq.(4.1) with subscript "p" instead of subscript "m." However, the scaling factors are utilized so that the governing equations of both systems can be compared and simplified. Comparing both equations, the vibration behavior of the model and of the prototype are similar if groups of the scaling factors in Eq.(4.2) are all equal. This implies that Eq.(4.2) can be reduced to Eq.(4.1) when the scaling factor groups are canceled out. Thus, the similitude requirement is obtained as

$$\frac{1}{C_x^4} = \frac{1}{C_x^2 C_y^2} = \frac{1}{C_y^4} = \frac{C_\omega^2 C_\rho}{C_D}.$$
(4.3)

By assuming that the model and prototype have a geometric similarity ($C_x = C_y = C_a = C_b$), the similarity requirement is simplified to

$$\frac{C_{\omega}^2 C_{\rho} C_b^4}{C_D} = 1. \tag{4.4}$$

Eq.(4.4) is the similitude invariant of the vibration behavior of rectangular plates. This invariant can be reduced to the scaling law of plate natural frequency as

$$\omega_p^2 = \omega_m^2 C_D \frac{b_m^4 \rho_m}{b_p^4 \rho_p} \,. \tag{4.5}$$

This scaling law relates the natural frequencies of the model to that of the corresponding prototype. The derived scaling law is valid for a model-prototype pair with complete geometric similarity, i.e. $C_a = C_b$ or both systems having the same aspect ratio. The scaling law can be verified with the theoretical solution shown in the previous section. The scaling law for the natural frequency of rectangular plate is verified, theoretically. The derived scaling law is applicable to a model and prototype pair with the same aspect ratio, although they are made of different materials.

4.3. Experimental study

4.3.1 Experimental setup

Several samples of thin rectangular plates were tested to determine their first three natural frequencies. The specimens were composed of aluminum, structural steel and stainless steel rectangular thin plates. The boundary conditions of the test panels were a combination of the knife-edge support and free boundary conditions. The knife-edge support was employed to simulate the theoretically simple supported boundary condition. Schematic drawings of the specimens' dimensions and boundary conditions are shown in Figure 4.1. The boundary of specimen supported by the knife-edge constraint is designated as "S," while the free supported edge is represented by "F." The boundary conditions of the specimens used in this study were SSSS, SFSS, SFSF, and SSFF, as

shown in the figure. The first and second letters represent the boundary condition on the y = 0 and y = b edges, respectively. Similarly, the last two letters symbolize the boundary conditions on the other edges. The specimens were mounted in the test setup and equipped with an impact hammer and an accelerometer as shown in Figure 4.2. The knife-edge support replicating the simply supported boundary condition was enforced by two stainless steel bars coupled on the specimen. The steel bars were machined in an inclined direction to form a knife-edge. With this support, the specimens were intentionally allowed to freely rotate but any out-of-plane displacement was restrained. The knife-edge supports were fixed with steel boxes with a number of machine screws. Additional machine screws were also used to push the knife-edge supports against the specimen surface. The assembly of steel boxes and knife-edge supports was also tested for natural frequency to confirm that their natural frequencies were not in the range of those of the specimens.

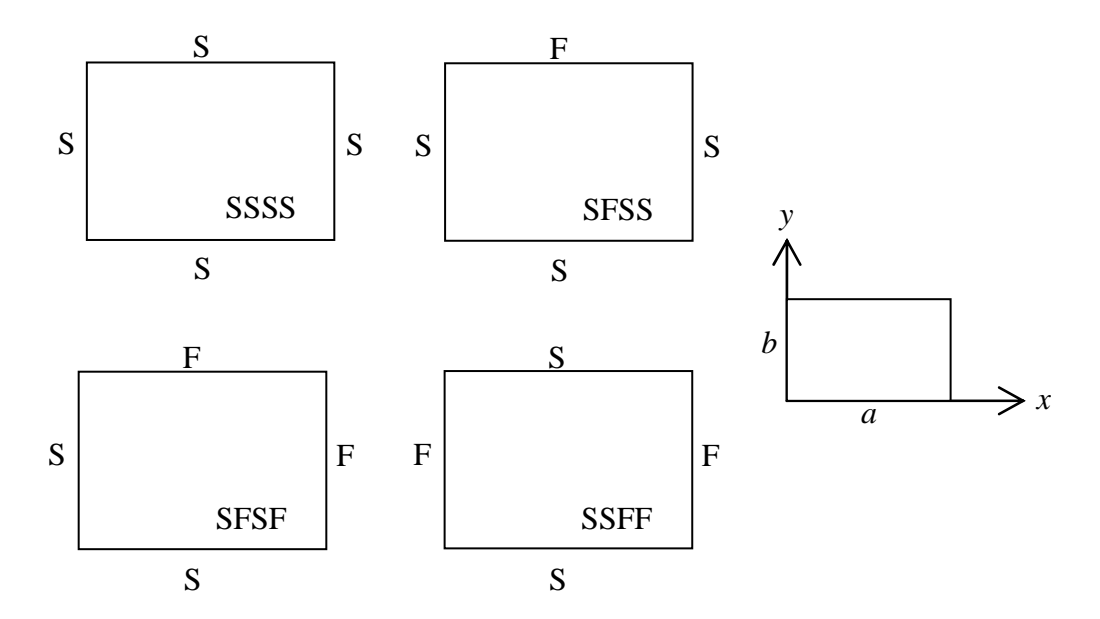


Figure 4.1 Schematic drawings of the rectangular test specimens

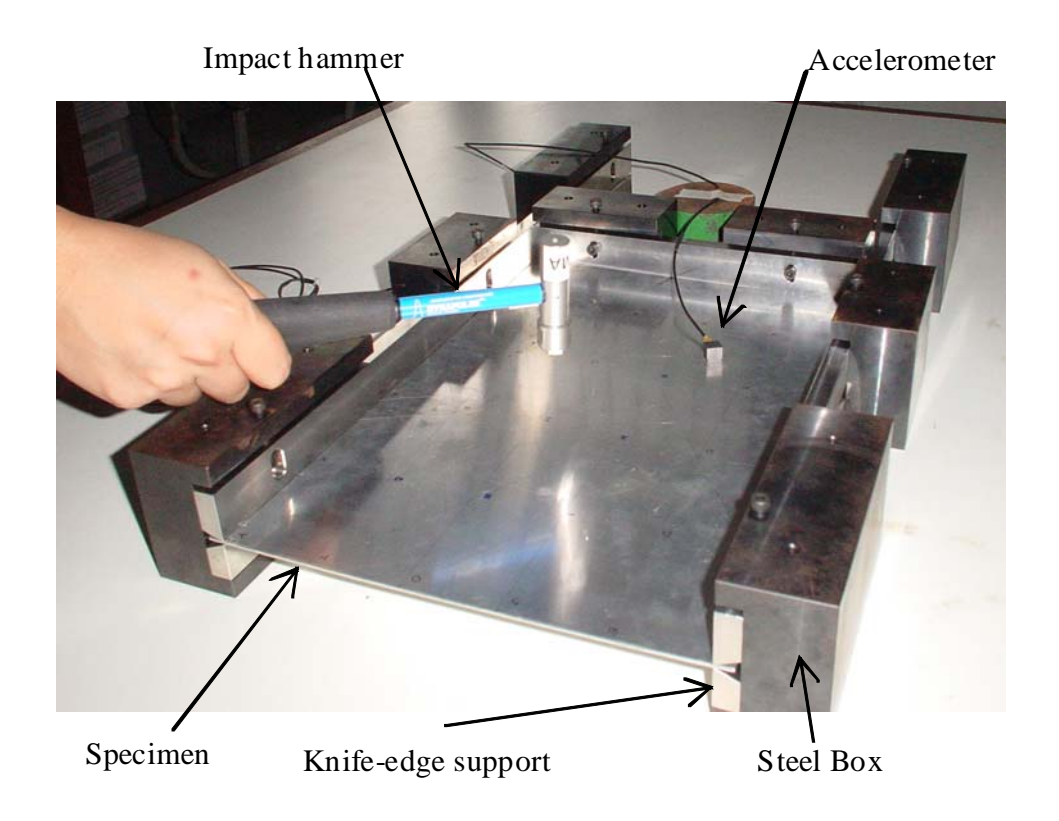


Figure 4.2 Experimental setup with accelerometer and impact hammer

The vibration test for natural frequency was performed using an impact test [29, 30]. Briefly, the specimens were excited by an impact hammer while the applied impulse was monitored by a dynamic signal analyzer. An accelerometer was placed on the specimen at a selected location to measure the plate response in terms of acceleration. It is recommended that the accelerometer should not be set on the node line of the vibration to avoid a low response signal. If the node line is unknown or uncertain, more than one measurement is recommended. In the present study, several pretests were conducted to determine a suitable location of the accelerometer. Besides the applied impulse from the impact hammer, the acceleration responses from the accelerometer were collected by a dynamic signal analyzer. The accelerations were recorded five times from five excitations of the impact hammer. These five sets of the acceleration data measured in the time domain were processed by a Fast Fourier Transform (FFT) algorithm using the dynamic

signal analyzer to obtain the response in the frequency domain. From the vibration response in the frequency domain, the natural frequencies of the specimen were identified from the peak of the response. Theoretically, there are infinite numbers of natural frequency; however, only the first three modes are of interest in this study. Figure 4.3 shows examples of the vibration response measured in the frequency domain obtained from the dynamic signal analyzer for a 300×300 mm² aluminum plate with various boundary conditions. The measured natural frequencies in Hz for the first three modes of the specimen with SSSS boundary conditions are 149.0, 293.5, and 322.5 Hz, respectively. A response similar to those of shown in Figure 3 can be obtained from experiments with excitation and accelerometer located at various positions. Ideally, the measured natural frequencies are independent of the location of either excitation or accelerometer. From the experiments, varying the position of excitation and the location of the response measurement has a minimal effect on the measured natural frequencies. In this study, a minimum of 5 experiments were performed for each specimen and the experimental natural frequency was determined from the average of each measurement.

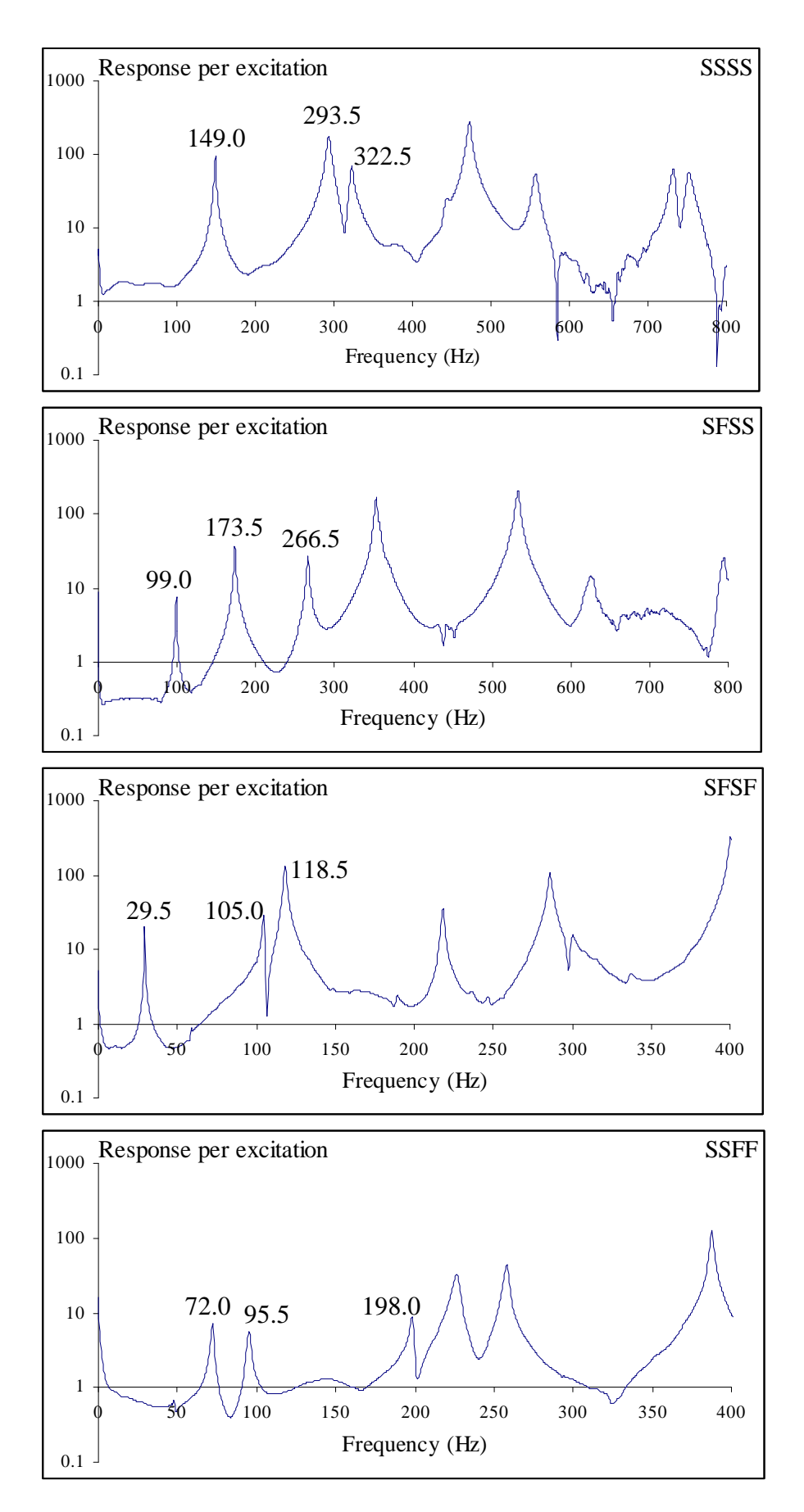


Figure 4.3 Vibration response in frequency domain of 300x300 mm² aluminum plate

4.3.2 Experimental results

A set of the experiments were conducted in this study. The test specimens were nine aluminum plates with aspect ratios (a/b) of 1, 1.5, and 2 and a specimen nominal width b of 200, 250, and 300 mm, respectively. The natural frequencies of all the specimens with four combinations of boundary conditions were experimentally determined and used to validate the accuracy of the measurement.

The measured natural frequencies for the SSSS aluminum plates with nine different dimensions are presented in Table 4.1. In the table, the test specimens are classified into three groups: rectangular plates with aspect ratios of 1, 1.5, and 2. The experimental data showed that the natural frequencies decreased with plate size. Similar experimental results were obtained for aluminum specimens with other boundary conditions but are not presented here. The specimens shown in Table 4.1 were assumed to be a model or a prototype and used to validate the scaling law, as shown in Table 4.2. From the three specimens with an aspect ratio of 1, three pairs of models and prototypes were assigned to the test specimens. As shown in column 2 and 3 of Table 4.2, a 200×200 mm² specimen was set as a model and used to model the 300×300 mm² prototype specimen. The other two model-prototype pairs were a 250×250 mm² model with 200×200 mm² prototype and a 300×300 mm² model with 250x250 mm² prototype. Specimens with aspect ratios of 1.5 and 2 were also assigned as models or prototypes in the same approach. In Table 4.2, column 5 and column 6 are the measured natural frequencies of the model and prototype, respectively. The next column labeled as " $\omega_{Scaling}$ " presents the scaling natural frequencies of the prototypes. These scaling natural frequencies were determined from the scaling law shown in Eq.(4.5) using the measured natural frequencies of the model in column 5. The experimental and scaling natural frequencies shown in column 6 and 7, respectively, were compared with each other. The percentage discrepancy of the scaling natural frequency shown in the last column was determined according to

% Dis =
$$\frac{\omega_{Scaling} - \omega_{Exp.}}{\omega_{Exp.}} \times 100\%$$
. (4.6)

Table 4.1 Measured natural frequencies of the SSSS aluminum specimens

Aspect	Specimen	Natural Frequency (Hz)							
Ratio	size, $a \times b$ (mm. ²)	1 st Mode	2 nd Mode	3 rd Mode					
	200x200	309.8	676.9	729.6					
1	250x250	196.7	409.0	444.6					
	300x300	148.8	293.2	321.8					
	300x200	221.2	376.3	580.7					
1.5	375x250	150.5	255.4	376.6					
	450x300	99.6	171.4	257.4					
	400x200	199.6	256.2	425.2					
2	500x250	132.4	173.6	275.5					
	600x300	90.1	117.8	193.4					

Most of the comparisons show a good agreement between the scaling and measured natural frequency. The average of the absolute values of percentage discrepancy for experiment on all 27 model-prototype pairs is 3.30% with a standard deviation of 4.05%. The minimum and maximum percentage discrepancies are -7.47% and +8.93%, respectively, while more than half of the comparisons have a percentage discrepancy within $\pm 3\%$. There was no significant difference in percentage discrepancy for each vibration mode or plate aspect ratio. The causes of discrepancy between the scaling and measured natural frequencies are probably related to the imperfections of the

boundary conditions and specimens. As described in the previous section, knife-edge supports of the test setup were controlled by several machine screws. In the experiments, the machine screws were tightened until the gaps between the specimen and support were invisible. Although it was desired to obtain identical boundary conditions for the model and its prototype, it was expected that the boundary conditions for each experiment would not be perfectly identical. Besides the imperfect boundary conditions, imperfections of specimens such as nonuniform thickness and the existence of plate curvature might be the cause of discrepancy between the scaling and measured behaviors. These two causes of error are classified as an experimental uncertainty which is typical in experimental study and is very difficult to completely eliminate.

Table 4.2 Measured and scaling natural frequencies for the SSSS aluminum specimens

Aspect	Model	Prototype	Mode	Model 309.8 676.9 729.6 196.7 409.0 444.6 148.8 293.2 321.8 221.2 376.3 580.7 150.5 255.4 376.6 99.6 171.4 257.4 199.6 256.2 425.2 132.4 173.6 275.5 90.1 117.8		Prototype	
Ratio	Model	Frototype	Mode	Model	ω_{Exp} $\omega_{Scaling}$ 8 148.8 137.7 9 293.2 300.8 6 321.8 324.3 7 309.8 307.3 0 676.9 639.1 6 729.6 694.7 8 196.7 214.3 2 409.0 422.2 8 444.6 463.4 2 99.6 98.3 3 171.4 167.2 7 257.4 258.1 5 221.2 235.2 4 376.3 399.1 6 580.7 588.4 6 150.5 143.4 4 255.4 246.8 4 376.6 370.7 6 90.1 88.7 2 117.8 113.9 2 193.4 189.0 4 199.6 206.9 6 256.2 271.3 5 425.2 430.5 1 132.4 129.7	%Dis	
			1	309.8	148.8	137.7	-7.47
	200×200	300×300	2	676.9	293.2	300.8	2.61
			3	729.6	321.8	324.3	0.77
			1	196.7	309.8	307.3	-0.79
1	250×250	200×200	2	409.0	676.9	639.1	-5.59
			3	444.6	729.6	694.7	-4.79
			1	148.8	196.7	214.3	8.93
	300×300	250×250	2	293.2	409.0	422.2	3.23
			3	321.8	444.6	463.4	4.23
	300×200	450×300	1	221.2	99.6	98.3	-1.29
			2	376.3	171.4	167.2	-2.42
			3	580.7	257.4	258.1	0.27
			1	150.5	221.2	235.2	6.31
1.5	375×250	300×200	2	255.4	376.3	399.1	6.05
			3	376.6	580.7	588.4	1.33
			1	99.6	150.5	143.4	-4.70
	450×300	375×250	2	171.4	255.4	246.8	-3.36
			3	257.4	376.6	370.7	-1.58
			1	199.6	90.1	88.7	-1.54
	400×200	600×300	2	256.2	117.8	113.9	-3.34
			3	425.2	193.4	189.0	-2.29
			1	132.4	199.6	206.9	3.64
2	500×250	400×200	2	173.6	256.2	271.3	5.87
			3	275.5	425.2	430.5	1.24
			1	90.1	132.4	129.7	-2.01
	600×300	500×250	2	117.8	173.6	169.6	-2.29
			3	193.4	275.5	278.5	1.09

Another three comparable studies were performed on the same test specimens with boundary conditions of SFSS, SFSF, and SSFF. An inconsistency between the

scaling and measured natural frequencies of all comparisons in terms of percentage discrepancy is shown in Table 4.3. The last two rows of the table show the average of absolute values of percentage discrepancy and the standard deviation of the percentage discrepancy, respectively. The overall average and standard deviations of the percentage discrepancy were 4.90% and 6.46%, respectively. The histogram in Figure 4.4 represents the frequency distribution of the percentage discrepancy which revealed that the distribution of the percentage discrepancy closely resembles a normal distribution and the percentage discrepancies of 95 from 108 comparisons were in the range of \pm 10 %. However, percentage errors for some pairs of model and prototype were slightly higher, especially for the experiments on the SFSF specimens. Eight values of percentage discrepancy from the experiments on this boundary condition resulted in a percentage discrepancy higher than ±10%, compared with only four values and one value for SSFF and SFSS cases, respectively. The average of the absolute percentage discrepancy for SFSF specimens was 7.47% which is higher than those of other boundary conditions. The higher percentage discrepancy of the scaling law observed in specimens with SFSF boundary conditions was probably caused by the particular characteristics of these boundary conditions. For SFSF specimens, the free boundary condition was imposed on two adjacent edges of the plate, i.e. two adjacent edges were free to move, as shown in Figure 4.1. As a result, the specimen with this combination of boundary conditions tended to be slightly curved at the free corner because of its own weight. The degree of nonflatness of the test specimens was probably different for specimens with different dimensions, that is, the size effect had an influence on the accuracy of the scaling law in this case. So, the model and prototype with these boundary conditions did not have a complete similarity, resulting in a slightly higher percentage discrepancy for these specific boundary conditions.

Table 4.3 Percentage discrepancy between scaling and measured natural frequencies

Aspect	Model	Prototype		SSSS			SFSS			
Ratio			Mode1	Mode2	Mode3	Mode1	Mode2	Mode3		
	200×200	300×300	-7.47	2.61	0.77	-0.86	3.75	0.06		
1	250×250	200×200	-0.79	-5.59	-4.79	2.91	-2.62	2.19		
	300×300	250×250	8.93	3.23	4.23	-1.98	-1.03	-2.20		
	300×200	450×300	-1.29	-2.42	0.27	7.26	2.83	6.84		
1.5	375×250	300×200	6.31	6.05	1.33	-11.91	-8.50	-5.50		
	450×300	375×250	-4.70	-3.36	-1.58	5.84	6.28	-0.95		
	400×200	600×300	-1.54	-3.34	-2.29	3.94	2.75	2.57		
2	500×250	400x200	3.64	5.87	1.24	2.06	1.00	-0.46		
	600×300	500x250	-2.01	-2.29	1.09	-5.73	-3.64	-2.06		
	Average			3.30		3.62				
	Standar	d deviation		4.05			4.63			

Table 4.3 Percentage discrepancy between scaling and measured natural frequencies (Continued)

Aspect	Model	Prototype	Mode1 Mode2 Mode3 Mode1 Mode2 Mode2 0 -5.56 -2.12 -4.52 3.55 2.80 2.30 0 1.37 0.45 -0.58 0.89 -4.90 -0 0 4.46 1.72 5.35 -4.28 2.30 -1 0 -17.74 -10.07 -10.96 -9.00 -15.54 -0 0 13.41 6.00 5.41 7.06 5.42 3. 0 7.19 4.90 6.54 2.64 12.31 -2 0 -11.22 -14.29 -9.69 -6.24 -12.66 -6 0 -6.78 -1.55 2.48 -3.51 8.36 5. 0 20.84 18.51 8.06 10.54 5.67 0.						
Ratio			Mode1	Mode2	Mode3	Mode1	Mode2	Mode3	
	200×200	300×300	-5.56	-2.12	-4.52	3.55	2.80	2.05	
1	250×250	200×200	1.37	0.45	-0.58	0.89	-4.90	-0.19	
	300×300	250×250	4.46	1.72	5.35	-4.28	2.30	-1.83	
	300×200	450×300	-17.74	-10.07	-10.96	-9.00	-15.54	-0.86	
1.5	375×250	300×200	13.41	6.00	5.41	7.06	5.42	3.15	
	450×300	375×250	7.19	4.90	6.54	2.64	12.31	-2.21	
	400×200	600×300	-11.22	-14.29	-9.69	-6.24	-12.66	-6.07	
2	500×250	400x200	-6.78	-1.55	2.48	-3.51	8.36	5.92	
	600×300	500x250	20.84	18.51	8.06	10.54	5.67	0.52	
	Average			7.47	1	5.20			
	Standar	d deviation		9.46			6.64		

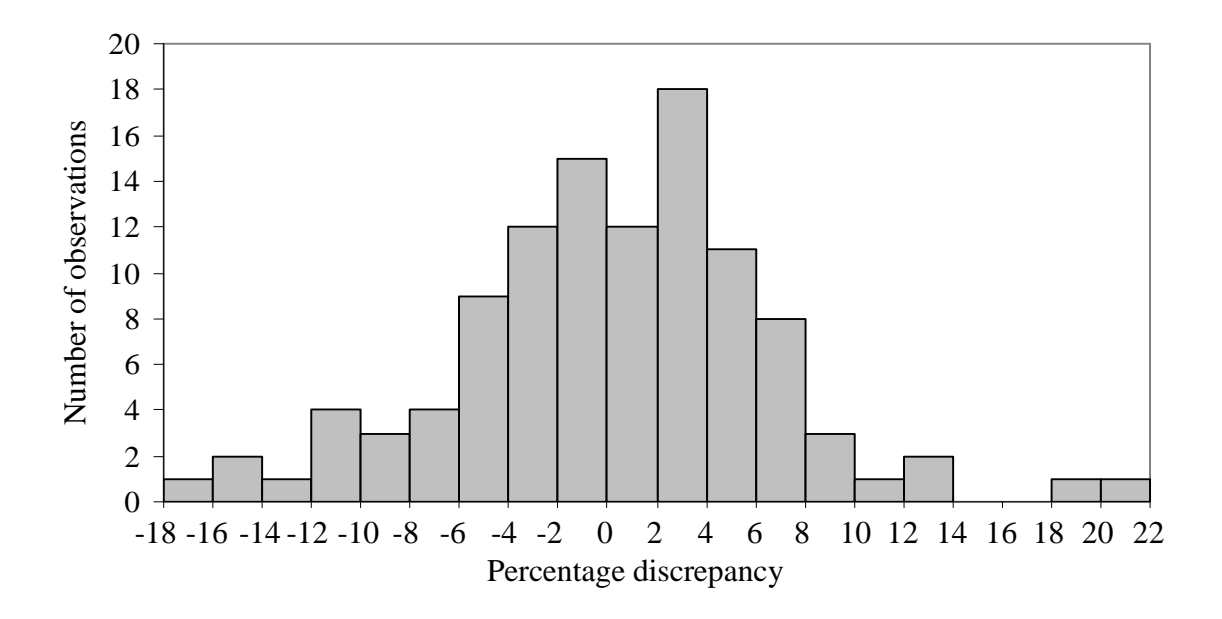


Figure 4.4 Histogram of the percentage discrepancy between scaling and measured natural frequencies.

4.4 Conclusions

From the experimental study, the scaling law provided reasonable accuracy for modeling a prototype using a model with different dimensions. Uncertainties of the experiments in boundary condition and thickness are believed to be the sources of the discrepancy. To obtain a decent prediction from the scaling law, the experiment on the model specimen should be carefully performed to assure near-complete, if not perfectly complete, similarity with the prototype. Therefore, with a careful experimental setup, the measured natural frequency is efficiently accurate and reliable to use as a data for buckling load identification.

Chapter 5. Vibration correlation technique

In this chapter, the derived scaling law for buckling of rectangular composite plates is verified with the experiment results. A compressive test frame was designed and built to conduct a buckling test. The specimens which are classified as models and prototypes were tested for buckling load using a plot of applied load vs. out-of-plane displacement. The experimental buckling load of the model was substituted into the scaling law to predict the similitude buckling load of the prototype which was then compared to the experimental one. Ideally, the similitude and experimental buckling loads are identical if all of the similarity requirements are satisfied.

5.1 Relationship between natural frequency and buckling load

In this part, the relationship between buckling and vibration behavior of thin plate is investigated. The relationship between applied in-plane load and the natural frequency of plates are derived from the differential governing equations of both problems. The derived relationship is verified using a numerical method. This relationship also implies that buckling load of plate can be obtained from the vibration data of the loaded plates. So, an alternative method for buckling load identification using dynamic approach is proposed.

In this study, the vibration and buckling behaviors of a rectangular composite plate as shown in Fig. 5.1 are investigated. The buckling load of plate represented by \bar{N}_x is the in-plane load N_x at which buckling occurs. For vibration behavior, the natural frequencies of plate can be determined for a specimen with a given tensile or compressive load N_x .

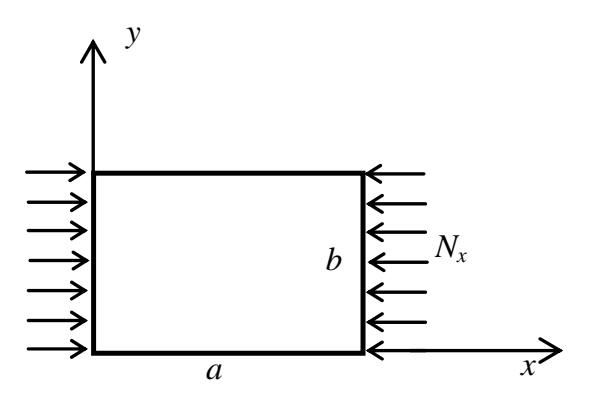


Figure 5.1 A rectangular plate subjected to a uniaxial in-plane load

The governing equation for buckling and vibration of thin isotropic plate can be written as;

$$D_{11} \frac{\partial^4 w}{\partial x^4} + 4D_{16} \frac{\partial^4 w}{\partial x^3 \partial y} + 2(D_{12} + 2D_{66}) \frac{\partial^4 w}{\partial x^2 \partial y^2} + 4D_{26} \frac{\partial^2 w}{\partial x \partial y^3} + D_{22} \frac{\partial^4 w}{\partial y^4} - \overline{N}_x \frac{\partial^2 w}{\partial x^2} = 0$$
 (5.1)

and

$$D_{11} \frac{\partial^4 w}{\partial x^4} + 4D_{16} \frac{\partial^4 w}{\partial x^3 \partial y} + 2(D_{12} + 2D_{66}) \frac{\partial^4 w}{\partial x^2 \partial y^2} + 4D_{26} \frac{\partial^2 w}{\partial x \partial y^3} + D_{22} \frac{\partial^4 w}{\partial y^4} - N_x \frac{\partial^2 w}{\partial x^2} - \rho \omega^{*2} w = 0$$
 (5.2)

respectively.

where w = Out-of-plane displacement

 ρ = Mass of plate per unit area

D = Plate flexural rigidity)

 $\overline{N}_x =$ Buckling load

 N_x = Applied in-plane load

 ω^* = natural frequency of the plate with applied in-plane load N_x

It should be noted that \overline{N}_x and N_x refer to the same in-plane load, however, \overline{N}_x is the buckling load which must be a compressive load (negative value), while N_x is the applied in-plane load which can be either tension or compression.

For a given rectangular plate, the relationship between the natural frequency and an applied in-plane load N_x can be determined by considering the governing equations, Eq.(5.1 and 5.2). For a specimen with a given boundary conditions, it is widely known that buckling mode and vibration mode of the plates are identical. Specifically, the out-of-plane displacement of the buckled plate is identical to the out-of-plane displacement of one of the vibration mode. So, for a given specimen, the governing of the buckling problem can be rewritten as.

$$L_{1}(w) - \overline{N}_{x}L_{2}(w) = 0 \tag{5.3}$$

where
$$L_1(w) = D_{11} \frac{\partial^4 w}{\partial x^4} + 4D_{16} \frac{\partial^4 w}{\partial x^3 \partial y} + 2(D_{12} + 2D_{66}) \frac{\partial^4 w}{\partial x^2 \partial y^2} + 4D_{26} \frac{\partial^2 w}{\partial x \partial y^3} + D_{22} \frac{\partial^4 w}{\partial y^4}$$

$$L_2(w) = \frac{\partial^2 w}{\partial x^2}$$

Similarly, the governing of the vibration of loaded plates is written as;

$$L_{1}(w) - N_{x}L_{2}(w) - \omega^{*2}L_{3}(w) = 0$$
(5.4)

where $L_3(w) = \rho w$

It should be noted that the terms contained derivatives of w for both problems are the same because the buckling mode and vibration mode are identical. From Eq.(5.3), the buckling load of plate can be written as;

$$\bar{N}_{x} = \frac{L_{1}(w)}{L_{2}(w)} \tag{5.5}$$

Similarly, the natural frequency of plate with and without the applied in-plane load can be written as;

$$\omega^{*2} = \frac{L_1(w) - N_x L_2(w)}{L_3(w)}$$
(5.6)

and
$$\omega^2 = \frac{L_1(w)}{L_3(w)}$$
 (5.7)

where ω^* is natural frequency of a plate with applied load N_x , and ω is natural frequency of a plate without applied load. From Eq.(5.7), ratio of the square of natural frequency of the loaded plate to that of the unloaded plate is written as;

$$\left(\frac{\omega^*}{\omega}\right)^2 = 1 - \frac{N_x}{\overline{N}_x} \tag{5.8}$$

Since buckling load \bar{N}_x and natural frequency of the unloaded plate ω is constant for a given specimen, it is concluded that square of the natural frequency of the loaded plate ω^{*2} is linearly varied with the applied load N_x . Since this relationship is derived from the governing, it is independent of boundary conditions.

From the linear relationship between ω^{*2} and N_x shown in Eq.(5.8), with the buckling load being a negative value, it is notice that the natural frequency of the plate increases with the applied tensile load. On the other hand, it is decreased with the applied compression. Moreover, if the applied load N_x equals the buckling load of the plate, the natural frequency ω^* theoretically equals zero. With this observation, ones can utilize the natural frequencies of the loaded plate to predict the buckling load of plate by plotting ω^{*2} versus the in-plane load N_x . The buckling load could be determined from the applied load N_x at which the natural frequency approaches zero.

5.2 Numerical validation

To numerically verify the VCT and the derived relationship shown in Eq. (5.8), a numerical simulation of the vibration and buckling of a plate was performed. The Ritz method with characteristic beam functions was used to solve the buckling and vibration problems. Detail information about the Ritz method which is beyond the scope of this

paper can be found in Ref.[31-36]. A 2-mm-thick aluminum plate with a dimension $a \times b$ of 400x200 mm² was chosen as a specimen. The plate was assumed to be simply supported on the loading edges and clamped supported on the other two edges. The buckling load of this specimen was numerically determined, and found to be 88.216 kN/m with buckling mode (3, 1). The buckling mode of this specimen is graphically shown in Fig.5.2. This numerical solution serves as the theoretical solution for this simulation, and is used to validate the buckling load from VCT. Buckling load and mode determined from VCT requires the vibration data, i.e. natural frequencies and vibration mode shapes, of the plate subjected to in-plane loading. These vibration parameters of the loaded plated were also simulated from the Ritz method. The applied in-plane load was increased step by step in both tensile and compressive loading range. The square of the natural frequencies for the first six modes was plotted versus applied load, as shown in Fig. 5.3. The mode shape of each vibration mode is shown in Fig. 5.4. The relationship between ω^{*2} and N_x of a particular vibration mode is linear, as expected according to the derived relationship. The predicted buckling load can be determined by extrapolating the vibration data to the in-plane load at which the square of the natural frequency approaches zero. Trend lines of each vibration mode intercept the N_x axis at a different load level. The lowest compressive load is the buckling load, and its corresponding vibration mode shape is the predicted buckling mode. In this simulation, the predicted buckling is 88.216 kN/m and the buckling mode is mode (3, 1). VCT predicted buckling mode as mode (3, 1) because the trend line of this vibration mode intersects N_x axis at the lowest load compared to those of other vibration modes. The buckling load determined from the vibration data compares perfectly with the numerical solution. Similarly, the buckling mode determined from VCT is also identical to the buckling mode of the numerical solution. In conclusion, the squares of natural frequencies are linearly varied with the applied in-plane load as expected from the relationship shown in Eq.(5.8). The natural frequency approaches zero as the in-plane compressive load approaches the buckling load of plate. The numerical simulation showed that buckling behaviors of a thin plate are very well predicted using VCT. The concept of using vibration parameters to identify buckling load and mode is theoretically verified. However, experimental study is required to determine the accuracy and reliability of the technique.

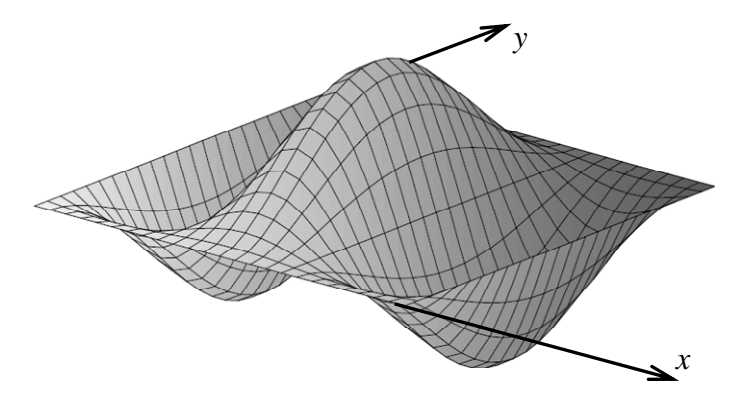


Figure 5.2 Buckling mode determined from the buckling problem

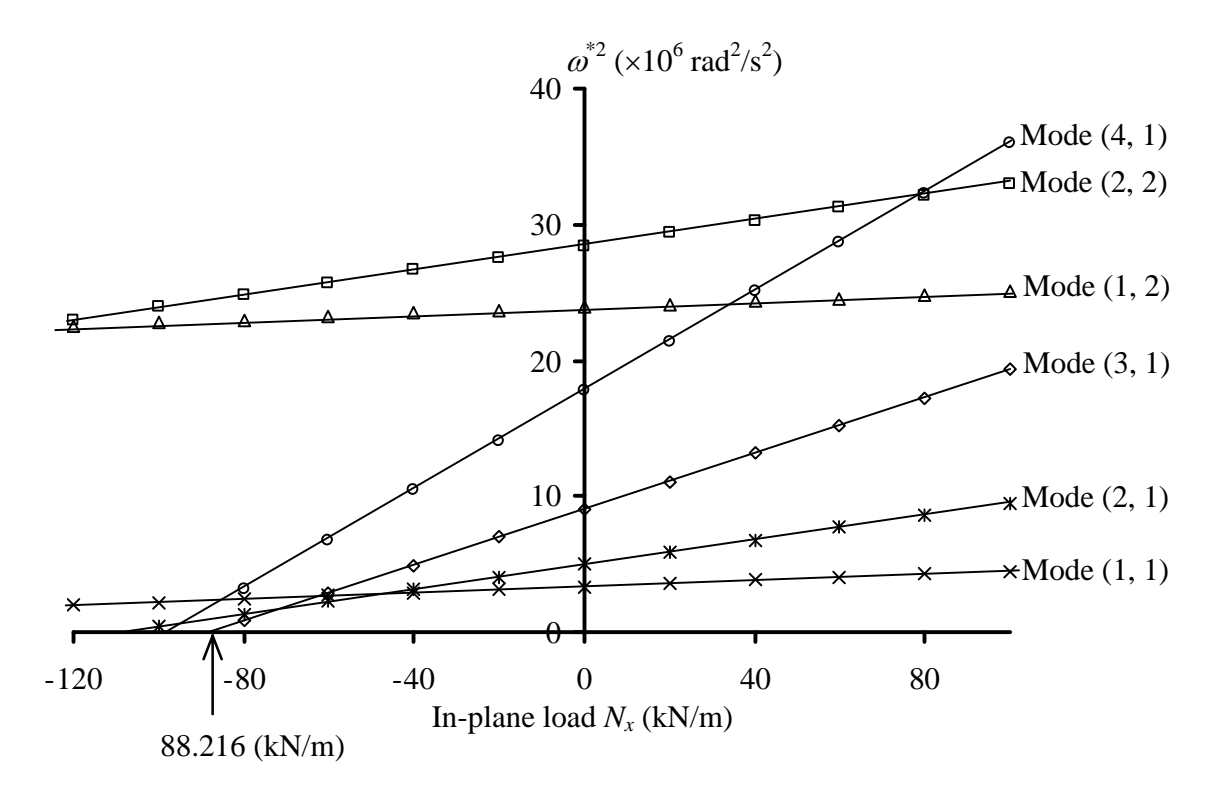


Figure 5.3 Square of the natural frequencies of an aluminum plate vs. applied loading.

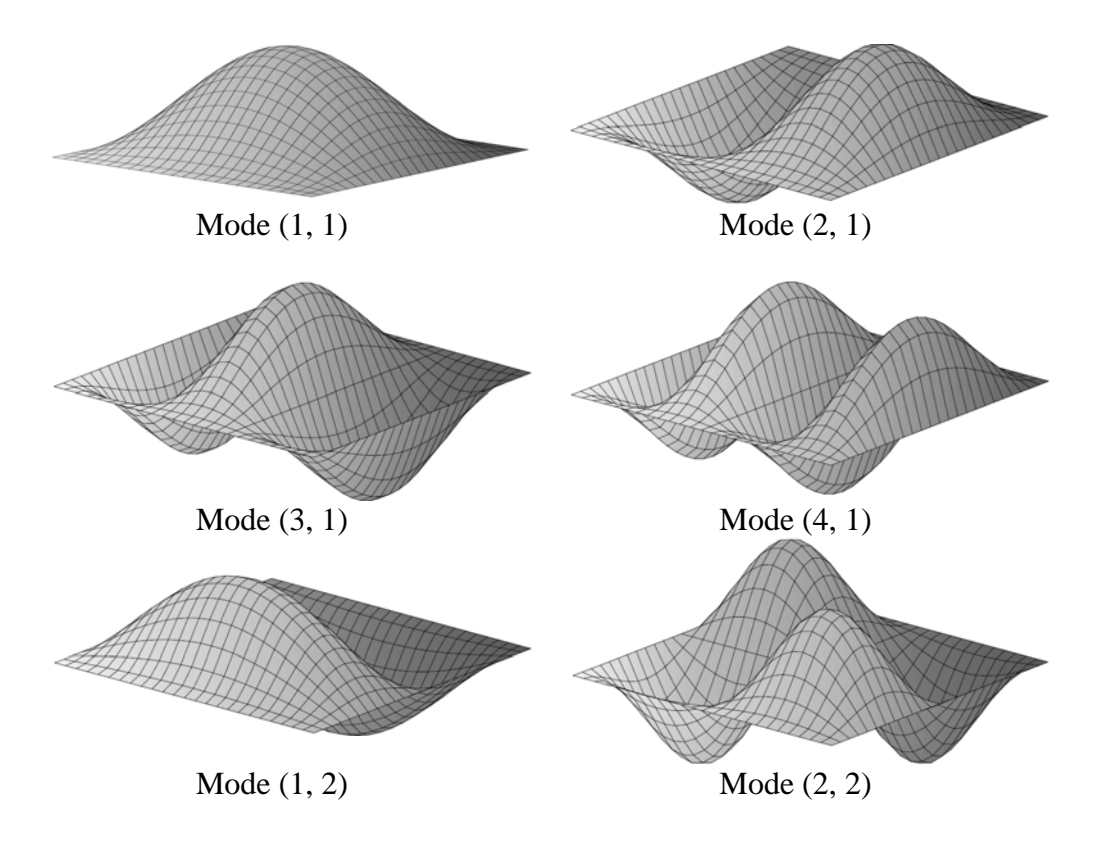


Figure 5.4 Vibration mode shapes of the first six vibration mode.

Chapter 6. Experimental study

Although the relationship between vibration and buckling behaviors of a thin plate is theoretically confirmed, the applicability of VCT as an experimental technique used to identify buckling load is needed to be investigated. A series of experiments was performed to determine the accuracy and reliability of the proposed technique. A set of aluminum and stainless steel plates was used; each plate was uniaxially loaded on a custom-made test frame. The experiment was then performed on the loaded specimens to determine natural frequencies and vibration mode shape. The vibration data was obtained for the specimens subjected to both tensile and compressive loading. The measured natural frequencies and applied loading were then plotted, with results similar to those shown in Fig. 3. The predicted buckling load was identified using the VCT, i.e. the relationship derived previously.

6.1 Experiment arrangement

The test setup, shown in Fig. 6.1, was specifically designed to accommodate the loading configurations and vibration testing. The test frame is capable of applying both clamped and free boundary conditions to the specimens. The simple supported boundary condition is not included in the experiment because it is difficult to obtain a perfect simple support comparing with other two conventional boundary conditions. Both tensile and compressive loads can be applied on the specimens. In-plane loads are applied horizontally using a hydraulic cylinder pressurized with a hand pump. The hydraulic cylinder is mounted on the right end frame, which is fixed to the left end frame using two guided columns. A rectangular thin plate is mounted on the loading edges with clamped support between crosshead #2 and crosshead #3. For a tensile testing configuration as shown in Fig. 6.1, the hydraulic ram applies a compressive force against crosshead #1. Loads are monitored using a load cell mounted between crosshead #1 and the hydraulic

cylinder. Two linear bearings are embedded within the crossheads such that they can move linearly along two guided columns. The applied loading on crosshead #1 is transferred through two tension rods to crosshead #2. So, crosshead #2 is pushed and trend to move to the left hand side. On the contrary, crosshead #3 is blocked by two stoppers mounted on the guided columns, as shown in figure. With this loading configuration, a specimen which is clamped between crosshead #2 and crosshead #3 is stretched when the compressive load is applied by the hydraulic ram. In the case of a compressive testing, the test frame shown in Fig. 6.1 has to be modified as the following. Crosshead #1 and the tension rods are removed in the compressive testing configuration. Two stoppers which are used to block crosshead #3 in the tensile testing configuration are moved to the left-hand side of crosshead #2 to prevent the horizontal motion of the crosshead. A compressive load from the hydraulic ram is applied directly on crosshead #3, in this loading configuration. With this setup, the specimen is uniformly compressed between crosshead #2 and crosshead #3. So, the designed test frame is capable of applying both tensile and compressive loads to a thin plate with changeable loading configurations.

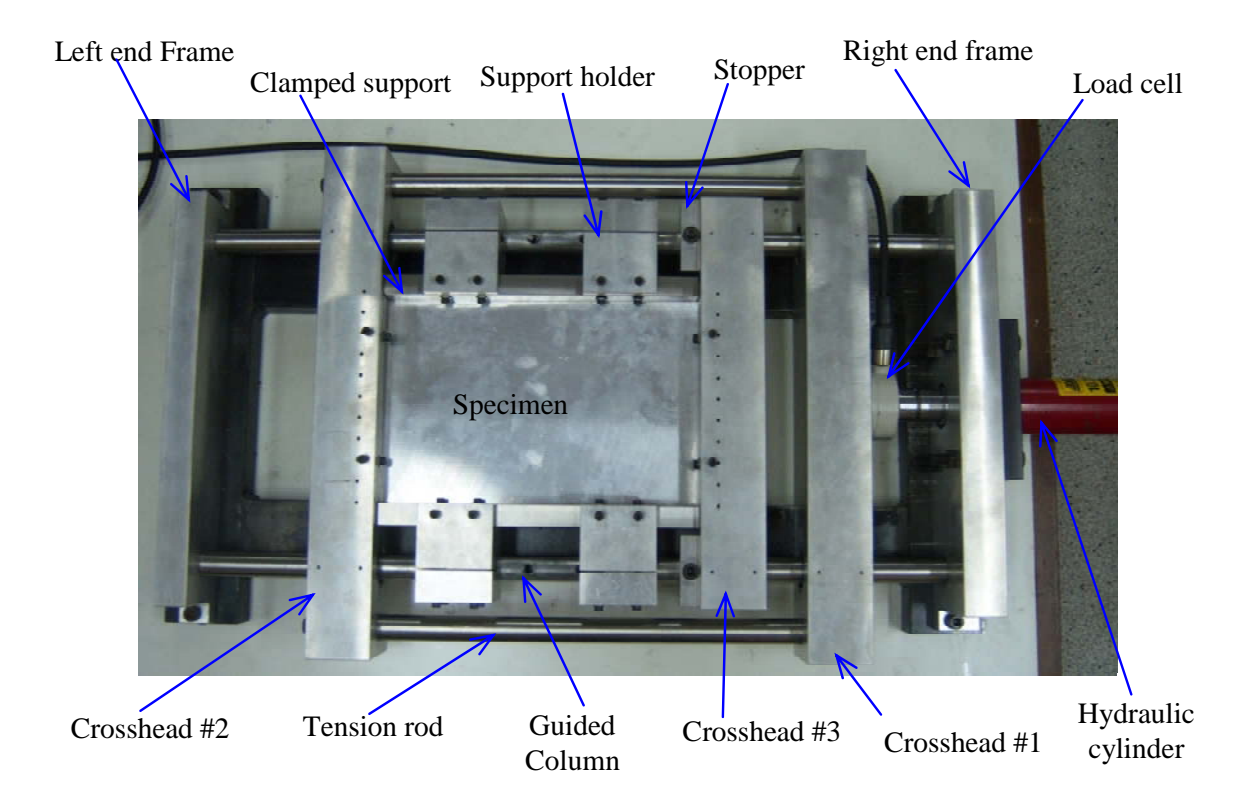


Figure 6.1 Experimental setup of a specimen with CCCC boundary condition

Besides the loading mechanism, the test frame is also equipped with restrained devices to apply desired boundary conditions to the test samples. In Fig. 6.1, the clamped boundary conditions of the specimen are enforced by 20-mm.-thick rigid stainless steel bars, denoted as "clamped support." For the unloaded edges, the clamped supports are mounted on the support holders, which are tightly clamped to the guided columns. Similarly, the rigid stainless steel bars are placed in the slot of the crossheads to assemble a clamped support on the loaded edges. On both loaded and unloaded edges, machine screws are used to push the steel supports against the specimen surface. To obtain a clamped support, machine screws are finger-tightened until the gap between the specimen and support is invisible. A clamped support on the unloaded edges of the specimen can be removed such that a free edge is formed on those boundaries. With the described constraint mechanism, the boundary conditions of a specimen are clamped support on the

loaded edges (on x = 0 and x = a), and either clamped or free edges on the unloaded edges (on y = 0 and y = b)

6.2 Specimens and boundary conditions

A series of experiment was performed on twelve thin isotropic plates with CCCC, CCCF and CFCF boundary conditions. The symbol "C" represents a clamped boundary condition, while "F" stands for a free boundary condition. The first and third letters symbolize the boundary condition on x = 0 and x = a, respectively. Similarly, the boundary conditions on y = 0 and y = b are represented by the second and forth letters, respectively. The specimens were prepared from 6061-T6 aluminum alloy and stainless steel AISI 304. The physical and mechanical properties of both materials are presented in Table 6.1. Nominal dimensions $a \times b$ of the specimen are 300x200, 200x200, and 150x200 mm². For each plate size, there were two specimens with different thicknesses. So, there were a total of six aluminum specimens and six stainless steel specimens. The aluminum and stainless steel specimens' dimensions are summarized in the first three columns of Table 6.2 and Table 6.3, respectively. It should be noted that the actual size of a specimen is slightly larger than the nominal size because a small portion on the boundary of the specimen is clamped by the rigid stainless steel bar, and is not regarded as an effective area. The schematic dimensions of the specimens are presented in Fig. 6.2. A specimen was originally prepared to be a CCCC specimen. The width and height of the specimen are 40 mm larger than those of the nominal dimensions. A 20-mm-width area on all four edges is an area to be clamped by the support. In the schematic of a CCCC specimen shown in Fig. 6.2, the effective area or nominal area of the specimen is represented by a clear area of $a \times b$, whereas the dashed area is an area to be clamped by the support. After an experiment on a CCCC specimen is concluded, a clamped area on one of the unloaded

edges is cut off to form a CCCF specimen. So, the actual size of a CCCF specimen is slightly smaller than a CCCC specimen with the same nominal size. Finally, the other clamped area on the unloaded edges is removed to obtain a CFCF specimen. Thus, specimens with an equal nominal size but different boundary conditions are actually the same specimen.

Material	Modulus of Elasticity, E (GPa)	Poisson ratio, <i>v</i>	Density, ρ (kg/m ³)
Aluminum 6061-T6	70	0.33	2700
Stainless steel AISI 304	193	0.30	8000

Table 6.1 Properties of materials used in the experiments.

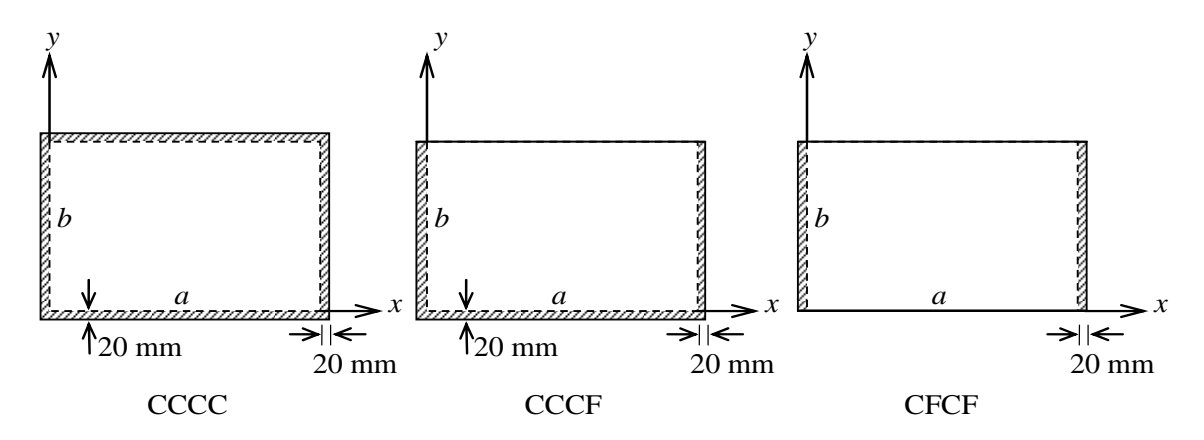


Figure 6.2 Nominal and actual dimensions of the specimens.

6.3 Experiment procedures and data reduction

In this study, the natural frequencies of a loaded plate are required data in order to predict the buckling behavior of the plate. Vibration testing was performed using an impact test, in which the specimen was excited by an impact hammer while the applied impulse was monitored by a dynamic signal analyzer. Acceleration response of the specimen was measured by an accelerometer placed on the specimen at a selected location. Acceleration data measured in the time domain were processed by a Fast Fourier

Transform algorithm using the dynamic signal analyzer to obtain the frequency response function (FRF). From the vibration response in the frequency domain, the natural frequencies of the specimen were identified from the peak of the response. Vibration mode shape was also obtained from an imaginary part of the response function. An overview of the vibration testing and modal analysis is beyond the scope of this paper; and the interested reader is referred to the articles by Avitabile [37]. Typical magnitude and imaginary part of the frequency response function are shown in Fig. 6.3.

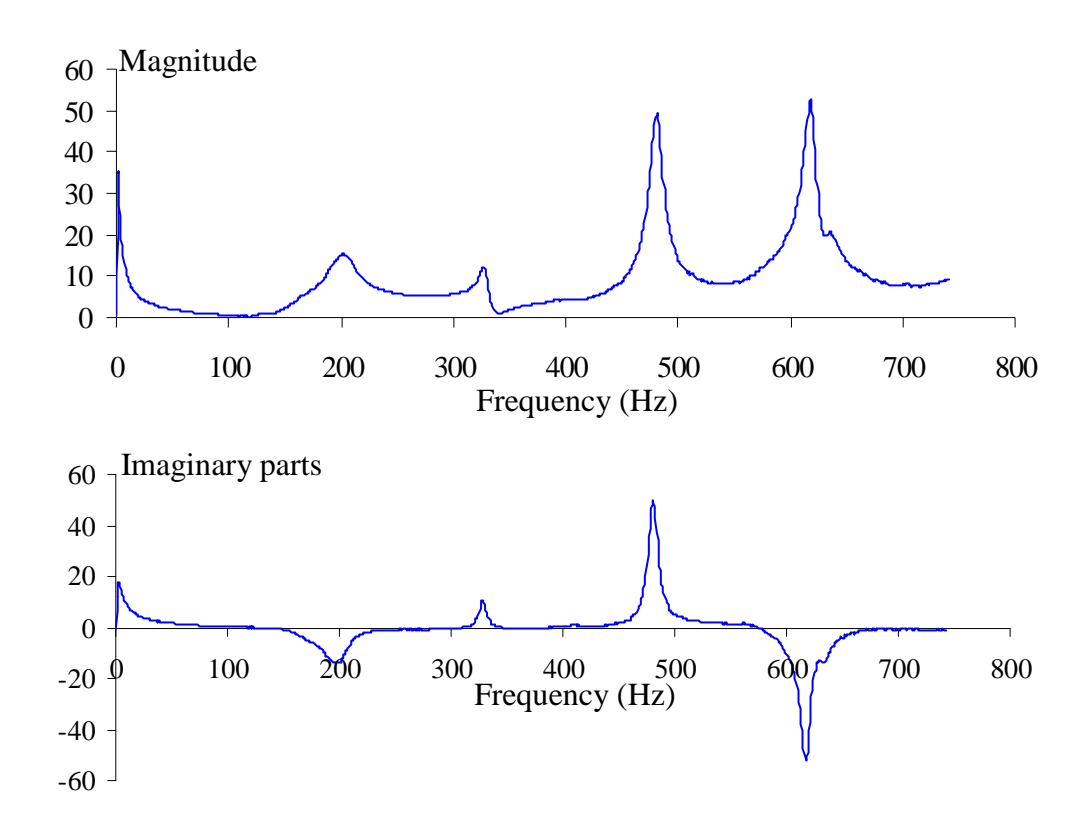


Figure 6.3. Magnitude and imaginary parts of the frequency response of the CCCC stainless specimen No. 2 without an in-plane load.

The experiment on a specimen was composed of two parts. The first part of the experiment was performed to verify the relationship shown in Eq.(5.8) and to determine the buckling mode of the plate. The specimen in this part of the experiment was loaded in

both tensile and compressive loading range. Natural frequencies of the specimen under unloaded, tensile-loaded and compressive-loaded conditions were determined, respectively. The square of the natural frequency was plotted against applied in-plane load. A typical relationship between ω^{*2} and N_x is presented in Fig. 6.4 which is the vibration behavior an aluminum specimen No.3 with CCCF boundary condition. Natural frequencies of vibration modes (1, 1), (1, 2) and (2, 1) are included in the plot. Numbers representing a vibration mode stand for a number of curves of an out-of-plane displacement in the x and y directions, respectively. Vibration mode shape is determined from the imaginary parts of the frequency response from several experiments. A plot of each mode shape is presented in Fig. 6.5. A symbol "-" and "+" represent the out-of-plane displacement in the different direction, and "0" indicate a zero displacement or a node line on the specimens. From Fig. 6.4, the buckling mode of the specimen was determined to be mode (1, 1), since the trend line of this mode intersects the N_x axis at the lowest value. It is observed that ω^{*2} varies linearly with the applied load in the tensile-loading range, as expected. The relationship between both parameters in the compressive-loading range is not as linear as the relationship in the tensile-loading range. This nonlinear relationship in the compressive-loading range was also observed in other specimens, and was also reported by Lurie and Monica [21]. This behavior is contradicted by the result from the numerical simulation shown in Fig. 5.3. It is speculated that the nonlinear behavior is a result of a premature curvature which develops before buckling of the specimen. For this reason, the buckling load was determined using only vibration data of the specimen subjected to tensile loading. So, the second part of the experiment emphasizes on determination of the buckling load. After plotting the relationship of ω^{*2} vs. N_x similar to Fig. 6.4 and determining the buckling mode, the specimen was reloaded under increased levels of tensile loading. At each load level, a vibration test was

performed to determine the natural frequency of the loaded plate. Only the natural frequencies of the relevant mode shape, i.e. the buckling mode, were collected. A plot of ω^{*2} versus N_x in the tensile-loading range was generated and extrapolated to determine the measured buckling load. Because the measurement of natural frequency is very sensitive to boundary conditions, the experiment was repeated 20 times by loosening and re-tightening the machine screws on the clamped supports. An average of the measured buckling load is reported as the buckling load obtained from VCT.

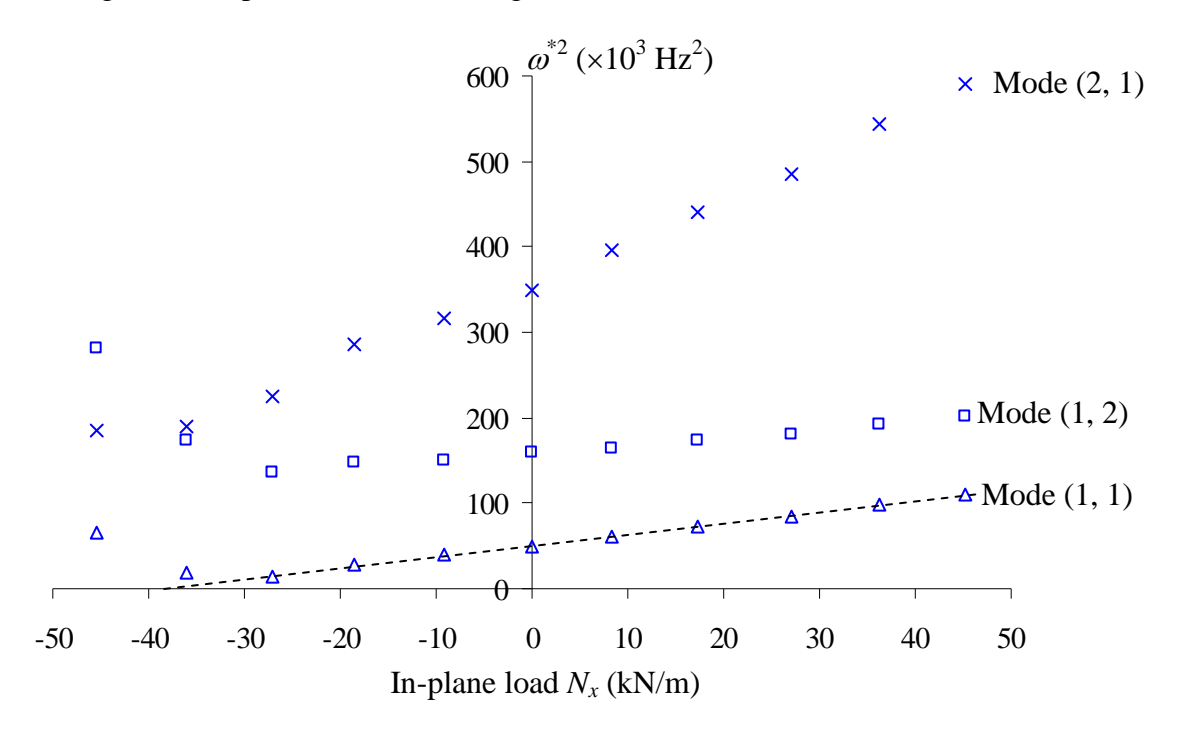


Figure 6.4 Plot of ω^{*2} vs. N_x of the aluminum specimen No.3 with CCCF boundary condition.

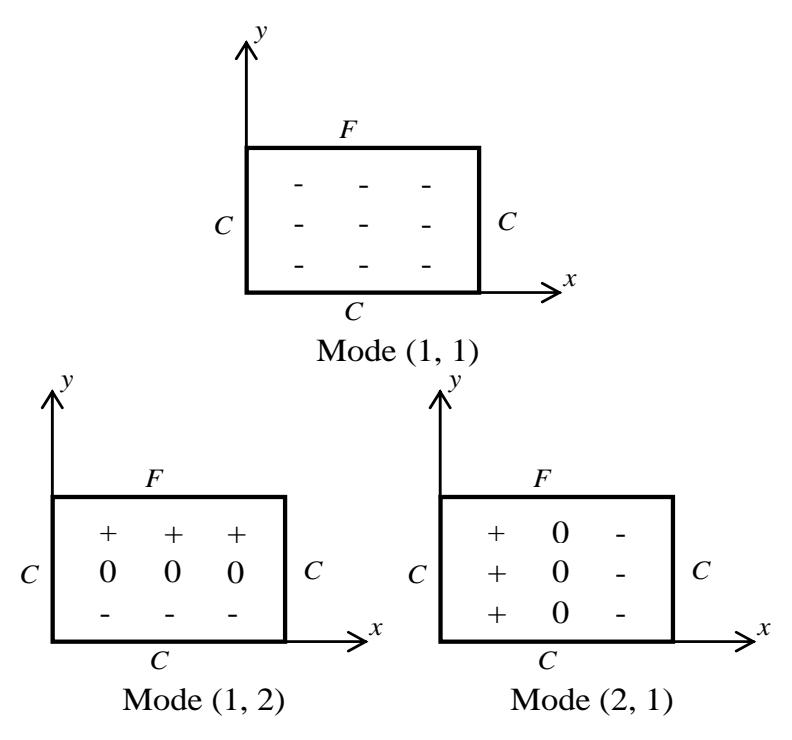


Figure 6.5 Vibration mode shapes of the experiments shown in Fig. 6.4

6.4 Experimental results and discussions.

All twelve specimens were tested to determine natural frequencies for each vibration mode. For each vibration mode, square of the natural frequency was plotted against an applied load to determine buckling load and buckling mode.

6.4.1 Buckling Mode

Experimental buckling mode is determined from the vibration mode whose trend line intersects the N_x -axis at the lowest load level. For all specimens, buckling modes determined from the experiment correspond very well to the numerical solutions. The plots of ω^{*2} vs. N_x of all specimens are similar to that of the aluminum specimen No.3 which is shown in Fig. 8. The relationship between both parameters is linear through out the tensile loading range and the low-load compressive loading range. In the high-load range, most of the experimental result showed that squares of the natural frequency are not linearly varied with the in-plane load. In Fig. 6.4, the nonlinear behavior is observed when the applied compressive load is higher than 30 kN/m, approximately. To investigate

the cause of this nonlinear behavior, the maximum out-of-plane displacement of the specimen subjected to compressive loading was measured and plotted, as shown in Fig. 6.6. From the figure, it is noticed that the out-of-plane displacement is observed as soon as the compressive load is applied. In the low-load range, i.e. N_x is lower than 25 kN/m, the measured out-of-plane displacement is less than 0.3 mm. The out-of-plane displacement is pronounced when the applied load approaches 30 kN/m. From linear buckling theory, the out-of-plane displacement is not existed before the specimen has buckled. So, this out-of-plane displacement is considered as a premature deformation in the experiment which reflects the imperfections of the specimen or the test setup. The inplane compressive load level at which the square of natural frequency begins to be nonlinear corresponds very well with the load level where the out-of-plane displacement of the specimen is well-defined. Other specimens also exhibited a similar correlation between the load level where a distinct out-of-plane displacement is observed and the load level where a nonlinear behavior between ω^{*2} and N_x is observed. It is reasonable to draw a conclusion that ω^{*2} is not linearly varied with the in-plane load in the high compressive loading region because of the premature out-of-plane displacement developed in that load region. Therefore, the proposal to use the vibration data in the tensile loading range to identify buckling load is justified.

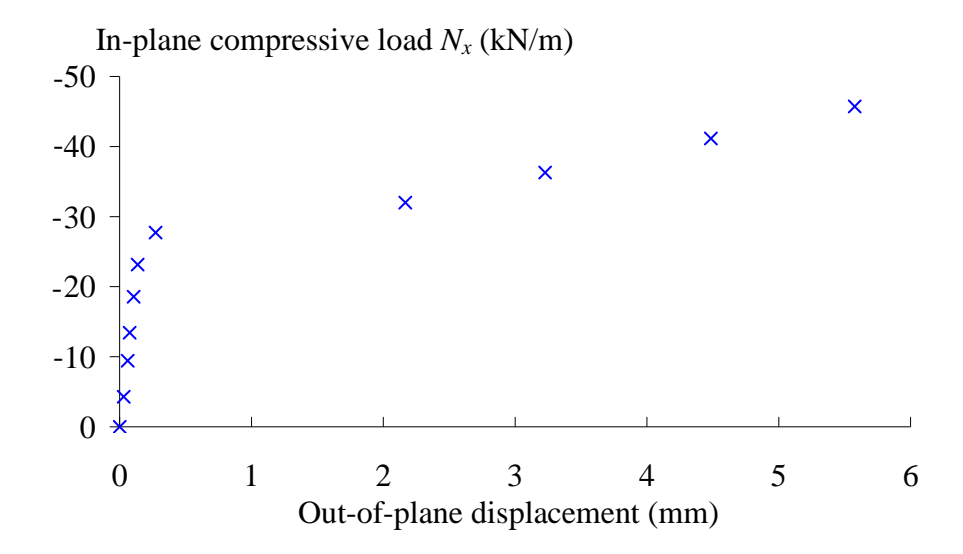


Figure 6.6 Plot of applied load vs. out-of-plane displacement of the specimen shown in Fig.6.4

6.4.2 Buckling load

The buckling loads determined from VCT for aluminum and stainless steel specimens are compared with the numerical solutions in Table 6.2 and 6.3, respectively. The experimental buckling load is determined from a plot of vibration data in the tensile loading range. In Table 6.2 and 6.3, dimensions of the specimens are presented in the first three columns. The next three columns compare experimental buckling loads of CCCC specimens with numerical solutions which are used as benchmark solutions. The last six columns show the experimental results of CCCF and CFCF specimens. It should be noted herein that the experimental result of the stainless steel specimen no.6 with CFCF is inapplicable because the specimen was permanently bended during the compressive test. It should be noted that each experimental buckling load presented in the tables is an average value from a set of 20 experiments. The discrepancy of the experimental buckling load from the benchmark solution is presented as percentage difference as shown in the column denoted by "% Diff." An average and standard deviation of the percent difference

between experimental and numerical solutions of specimens with the same boundary conditions is shown in the bottom of the tables. Since the experimental buckling loads shown in the Tables are an average value from 20 experiments, standard deviations shown in the last row are calculated from 120 experiments for each set of boundary condition, except stainless steel specimens with CFCF boundary conditions which have only 100 experiments. For aluminum specimens shown in Table 6.2, the percent difference of the measured buckling loads from the benchmarks varies from -5.95 % to 4.10 %. However, the averages of the percent discrepancy for specimens with the same boundary conditions shown at the bottom of the table are lower than ± 2 %. It is also observed that the average percent difference is independent of sizes, thickness and boundary conditions of the specimen. In general, the buckling load of an aluminum specimen obtained from VCT match the numerical solution very well. On the other hand, measured buckling loads of stainless steel plates are not as well agreed with the numerical ones. From Table 6.3, percent discrepancies of the measured buckling loads of CCCF and CFCF specimens are comparable to those of aluminum plates. The average percent differences of buckling load for both boundary conditions are less than 1%. However, an average percent different of 11.41 % for CCCC specimens is fairly high compared with those of other experiments. It is also noticed that the measured buckling load of a thicker plate deviates from the expected solution more than that of the thinner one. Specifically, the percent differences of the thicker plates (specimen No. 2, 4 and 6) which vary from 13.45% to 16.15% are higher than those of the thinner plates (specimen No. 1, 3 and 5) which are less than 10%.

Table 6.2 Buckling load in kN/m of aluminum specimens compared to numerical solutions.

			CCCC			CCCF			CFCF		
Specimen No.	Dimension $(a \times b) \text{ mm}^2$	Thickness, mm	Numerical	Exp.	%	Numerical	Exp.	%	Numerical	Exp.	%
NO.	(<i>a</i> × <i>b</i>) IIIII	ШШ	Solution	Measurement	Diff	Solution	Measurement	Diff	Solution	Measurement	Diff
1	300 x 200	2.032	113.198	115.7014	2.21	34.01854	34.84576	2.43	23.52831	24.09362	2.40
2	300 x 200	2.298	163.727	165.6002	1.14	49.20334	46.57304	-5.35	34.03061	34.19524	0.48
3	200 x 200	1.765	89.483	89.01088	-0.53	40.72324	38.30099	-5.95	34.89764	33.70079	-3.43
4	200 x 200	1.955	121.604	125.1282	2.90	55.34119	54.84334	-0.90	47.42444	46.76728	-1.39
5	150 x 200	1.745	100.1397	101.0814	0.94	65.48127	64.8182	-1.01	60.17814	57.05806	-5.18
6	150 x 200	1.976	145.4055	146.4931	0.75	95.08054	98.98151	4.10	87.38025	84.51399	-3.28
			Av	verage	1.24			-1.11			-1.73
			Standar	d deviation	4.44			6.30			3.38

Table 6.3 Buckling load in kN/m of stainless steel specimens compared to numerical solutions.

Specimen	Specimen Dimension		CCCC			CCCF			CFCF		
_		, i	Numerical	Exp.	%	Numerical	Exp.	%	Numerical	Exp.	%
Specimen No. Dimension (a×b) mm² Thickness, mm Numerical Solution Exp. Measurement % Numerical Diff Numerical Solution Exp. Measurement % Numerical Diff Numerical Solution Numerical Measurement Numerical Diff Numerical Solution Numerical Measurement Numerical Diff Numerical Solution Numerical Measurement Numerical Diff Numerical Solution Numerical Solution	Measurement	Diff									
1	300 x 200	1.173	58.79079	62.52427	6.35	18.04255	18.9684477	5.13	12.27434	12.044275	-1.87
2	300 x 200	1.389	97.61622	112.625	15.38	29.67785	28.4294318	-4.21	20.38031	20.558505	0.87
3	200 x 200	1.110	60.0928	64.64974	7.58	27.517	28.3914568	3.18	23.51676	23.63024	0.48
4	200 x 200	1.389	117.748	133.5815	13.45	53.91863	55.1761545	2.33	46.0803	46.689305	1.32
5	150 x 200	1.124	72.25424	79.15339	9.55	47.4231	48.327375	1.91	43.54222	44.1669325	1.43
6	150 x 200	1.406	141.423	164.2616	16.15	92.82115	87.3316045	-5.91	85.22511	N/A	N/A
			Av	erage	11.41			0.40			0.45
			Standar	d deviation	6.23			5.95			3.76

Imperfection of boundary conditions

From the experimental results of CCCC stainless steel specimens, it is speculated that the boundary condition of those specimens is significantly deviated from the theoretical one. For a clamped support, the specimen should be fixed with zero out-ofplane displacement and zero slope on the boundary. After a careful consideration, it was hypothesized that the supports on the unloaded edges were vulnerable to be a cause of imperfection. These supports are restrained by two support holders which are clamped on the guided columns, as shown in Fig. 5. Preferably, the support holder may not rotate around the guided column, such that the specimen is tightly clamped by the clamped supports. However, if the bending moment on the specimen's edge is sufficiently high, the support holder could be rotated by the reaction moment, resulting in a movement of the support in the out-of-plane direction. As a result, imperfection of the clamped boundary condition can be observed by monitoring the movement of the support bar on the unloaded edge. An additional measurement was conducted on both aluminum and stainless steel specimens to investigate the perfection of the clamped boundary condition. Specimens number 1 and 2 were mounted on the test frame and loaded with tensile loading, similar to that of the vibration test to determine natural frequencies. A dial indicator was placed in the middle of a clamped support to monitor the motion of the support after the specimen was loaded with tensile loading. A Plot of the displacement in the out-of-plane direction of the support versus applied tension is presented in Fig. 11. In an ideal world, this displacement should not be existed at any load levels. However, this displacement could be detected if (a) the specimen is not perfectly flat, or (b) the tensile load is not uniformly applied. It should also be noted that nominal sizes of specimen No. 1 and 2 are identical but specimen No. 1 is thinner than specimen No. 2. It is clearly seen that displacements of the support on the stainless steel plates are considerably higher than those of on the aluminum plates. Furthermore, the displacement measured on a thinner plate is less than those of on a thicker plate. This out-of-plane displacement of the support indicates the imperfection of that support. So, with the test frame used in this study, it can be concluded that aluminum specimens are supported by a better clamped boundary condition on the unloaded edges than those of the stainless steel specimens. Similarly, a clamped support on a thinner specimen is closed to an ideal boundary condition than that of on a thicker specimen. Although all specimens are clamped with the same supports and comparable clamping force, they are probably not subjected to similar boundary conditions because of the difference of the plate's bending stiffness. Bending stiffness of a stainless steel plate is higher than that of an aluminum plate, so does a thicker plate comparing with a thinner plate. Because of the imperfections of plates and loading conditions, such as pre-existed curvatures and uniformity of tensile loading, a specimen has a tendency to move in the out-of-plane direction. With an ideal boundary condition, all of this motion will be suppressed by the clamped support. It is confirmed in the additional measurement that the support can not perfectly restrain the specimen, as shown in Fig. 6.7. Specimens with lower stiffness, i.e. aluminum plates and thinner plates, are supported with a better clamped boundary condition. Thus, buckling loads of CCCC stainless steel specimens are not well predicted compared with those of other specimens because boundary conditions of these specimens are significantly diverged from an ideal boundary condition. In addition, a support on thinner specimens (specimen No. 1, 3 and 5) assembles a near-ideal boundary condition than that of the thicker ones. This remark is supported by the plot in Fig. 6.7, and justifies the obtained percent differences of the CCCC stainless steel specimens.

An imperfection of the clamped support, i.e., rotation of the support holder is encountered only on the unloaded edges. The clamped supports on the loaded edges are

mounted in crossheads #2 and #3 which are only allowed to move along two guided columns. With the described arrangement, both crossheads can not be rotated as long as the guided column remains straight, so the supports on these edges closely assemble an ideal clamped boundary condition. Therefore, the boundary conditions of the CFCF specimens were well setup, and the buckling loads of CFCF specimens are very well identified using VCT. For CCCF boundary conditions, although one of the unloaded edges is supported with a clamped boundary condition, experimental buckling loads from VCT still match the numerical solutions very well. The unloaded edges on CCCF specimens are clamped on one side and free on the other side. The free edge of these specimens is allowed to deform or bend; consequently, the bending moment on the other unloaded edges is probably not high enough to nullify a clamped boundary condition.

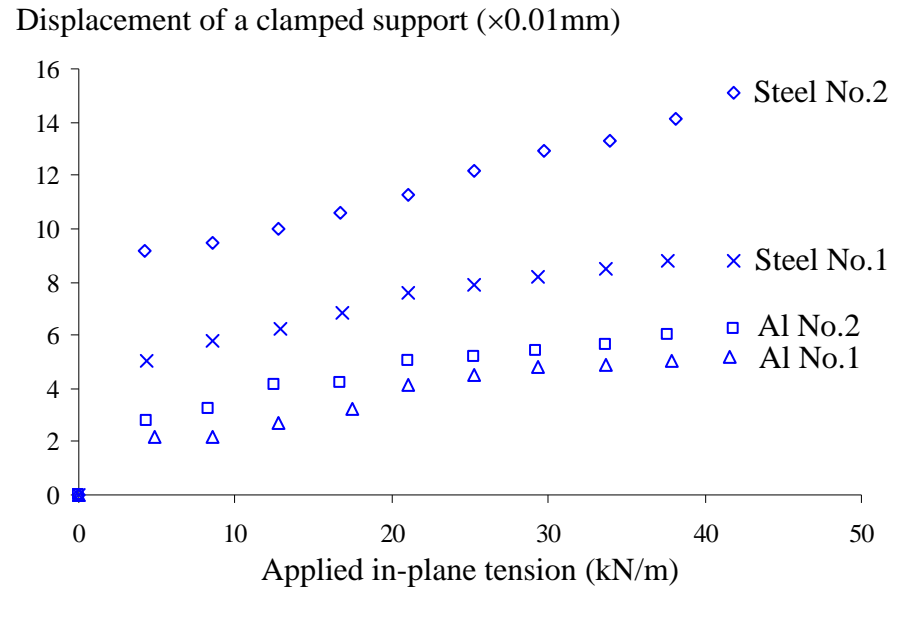


Figure 6.7 Plot of support displacement vs. in-plane tension of CCCC specimens

It is noticed from the experimental results that all of the measured buckling loads of CCCC stainless steel specimens are higher than the theoretical ones, i.e. percent differences are positive. This observation is contradicted by the fact that the specimen is not perfectly clamped, so its buckling load should be lower than that of the numerical

solution. However, this contradiction is rational because the measured buckling load is obtained from the measured vibration data. Because of the diverged boundary conditions, the specimen is not perfectly restrained, so its boundary condition is somewhat between simple support and clamped support. Thus, the measured natural frequencies of the specimens subjected to tensile load are lower than those of the perfectly clamped specimen. The degree of divergence of the boundary conditions is greater when the specimen is loaded with higher in-plane load. As a result, the slope of the trend line of ω^{*2} vs. N_x is lower than expected and the intersection of the trend line with N_x -axis is further away from the origin than it should be. Therefore the buckling load obtained from VCT using vibration data in the tensile loading region is higher than the theoretical one.

In conclusion, specimens used in this study are supported with either a clamped support or free boundary condition. The clamped boundary conditions on the loaded edges as well as the free boundary conditions on the unloaded edges were very well set up. Imperfection of the clamped boundary condition on the unloaded edge was minimized if the boundary condition on the other edge was free boundary condition. The imperfection of the support was also decreased on an aluminum specimen because of the lower plate's stiffness. With these remarks, only CCCC stainless steel plates were not well supported with an intended clamped boundary condition. This observation clarifies the fact that the measured buckling loads of these specimens from VCT are diverged from the numerical solutions. Buckling loads of other sets of specimens are accurately indicated using the proposed technique.

Derivation the buckling load

Although the average percent differences of the measured buckling loads from the numerical solutions are very low for most of the experiments with properly-prepared

boundary conditions. The standard deviations of the percent differences for each group of the specimens are, on the other hand, fairly high. The standard deviation for specimens with the same material and boundary condition is shown in the last row of Table 6.2 and 6.3. Unlike an average of the percent discrepancy, the standard deviations in each case of the experiments are not noticeably different. For CCCC and CCCF specimens, the standard deviations of the percent difference are varied from 4% to 6.5% for both materials. The standard deviations of CFCF specimens are 3.38% and 3.76 % for aluminum and stainless steel plates, respectively. These deviations are moderately less than those of the specimens with CCCC and CCCF boundary conditions. The standard derivation of the percent difference indicates the precision or repeatability of the measurements. In the experiment, to obtain a buckling load, a specimen was clamped by tightening machine screws and tested for natural frequencies under an increasing tensile loading. Then, the supports on the specimen was loosened and retightened again for the next experiment. So, it is noticed that boundary conditions of the specimen for each measurement are not identical. Additional tests were conducted by repeating the experiment without loosening the machine screws, i.e. the same boundary conditions were maintained. The measured buckling loads were not significantly different. Therefore, a measured buckling load of one experiment deviates from those of other experiments because of the nonidentical boundary condition between each experiment. It is also notice that the boundary condition on the unloaded edges of a CFCF specimen is free or unsupported. So, the boundary condition on these edges is identical for all experiments. Accordingly, the boundary conditions of CFCF specimens are deviated from an experiment to another experiment less than those of specimens with other boundary condition. So, the standard deviations of percent difference of CFCF specimens are fairly less than those of the specimens with other boundary conditions.

The distribution of the percent differences of the experiments with proper-setting boundary conditions is presented as a histogram shown in Fig. 12. The experimental results of CCCC stainless steel plates are not included in the plot because of their illdefined boundary conditions. There are a total of 580 comparisons between the measured and numerical buckling loads. It is seen that the histogram assemble a very symmetric bell curve with the tip of the curve right around 0%. The average percent difference from 580 comparisons is -0.18% with the standard deviation of 5.05%. A total of 397 comparisons, or approximately 68%, have percent difference between measured and numerical buckling loads within ±5%. In conclusion, the accuracy of using VCT with vibration data in the tensile loading region to identify a buckling load of plates is very well demonstrated. The precision or repeatability of the technique is fairly acceptable, given the fact that the boundary conditions of the specimen for each experiment in this study are not exactly identical. In practice, the precision of using the VCT can be kept at maximum if the boundary conditions of the specimen are suitably arranged. The advantage of using VCT is that the technique is applicable for specimens with any boundary conditions. As long as the specimen is supported in the vibration test in the same manner as that of in the buckling problem, the buckling load obtained from the VCT should be accurate and precise without knowing the boundary conditions of the specimen.

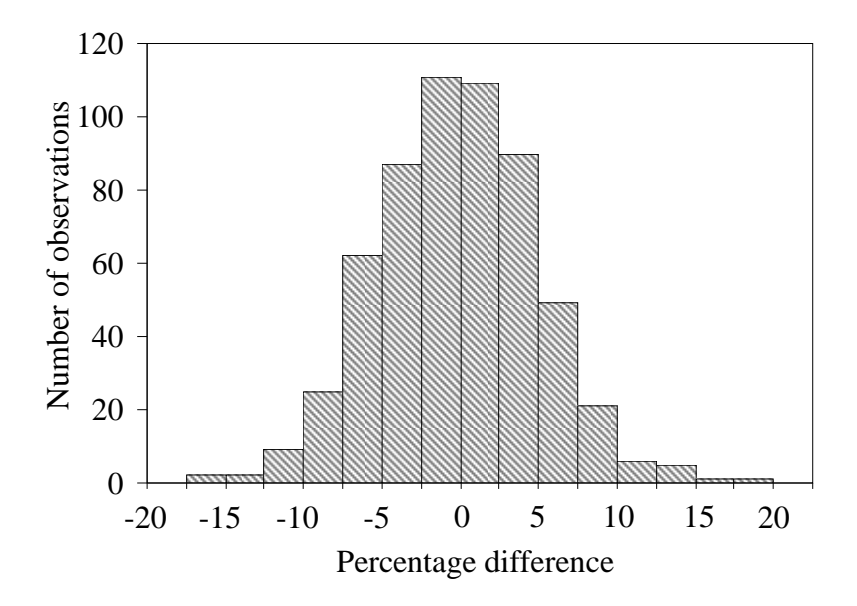


Figure 12. Histogram of the percentage difference between measured and predicted

buckling loads of the experiment except CCCC of stainless steel

6.5 Conclusions

The relationship between the natural frequency and the buckling load of a rectangular thin plate is developed in this study. It is shown that the square of natural frequency of a loaded plate is linearly varied with the in-plane load. By comparing the governing equations of both problems, the natural frequency of the plate decreases to be zero when the applied in-plane load approaches the buckling load of plate. The derived relationship is utilized as a technique to identify the buckling load and buckling mode of the structure. Due to a premature curvature which usually develops before buckling, the use of vibration data in the tensile-loading range, where the premature curvature is negligible, is proposed in this study. To verify the accuracy of the technique, the experiment was performed on a test frame in which the specimen was loaded and tested for natural frequencies. Both aluminum and stainless steel specimen with CCCC, CCCF and CFCF boundary conditions are included in the specimen. The measured vibration data is plotted against the in-plane load to determine the buckling load and buckling

mode. Square of the measured natural frequency is linearly varied with the applied load as expected. The experimental results show that all buckling modes obtained from VCT agree with numerical solutions very well, while most of the measured buckling loads conform to the numerical solutions. Buckling loads of CCCC stainless steel specimens were not well indicated using the proposed technique. The imperfection of boundary conditions of this group of specimens is believed to be a considerable factor in the high percentage difference between the measured and numerical buckling loads. If the experiments of stainless steel specimens with CCCC boundary condition are excluded, the average of the percent difference between measured buckling loads and numerical solutions is -0.18% with the standard deviation of 5.05%. The obtained percent difference assembles a bell-shape normal distribution. The standard deviation of the percent difference is fairly high because of the variation of the boundary conditions from one experiment to another experiment. In conclusion, the experimental study demonstrates the accuracy and reliability of using vibration data in the tensile-loading range to determine the buckling load. Boundary conditions of the specimen have a considerable effect on the precision of the measured buckling load. The proposed technique of identifying buckling load of plate has an advantage over the static methods for the fact that this method does not need human's judgment to draw two lines in the pre- and post- buckling regions. However, the boundary conditions of the specimen must be carefully set to get an accurate and precise measurement. The measured natural frequency of the specimen is sensitive to the boundary conditions and, hence, is a critical parameter in applying VCT to buckling of plate problem.

Chapter 7. Discussions and Conclusions

Buckling is one of the important failure modes of thin-walled structures, especially structures subjected to compressive load. There are mainly three approaches used to determine buckling load; i.e. analytical, numerical, or experimental approaches. In this project the experimental method is investigated. Several studies available in the literature compared experimental results with theoretical or numerical ones, and found a moderately high degree of discrepancy. Imperfection of plate and boundary condition of the experiment specimens are frequently cited as sources of the inconsistency. Also, the methods used to identify buckling load can be a source of discrepancy between the experimental result and the prediction. Usually, the static method, which is a plot some parameters such as out-of-plane displacement versus an in-plane load, requires some human judgments. That is it needs to draw two lines in the pre- and post- buckling regions to obtain the buckling load. Drawing these two lines could be a cause of error of the experimental buckling load. So, there is a need for an alternative approach of buckling load identification. In this study, a VCT is proposed as a technique which used the measured vibration data to identify buckling point of the structures. It is hypothesized that this approach might improve the accuracy of the measurement because there is no need to draw a line in the process so human error is avoided.

Since VCT utilizes the vibration data, the measured natural frequency need to be certain and reliable, unless the obtained buckling load is vulnerable to further critical error. Thus, in the first part of the study, the accuracy of vibration measurement is investigated. Because of the difficulty of setting up the theoretical boundary conditions, the scaling law is employed to predict the natural frequency of the prototype using the measured vibration data from the model. It is concluded that the vibration measurement is

satisfactorily accurate to further use in buckling load problem. Boundary conditions of the specimens are proved to be the most significant factor which can affect the measured natural frequency.

The second part of the study is focused on using VCT to identify the buckling load and mode of rectangular thin plate. The relationship between the natural frequency and the buckling load of a rectangular thin plate is developed. By comparing the governing equations of both problems, the natural frequency of the plate decreases to be zero when the applied in-plane load approaches the buckling load of plate. It is shown that the square of natural frequency of a loaded plate is linearly varied with the in-plane load. The derived relationship is utilized as a technique to identify the buckling load and buckling mode of the structure. Because of a premature curvature which usually develops before the specimen has buckled, the use of natural frequency in the tensile-loading range, where the premature curvature is negligible, is proposed in this study. The experimental investigation was performed to determine the accuracy and reliability of the technique. A test frame which can apply both tensile and compressive loads to the specimen was prepared and used in the experimental study. The measured vibration data is plotted against the in-plane load to determine the buckling load and buckling mode. Square of the measured natural frequency is linearly varied with the applied load as expected. The experimental results show that all buckling modes obtained from VCT agree with numerical solutions very well, while most of the measured buckling loads conform to the numerical solutions. There are some cases of the experiment that the measured buckling loads from VCT are not well agreed with the benchmark solution because the boundary conditions of the specimens are not closed to the ideal case. The experiment demonstrates the accuracy and reliability of using vibration data in the tensile-loading range to determine the buckling load. Similar to the case of vibration study, boundary conditions

of the specimen have a considerable effect on the precision of the measured buckling load.

The proposed VCT used to identify buckling load of plate has an advantage over the static methods for the fact that this method does not need human's judgment to draw two lines in the pre- and post- buckling regions. This technique is also appropriate for structures with imperfection or unknown boundary conditions. However, the boundary conditions of the specimen in vibration experiment must be carefully set to get an accurate and precise measurement. The measured natural frequency of the specimen is sensitive to the boundary conditions and, hence, is a critical parameter in applying VCT to buckling of plate problem.

References

- [1] Whitney JM. Structural analysis of laminated anisotropic plates, Technomic Pub. Co., Lancaster, Pa., 1987.
- [2] Lagace PA, Jensen DW, Finch DC. Buckling of unsymmetric composite laminates. Composite Structures 1986;5:101-23.
- [3] Narita Y, Leissa, AW. Buckling studies for simply supported symmetrically laminated rectangular plates. International Journal of Mechanical Sciences 1990;32:909-24.
- [4] Chai GB, Hoon KH. Buckling of generally laminated composite plates, Composites Science and Technology 1992;45:125-33.
- [5] Chai GB, Hoon KH, Chin SS. Buckling response of symmetric laminated plates.

 Mechanics of Structures and Machines 1996;24:439-52.
- [6] Chai GB, Banks WM, Rhodes J. The instability behaviour of laminated panels with elastically rotationally restrained edges. Composite Structures 1991;19:41-65.
- [7] Chai GB, Banks WM, Rhodes J. An experimental study on laminated panels in compression. Composite Structures 1991;19:67-87.
- [8] Chai GB, Khong PW. Stability study of coupling responses in laminates. Journal of Composites Technology & Research 1991;13:187-90.
- [9] Tuttle M, Singhatanadgid P, Hinds G. Buckling of Composite Panels Subjected to Biaxial Loading. Experimental Mechanics 1999;39:191-201.
- [10] Simitses GJ. Structural similitude for flat laminated surfaces. Composite Structures 2001;51:191-194.

- [11] Rezaeepazhand J, Simitses GJ, Starnes Jr. JH. Use of scaled-down models for predicting vibration response of laminated plates. Composite Structures 1995;30:419-426.
- [12] Singhatanadgid P, Ungbhakorn V. Buckling similitude invariants of symmetrically laminated plates subjected to biaxial loading, SEM Annual Conference and Exposition. Milwaukee, WI, USA. June, 2002.
- [13] Ungbhakorn V, Singhatanadgid P. Scaling laws for vibration response of antisymmetrically laminated plates. Structural Engineering and Mechanics 2002;14:345-364.
- [14] Ungbhakorn V, Singhatanadgid P. Similitude invariants and scaling laws for buckling experiments on anti-symmetrically laminated plates subjected to biaxial loading. Composite Structures 2003;59:455-465.
- [15] Wu JJ. Letter to the Editor: The complete-similitude scale models for predicting the vibration characteristics of the elastically restrained flat plates subjected to dynamic loads. Journal of Sound and Vibration 2003;268:1041–1053.
- [16] Wu JJ. Dynamic analysis of a rectangular plate under a moving line load using scale beams and scaling laws. Computers and Structures 2005;83:1646–1658.
- [17] Wu JJ. Cartmell MP, Whittaker AR. Prediction of the vibration characteristics of a full-size structure from those of a scale model. Computers and Structures 2002;80:1461–1472.
- [18] Singer J, Arbocz J, Weller, T. Buckling experiments: experimental methods in buckling of thin-walled structures Vol. 1. Chichester, UK: John Wiley & Sons, 1992.

- [19] Chai GB, Banks WM, Rhodes J. An experimental study on laminated panels in compression. Composite Structures 1991;19(1):67-87.
- [20] Tuttle M, Singhatanadgid P, Hinds G. Buckling of composite panels subjected to biaxial loading. Experimental Mechanics 1999;39(3):191-201.
- [21] Lurie H, Monica S. Lateral vibrations as related to structural stability. Journal of Applied Mechanics1952;19:195-204.
- [22] Chailleux A, Hans Y, Verchery G. Experimental study of the buckling of laminated composite columns and plates. International Journal of Mechanical Sciences 1975;17:489-498.
- [23] Segall A, Springer GS. A dynamic method for measuring the critical loads of elastic flat plates. Experimental Mechanics 1986;26(4):354-359.
- [24] Souza MA, Assaid LMB. A new technique for the prediction of buckling loads from nondestructive vibration tests. Experimental Mechanics 1991;31(2):93-97.
- [25] Go CG, Lin YS, Khor EH. Experimental determination of the buckling load of a straight structural member by using dynamic parameters. Journal of Sound and Vibration 1997;205(3):257-264.
- [26] Go CG, Liou CD. Experimental determination of the buckling load of a flat plate by the use of dynamic parameters. Structural Engineering and Mechanics 2000;9(5):483-490.
- [27] Gibson, R.F., Principles of composite material mechanics, MdGraw-Hill, Inc., New York, 1994.
- [28] E. Szucs, Similitude and Modelling, Elsevier Scientific Publishing Co., New York, 1980.

- [29] J.P. Lecointea, R. Romarya, J.F. Brudnya, T. Czaplab, Five methods of stator natural frequency determination: case of induction and switched reluctance machines, Mechanical Systems and Signal Processing 18 (2004) 1133–1159.
- [30] G.P. Zou, M. Naghipour, F. Taheri, A Nondestructive method for evaluating natural frequency of glued-laminated beams reinforced with GRP, Nondestructive Testing and Evaluation 19 (2003) 53–65.
- [31] Ding Z. Natural frequencies of rectangular plates using a set of static beam functions in Rayleigh-Ritz method. Journal of Sound and Vibration 1996;189(1):81-87.
- [32] Rajalingham C, Bhat RB, Xistris GD. Vibration of rectangular plates using plate characteristic functions as shape functions in the Rayleigh-Ritz method. Journal of Sound and Vibration 1996;193(2):497-509.
- [33] Lee JM, Chung JH, Chung TY. Free vibration analysis of symmetrically laminated composite rectangular plates. Journal of Sound and Vibration 1997;199(1):71-85.
- [34] Wang G, Wereley NM, Chang DC. Analysis of bending vibration of rectangular plates using two-dimensional plate modes. Journal of Aircraft 2005;42(2):542-550.
- [35] Timarci T, Aydogdu M. Buckling of symmetric cross-ply square plates with various boundary conditions. Composite Structures 2005;68(4):381-389.
- [36] Ni QQ, Xie J, and Iwamoto M. Buckling analysis of laminated composite plates with arbitrary edge supports. Composite Structures 2005;69(2):209-217.
- [37] Avitabile P, Experimental Modal Analysis: A Simple Non-Mathematical Presentation. Sound and Vibration 2001;35(1):20-31.

Appendix

Outputs of the project can be summarized as the following:

Manuscript:

 Singhatahadgid, P. and Sukajit, P., "Experimental determination of the buckling load of rectangular plates using vibration correlation technique," submitted to Thin-Walled Structures.

Reprint:

- Singhatanadgid, P. and Na Songkhla, A., "An experimental investigation into the use of scaling laws for predicting vibration responses of rectangular thin plates," Journal of Sound and Vibration 2008;311:314–327.
- Singhatanadgid, P. and Sukajit, P., "Determination of buckling load of rectangular plates using measured vibration data." International Conference on Experimental Mechanics (ICEM2008), Nanjing, China, 8-11 November 2008.
- 3. Sukajit, P.. and Singhatanadgid, P. "Identification of buckling load of thin plate using the vibration correlation technique," Proceedings of the 21st Conference of the Mechanical Engineering Network of Thailand (ME-NETT 21), Chonburi, Thailand, 17-19 October 2007, code AMM10.

Experimental determination of the buckling load of rectangular plates using vibration correlation technique

Pairod Singhatanadgid¹, Padol Sukajit

Department of Mechanical Engineering, Faculty of Engineering, Chulalongkorn

University,

Bangkok, 10330, Thailand

Tel: +66-2-218-6595, Fax: +66-2-252-2889, E-mail: Pairod.S@chula.ac.th

Abstract

This study investigates the use of a vibration correlation technique (VCT) to

identify the buckling load of a rectangular thin plate. It is proposed that the buckling load

is determined experimentally using the natural frequencies of plates under tensile loading.

A set of rectangular plates was tested for natural frequencies using an impact test method.

Aluminum and stainless steel specimens with CCCC, CCCF and CFCF boundary

conditions were included in the experiment. The measured buckling load was determined

from the plot of the square of a measured natural frequency versus an in-plane load. The

buckling loads from the measured vibration data match the numerical solutions very well.

For specimens with well-defined boundary conditions, the average percentage difference

between buckling loads from VCT and numerical solutions is -0.18 % with a standard

deviation of 5.05 %. The proposed technique using vibration data in the tensile loading

region is proven to be an accurate and reliable method which might be used to identify the

buckling load of plates. Unlike other static methods, this correlation approach does not

¹ Corresponding Author

require to draw lines in the pre-buckling and post-buckling regions, thus, bias in data interpretation is avoided.

Keywords: buckling load, vibration, natural frequency, thin plate, experiment

1. Introduction

Buckling load is one of the important parameters which should be considered in the design of thin or slender structures subjected to compressive loading. Buckling behavior of several engineering structures such as columns, plates, frames, and shells has been continuously investigated in the past several decades. Among several types of structure, a thin plate is one of the most important types of structure used in engineering applications. Mainly, the stability problem of plate is investigated using theoretical, numerical and experimental approaches. The theoretical method is applicable to a limited type of problems where a closed-form solution is possible. For more complicated structures, the numerical methods such as a finite element method are required. Solutions from both theoretical and numerical methods are generally verified with the experimental results. Experimental method involves in a number of costly and time consuming processes, however, imperfections and complicated effects of the problem are naturally included. For an experimental study of buckling of plate, identification of the buckling point is an important process, since it directly affects the accuracy of the measurement. In the experiment, the buckling load of plates can be identified using various kinds of plots; for example: 1) a plot of in-plane loads vs. out-of-plane displacement; 2) a plot of inplane loads vs. end-shortening; and 3) a plot of in-plane loads vs. difference of surface strains. These methods which may be classified as static methods utilize the change of the slope of the curve in pre-buckling and post-buckling regions to identify buckling load. The plots mentioned above and other static methods are properly summarized in Ref. [1]. There are several studies employed the static methods to identify the buckling load of

plates. Chai et al.[2] verified the theoretical buckling load of composite plates using the experimental method. Buckling load was determined from the intersection of the tangents drawn in the pre-buckling and post-buckling slopes of the load versus membrane strain curve. The discrepancies between the experimental and theoretical solutions between -7 % and +11 % were reported. Tuttle et al. [3] determined buckling loads of composite panels from the plots of applied in-plane load vs. out-of-plane displacement, and compared the experimental results to numerical predictions obtained using a Galerkin method. Although the average percentage error between the measured and predicted buckling loads is low, the standard deviation of the percentage error is as high as 15%. The difficulties of identifying the buckling load using a static test method were documented. In particular, drawing two lines in the pre-buckling and post-buckling regions to identify the buckling point depended on personal judgment, and could be a cause of error. To use the experimental result as a benchmark solution, the method used to identify buckling load must be accurate and reliable.

There is a need for an alternative approach to experimentally identify the buckling load of a plate. In this paper, the vibration correlation technique (VCT) is explored and modified to determine buckling load of a plate. The VCT is a nondestructive testing utilizing the measured vibration data. This concept has been applied to buckling problems in the past with a variety of amount of success. Lurie and Monica [4] showed that the square of the frequency of the lateral vibration of a thin plate with simple supports on all edges is linearly related to the end load. They also conducted some experiments on elastically restrained columns, rigid-joint trusses, and thin flat plates. The authors reported that VCT was successfully employed to predict the buckling load of only columns and trusses. For flat plates, because of the initial curvature, the buckling load cannot be predicted by the proposed method. However, Chailleux et al. [5] later showed

that with a carefully designed experimental setting, VCT can be used to determine the buckling load with satisfactory accuracy. The experimental dynamical curved is linear in the low load region, such that it is possible to extrapolate the data to obtain the buckling load. Segall and Springer [6] proposed a dynamic method to determine linear buckling loads of elastic rectangular plates. With an integral equation representation of the elastic stability, the proposed technique does not require the application of an in-plane load. A few studies [7-9] concerning the use of vibration data to investigate buckling behavior can be found in the literature.

In this study, the relationship between buckling and vibration behavior of thin plates is investigated. The relationship between applied in-plane load and the natural frequency of plates is derived from the differential governing equations of both problems. The derived relationship, which is applicable to thin plates with any boundary conditions, is numerically verified by simulating a plot of the derived relationship. Because of the premature curvature, which is usually detected even before the specimen has buckled, it is proposed in this study that the buckling load be determined from the vibration data of a plate subjected to tensile loading. A test frame, capable of applying tensile and compressive loading to a specimen, was prepared. A series of vibration tests was performed to determine the natural frequencies of the plates. The vibration data, along with the derived relationship, are used to predict the buckling load. Experimental buckling loads are compared to the numerical solutions to verify the proposed technique.

2. Relationship between natural frequency and buckling load

The vibration correlation technique utilizes the relationship between vibration parameters and buckling parameters. If the relationship between both parameters is established, the buckling behavior can be determined from the known or measured

vibration parameters. In this section, vibration and buckling behaviors of a thin plate are investigated and their relationship is derived. As shown in Fig. 1, a rectangular plate with a dimension of $a \times b$, and subjected to a uniform uniaxial loading N_x is a system of interest. For a buckling problem, an applied in-plane load N_x is always a compressive load. The desired parameters to be determined are buckling load and buckling mode. The buckling load of a plate – represented by \bar{N}_x – is the in-plane compressive load N_x at which buckling occurs, while the buckling mode is the out-of-plane configuration w of the buckled plate. In addition, natural frequencies and vibration mode shapes are two parameters to be determined in a vibration problem. The natural frequencies of a plate can be determined for a specimen with a given N_x . It should be noted that \bar{N}_x and N_x refer to the same in-plane load; however, \bar{N}_x is the buckling load which must be a compressive load (negative value), while N_x is the applied in-plane load which can be either tension or compression in the vibration problem. To derive the relationship between both phenomena, the governing equations of both problems are considered. The governing equations for buckling and vibration of a thin isotropic plate are written as:

$$\frac{\partial^4 w}{\partial x^4} + 2 \frac{\partial^4 w}{\partial x^2 \partial y^2} + \frac{\partial^4 w}{\partial y^4} - \frac{\overline{N}_x}{D} \frac{\partial^2 w}{\partial x^2} = 0$$
 (1)

and

$$\frac{\partial^4 w}{\partial x^4} + 2 \frac{\partial^4 w}{\partial x^2 \partial y^2} + \frac{\partial^4 w}{\partial y^4} - \frac{N_x}{D} \frac{\partial^2 w}{\partial x^2} - \frac{\omega^{*2} \rho}{D} w = 0, \qquad (2)$$

respectively. For a given plate with particular boundary conditions, it is widely known that the buckling mode is identical to one of the vibration modes. Specifically, the out-of-plane displacement of the buckled plate is the same as the out-of-plane displacement of one of the vibration modes. So, the governing equation of the buckling problem can be rewritten as:

$$L_1(w) - \bar{N}_x L_2(w) = 0,$$
 (3)

where
$$L_1(w) = \frac{\partial^4 w}{\partial x^4} + 2 \frac{\partial^4 w}{\partial x^2 \partial y^2} + \frac{\partial^4 w}{\partial y^4}$$
 and $L_2(w) = \frac{1}{D} \frac{\partial^2 w}{\partial x^2}$.

Similarly, the governing equation of the vibration of loaded plates is written as:

$$L_{1}(w) - N_{x}L_{2}(w) - \omega^{*2}L_{3}(w) = 0$$
(4)

where $L_3(w) = \frac{\rho w}{D}$.

It should be noted that the terms containing derivatives of w are the same for both problems because the buckling mode and vibration mode are identical. From Eq. (3), the buckling load of a plate can be written as:

$$\bar{N}_{x} = \frac{L_{1}(w)}{L_{2}(w)}.$$
(5)

Similarly, the natural frequency of a plate, with the applied in-plane load N_x , can be determined from Eq. (4), and written as:

$$\omega^{*2} = \frac{L_1(w) - N_x L_2(w)}{L_3(w)},$$
(6)

where ω^* is the natural frequency of a plate with applied load N_x . It is noticed that the natural frequency of plate varies with the in-plane loading. For an unloaded plate, the natural frequency is easily described as:

$$\omega^2 = \frac{L_1(w)}{L_3(w)},\tag{7}$$

where ω is the natural frequency of a plate without an applied load. By dividing Eq. (5) by Eq.(6) and utilizing Eq.(7), the ratio of the square of the natural frequency of a loaded plate to that of an unloaded plate is written as:

$$\left(\frac{\omega^*}{\omega}\right)^2 = 1 - \frac{N_x}{\bar{N}_x}.\tag{8}$$

From the relationship shown in Eq.(8), the buckling load \bar{N}_x and the natural frequency of an unloaded plate ω may be considered as a constant for a specific specimen. The variables in that equation are the natural frequency of the loaded plate ω^* and the applied in-plane load N_r . Thus, the square of the natural frequency (ω^{*2}) varies linearly with the applied load N_x . With the buckling load being a negative value, it is observed that the natural frequency of the plate increases with the applied tensile load. On the other hand, it decreases with the applied compression. Moreover, if the applied load N_x equals the buckling load of the plate, the natural frequency ω^* theoretically equals zero. With this observation, the natural frequencies of the loaded plate can be utilized to predict its buckling load by plotting ω^{*2} versus the in-plane load N_x . The buckling load can be determined from the applied load N_x at which the natural frequency approaches zero. Since this relationship is derived from the governing equations, it is applicable to specimens with any boundary conditions. Besides conventional boundary conditions, this relationship is also applicable for thin plates with unknown or imperfect boundary conditions. As long as the vibration data is obtained from the specimen with boundary conditions of interest, the buckling load determined using VCT will be the buckling load of the specimen with those boundary conditions.

To numerically verify the VCT and the derived relationship shown in Eq. (8), a numerical simulation of the vibration and buckling of a plate was performed. The Ritz method with characteristic beam functions was used to solve the buckling and vibration problems. Detail information about the Ritz method which is beyond the scope of this paper can be found in Ref.[10-15]. A 2-mm-thick aluminum plate with a dimension $a \times b$ of $400 \times 200 \text{ mm}^2$ was chosen as a specimen. The plate was assumed to be simply supported on the loading edges and clamped supported on the other two edges. The buckling load of this specimen was numerically determined, and found to be 88.216

kN/m with buckling mode (3, 1). The buckling mode of this specimen is graphically shown in Fig.2. This numerical solution serves as the theoretical solution for this simulation, and is used to validate the buckling load from VCT. Buckling load and mode determined from VCT requires the vibration data, i.e. natural frequencies and vibration mode shapes, of the plate subjected to in-plane loading. These vibration parameters of the loaded plated were also simulated from the Ritz method. The applied in-plane load was increased step by step in both tensile and compressive loading range. The square of the natural frequencies for the first six modes was plotted versus applied load, as shown in Fig. 3. The mode shape of each vibration mode is shown in Fig. 4. The relationship between ω^{*2} and N_x of a particular vibration mode is linear, as expected according to the derived relationship. The predicted buckling load can be determined by extrapolating the vibration data to the in-plane load at which the square of the natural frequency approaches zero. Trend lines of each vibration mode intercept the N_x axis at a different load level. The lowest compressive load is the buckling load, and its corresponding vibration mode shape is the predicted buckling mode. In this simulation, the predicted buckling is 88.216 kN/m and the buckling mode is mode (3, 1). VCT predicted buckling mode as mode (3, 1) because the trend line of this vibration mode intersects N_x axis at the lowest load compared to those of other vibration modes. The buckling load determined from the vibration data compares perfectly with the numerical solution. Similarly, the buckling mode determined from VCT is also identical to the buckling mode of the numerical solution. In conclusion, the squares of natural frequencies are linearly varied with the applied in-plane load as expected from the relationship shown in Eq. (8). The natural frequency approaches zero as the in-plane compressive load approaches the buckling load of plate. The numerical simulation showed that buckling behaviors of a thin plate are very well predicted using VCT. The concept of using vibration parameters to identify buckling

load and mode is theoretically verified. However, experimental study is required to determine the accuracy and reliability of the technique.

3. Experimental Arrangement

Although the relationship between vibration and buckling behaviors of a thin plate is theoretically confirmed, the applicability of VCT as an experimental technique used to identify buckling load is needed to be investigated. A series of experiments was performed to determine the accuracy and reliability of the proposed technique. A set of aluminum and stainless steel plates was used; each plate was uniaxially loaded on a custom-made test frame. The experiment was then performed on the loaded specimens to determine natural frequencies and vibration mode shape. The vibration data was obtained for the specimens subjected to both tensile and compressive loading. The measured natural frequencies and applied loading were then plotted, with results similar to those shown in Fig. 3. The predicted buckling load was identified using the VCT, i.e. the relationship derived previously.

Test frame

The test setup, shown in Fig. 5, was specifically designed to accommodate the loading configurations and vibration testing. The test frame is capable of applying both clamped and free boundary conditions to the specimens. The simple supported boundary condition is not included in the experiment because it is difficult to obtain a perfect simple support comparing with other two conventional boundary conditions. Both tensile and compressive loads can be applied on the specimens. In-plane loads are applied horizontally using a hydraulic cylinder pressurized with a hand pump. The hydraulic cylinder is mounted on the right end frame, which is fixed to the left end frame using two guided columns. A rectangular thin plate is mounted on the loading edges with clamped

support between crosshead #2 and crosshead #3. For a tensile testing configuration as shown in Fig. 5, the hydraulic ram applies a compressive force against crosshead #1. Loads are monitored using a load cell mounted between crosshead #1 and the hydraulic cylinder. Two linear bearings are embedded within the crossheads such that they can move linearly along two guided columns. The applied loading on crosshead #1 is transferred through two tension rods to crosshead #2. So, crosshead #2 is pushed and trend to move to the left hand side. On the contrary, crosshead #3 is blocked by two stoppers mounted on the guided columns, as shown in figure. With this loading configuration, a specimen which is clamped between crosshead #2 and crosshead #3 is stretched when the compressive load is applied by the hydraulic ram. In the case of a compressive testing, the test frame shown in Fig. 5 has to be modified as the following. Crosshead #1 and the tension rods are removed in the compressive testing configuration. Two stoppers which are used to block crosshead #3 in the tensile testing configuration are moved to the left-hand side of crosshead #2 to prevent the horizontal motion of the crosshead. A compressive load from the hydraulic ram is applied directly on crosshead #3, in this loading configuration. With this setup, the specimen is uniformly compressed between crosshead #2 and crosshead #3. So, the designed test frame is capable of applying both tensile and compressive loads to a thin plate with changeable loading configurations.

Besides the loading mechanism, the test frame is also equipped with restrained devices to apply desired boundary conditions to the test samples. In Fig.5, the clamped boundary conditions of the specimen are enforced by 20-mm.-thick rigid stainless steel bars, denoted as "clamped support." For the unloaded edges, the clamped supports are mounted on the support holders, which are tightly clamped to the guided columns. Similarly, the rigid stainless steel bars are placed in the slot of the crossheads to assemble

a clamped support on the loaded edges. On both loaded and unloaded edges, machine screws are used to push the steel supports against the specimen surface. To obtain a clamped support, machine screws are finger-tightened until the gap between the specimen and support is invisible. A clamped support on the unloaded edges of the specimen can be removed such that a free edge is formed on those boundaries. With the described constraint mechanism, the boundary conditions of a specimen are clamped support on the loaded edges (on x = 0 and x = a), and either clamped or free edges on the unloaded edges (on y = 0 and y = b)

Test specimens

A series of experiment was performed on twelve thin isotropic plates with CCCC, CCCF and CFCF boundary conditions. The symbol "C" represents a clamped boundary condition, while "F" stands for a free boundary condition. The first and third letters symbolize the boundary condition on x = 0 and x = a, respectively. Similarly, the boundary conditions on y = 0 and y = b are represented by the second and forth letters, respectively. The specimens were prepared from 6061-T6 aluminum alloy and stainless steel AISI 304. The physical and mechanical properties of both materials are presented in Table 1. Nominal dimensions $a \times b$ of the specimen are 300x200, 200x200, and 150x200 mm². For each plate size, there were two specimens with different thicknesses. So, there were a total of six aluminum specimens and six stainless steel specimens. The aluminum and stainless steel specimens' dimensions are summarized in the first three columns of Table 2 and Table 3, respectively. It should be noted that the actual size of a specimen is slightly larger than the nominal size because a small portion on the boundary of the specimen is clamped by the rigid stainless steel bar, and is not regarded as an effective area. The schematic dimensions of the specimens are presented in Fig. 6. A specimen was originally prepared to be a CCCC specimen. The width and height of the specimen are 40

mm larger than those of the nominal dimensions. A 20-mm-width area on all four edges is an area to be clamped by the support. In the schematic of a CCCC specimen shown in Fig. 6, the effective area or nominal area of the specimen is represented by a clear area of $a \times b$, whereas the dashed area is an area to be clamped by the support. After an experiment on a CCCC specimen is concluded, a clamped area on one of the unloaded edges is cut off to form a CCCF specimen. So, the actual size of a CCCF specimen is slightly smaller than a CCCC specimen with the same nominal size. Finally, the other clamped area on the unloaded edges is removed to obtain a CFCF specimen. Thus, specimens with an equal nominal size but different boundary conditions are actually the same specimen.

Testing procedures

In this study, the natural frequencies of a loaded plate are required data in order to predict the buckling behavior of the plate. Vibration testing was performed using an impact test, in which the specimen was excited by an impact hammer while the applied impulse was monitored by a dynamic signal analyzer. Acceleration response of the specimen was measured by an accelerometer placed on the specimen at a selected location. Acceleration data measured in the time domain were processed by a Fast Fourier Transform algorithm using the dynamic signal analyzer to obtain the frequency response function (FRF). From the vibration response in the frequency domain, the natural frequencies of the specimen were identified from the peak of the response. Vibration mode shape was also obtained from an imaginary part of the response function. An overview of the vibration testing and modal analysis is beyond the scope of this paper; and the interested reader is referred to the articles by Avitabile [16]. Typical magnitude and imaginary part of the frequency response function are shown in Fig. 7.

The experiment on a specimen was composed of two parts. The first part of the experiment was performed to verify the relationship shown in Eq.(8) and to determine the buckling mode of the plate. The specimen in this part of the experiment was loaded in both tensile and compressive loading range. Natural frequencies of the specimen under unloaded, tensile-loaded and compressive-loaded conditions were determined, respectively. The square of the natural frequency was plotted against applied in-plane load. A typical relationship between ω^{*2} and N_x is presented in Fig. 8 which is the vibration behavior an aluminum specimen No.3 with CCCF boundary condition. Natural frequencies of vibration modes (1, 1), (1, 2) and (2, 1) are included in the plot. Numbers representing a vibration mode stand for a number of curves of an out-of-plane displacement in the x and y directions, respectively. Vibration mode shape is determined from the imaginary parts of the frequency response from several experiments. A plot of each mode shape is presented in Fig. 9. A symbol "-" and "+" represent the out-of-plane displacement in the different direction, and "0" indicate a zero displacement or a node line on the specimens. From Fig. 8, the buckling mode of the specimen was determined to be mode (1, 1), since the trend line of this mode intersects the N_x axis at the lowest value. It is observed that ω^{*2} varies linearly with the applied load in the tensile-loading range, as expected. The relationship between both parameters in the compressive-loading range is not as linear as the relationship in the tensile-loading range. This nonlinear relationship in the compressive-loading range was also observed in other specimens, and was also reported by Lurie and Monica [4]. This behavior is contradicted by the result from the numerical simulation shown in Fig. 3. It is speculated that the nonlinear behavior is a result of a premature curvature which develops before buckling of the specimen. For this reason, the buckling load was determined using only vibration data of the specimen subjected to tensile loading. So, the second part of the experiment emphasizes on

determination of the buckling load. After plotting the relationship of ω^{*2} vs. N_x similar to Fig. 8 and determining the buckling mode, the specimen was reloaded under increased levels of tensile loading. At each load level, a vibration test was performed to determine the natural frequency of the loaded plate. Only the natural frequencies of the relevant mode shape, i.e. the buckling mode, were collected. A plot of ω^{*2} versus N_x in the tensile-loading range was generated and extrapolated to determine the measured buckling load. Because the measurement of natural frequency is very sensitive to boundary conditions, the experiment was repeated 20 times by loosening and re-tightening the machine screws on the clamped supports. An average of the measured buckling load is reported as the buckling load obtained from VCT.

4. Experimental results and discussions.

All twelve specimens were tested to determine natural frequencies for each vibration mode. For each vibration mode, square of the natural frequency was plotted against an applied load to determine buckling load and buckling mode.

4.1 Buckling Mode

Experimental buckling mode is determined from the vibration mode whose trend line intersects the N_x -axis at the lowest load level. For all specimens, buckling modes determined from the experiment correspond very well to the numerical solutions. The plots of ω^{*2} vs. N_x of all specimens are similar to that of the aluminum specimen No.3 which is shown in Fig. 8. The relationship between both parameters is linear through out the tensile loading range and the low-load compressive loading range. In the high-load range, most of the experimental result showed that squares of the natural frequency are not linearly varied with the in-plane load. In Fig. 8, the nonlinear behavior is observed when the applied compressive load is higher than 30 kN/m, approximately. To investigate

the cause of this nonlinear behavior, the maximum out-of-plane displacement of the specimen subjected to compressive loading was measured and plotted, as shown in Fig. 10. From the figure, it is noticed that the out-of-plane displacement is observed as soon as the compressive load is applied. In the low-load range, i.e. N_x is lower than 25 kN/m, the measured out-of-plane displacement is less than 0.3 mm. The out-of-plane displacement is pronounced when the applied load approaches 30 kN/m. From linear buckling theory, the out-of-plane displacement is not existed before the specimen has buckled. So, this out-of-plane displacement is considered as a premature deformation in the experiment which reflects the imperfections of the specimen or the test setup. The in-plane compressive load level at which the square of natural frequency begins to be nonlinear corresponds very well with the load level where the out-of-plane displacement of the specimen is well-defined. Other specimens also exhibited a similar correlation between the load level where a distinct out-of-plane displacement is observed and the load level where a nonlinear behavior between ω^{*2} and N_x is observed. It is reasonable to draw a conclusion that ω^{*2} is not linearly varied with the in-plane load in the high compressive loading region because of the premature out-of-plane displacement developed in that load region. Therefore, the proposal to use the vibration data in the tensile loading range to identify buckling load is justified.

4.2 Buckling load

The buckling loads determined from VCT for aluminum and stainless steel specimens are compared with the numerical solutions in Table 2 and 3, respectively. The experimental buckling load is determined from a plot of vibration data in the tensile loading range. In Table 2 and 3, dimensions of the specimens are presented in the first three columns. The next three columns compare experimental buckling loads of CCCC

specimens with numerical solutions which are used as benchmark solutions. The last six columns show the experimental results of CCCF and CFCF specimens. It should be noted herein that the experimental result of the stainless steel specimen no.6 with CFCF is inapplicable because the specimen was permanently bended during the compressive test. It should be noted that each experimental buckling load presented in the tables is an average value from a set of 20 experiments. The discrepancy of the experimental buckling load from the benchmark solution is presented as percentage difference as shown in the column denoted by "% Diff." An average and standard deviation of the percent difference between experimental and numerical solutions of specimens with the same boundary conditions is shown in the bottom of the tables. Since the experimental buckling loads shown in the Tables are an average value from 20 experiments, standard deviations shown in the last row are calculated from 120 experiments for each set of boundary condition, except stainless steel specimens with CFCF boundary conditions which have only 100 experiments. For aluminum specimens shown in Table 2, the percent difference of the measured buckling loads from the benchmarks varies from -5.95 % to 4.10 %. However, the averages of the percent discrepancy for specimens with the same boundary conditions shown at the bottom of the table are lower than ± 2 %. It is also observed that the average percent difference is independent of sizes, thickness and boundary conditions of the specimen. In general, the buckling load of an aluminum specimen obtained from VCT match the numerical solution very well. On the other hand, measured buckling loads of stainless steel plates are not as well agreed with the numerical ones. From Table 3, percent discrepancies of the measured buckling loads of CCCF and CFCF specimens are comparable to those of aluminum plates. The average percent differences of buckling load for both boundary conditions are less than 1%. However, an average percent different of 11.41 % for CCCC specimens is fairly high compared with those of other

experiments. It is also noticed that the measured buckling load of a thicker plate deviates from the expected solution more than that of the thinner one. Specifically, the percent differences of the thicker plates (specimen No. 2, 4 and 6) which vary from 13.45% to 16.15% are higher than those of the thinner plates (specimen No. 1, 3 and 5) which are less than 10%.

4.2.1 Imperfection of boundary conditions

From the experimental results of CCCC stainless steel specimens, it is speculated that the boundary condition of those specimens is significantly deviated from the theoretical one. For a clamped support, the specimen should be fixed with zero out-ofplane displacement and zero slope on the boundary. After a careful consideration, it was hypothesized that the supports on the unloaded edges were vulnerable to be a cause of imperfection. These supports are restrained by two support holders which are clamped on the guided columns, as shown in Fig. 5. Preferably, the support holder may not rotate around the guided column, such that the specimen is tightly clamped by the clamped supports. However, if the bending moment on the specimen's edge is sufficiently high, the support holder could be rotated by the reaction moment, resulting in a movement of the support in the out-of-plane direction. As a result, imperfection of the clamped boundary condition can be observed by monitoring the movement of the support bar on the unloaded edge. An additional measurement was conducted on both aluminum and stainless steel specimens to investigate the perfection of the clamped boundary condition. Specimens number 1 and 2 were mounted on the test frame and loaded with tensile loading, similar to that of the vibration test to determine natural frequencies. A dial indicator was placed in the middle of a clamped support to monitor the motion of the support after the specimen was loaded with tensile loading. A Plot of the displacement in the out-of-plane direction of the support versus applied tension is presented in Fig. 11. In

an ideal world, this displacement should not be existed at any load levels. However, this displacement could be detected if (a) the specimen is not perfectly flat, or (b) the tensile load is not uniformly applied. It should also be noted that nominal sizes of specimen No. 1 and 2 are identical but specimen No. 1 is thinner than specimen No. 2. It is clearly seen that displacements of the support on the stainless steel plates are considerably higher than those of on the aluminum plates. Furthermore, the displacement measured on a thinner plate is less than those of on a thicker plate. This out-of-plane displacement of the support indicates the imperfection of that support. So, with the test frame used in this study, it can be concluded that aluminum specimens are supported by a better clamped boundary condition on the unloaded edges than those of the stainless steel specimens. Similarly, a clamped support on a thinner specimen is closed to an ideal boundary condition than that of on a thicker specimen. Although all specimens are clamped with the same supports and comparable clamping force, they are probably not subjected to similar boundary conditions because of the difference of the plate's bending stiffness. Bending stiffness of a stainless steel plate is higher than that of an aluminum plate, so does a thicker plate comparing with a thinner plate. Because of the imperfections of plates and loading conditions, such as pre-existed curvatures and uniformity of tensile loading, a specimen has a tendency to move in the out-of-plane direction. With an ideal boundary condition, all of this motion will be suppressed by the clamped support. It is confirmed in the additional measurement that the support can not perfectly restrain the specimen, as shown in Fig. 11. Specimens with lower stiffness, i.e. aluminum plates and thinner plates, are supported with a better clamped boundary condition. Thus, buckling loads of CCCC stainless steel specimens are not well predicted compared with those of other specimens because boundary conditions of these specimens are significantly diverged from an ideal boundary condition. In addition, a support on thinner specimens (specimen No. 1, 3 and

5) assembles a near-ideal boundary condition than that of the thicker ones. This remark is supported by the plot in Fig. 11, and justifies the obtained percent differences of the CCCC stainless steel specimens.

An imperfection of the clamped support, i.e., rotation of the support holder is encountered only on the unloaded edges. The clamped supports on the loaded edges are mounted in crossheads #2 and #3 which are only allowed to move along two guided columns. With the described arrangement, both crossheads can not be rotated as long as the guided column remains straight, so the supports on these edges closely assemble an ideal clamped boundary condition. Therefore, the boundary conditions of the CFCF specimens were well setup, and the buckling loads of CFCF specimens are very well identified using VCT. For CCCF boundary conditions, although one of the unloaded edges is supported with a clamped boundary condition, experimental buckling loads from VCT still match the numerical solutions very well. The unloaded edges on CCCF specimens are clamped on one side and free on the other side. The free edge of these specimens is allowed to deform or bend; consequently, the bending moment on the other unloaded edges is probably not high enough to nullify a clamped boundary condition.

It is noticed from the experimental results that all of the measured buckling loads of CCCC stainless steel specimens are higher than the theoretical ones, i.e. percent differences are positive. This observation is contradicted by the fact that the specimen is not perfectly clamped, so its buckling load should be lower than that of the numerical solution. However, this contradiction is rational because the measured buckling load is obtained from the measured vibration data. Because of the diverged boundary conditions, the specimen is not perfectly restrained, so its boundary condition is somewhat between simple support and clamped support. Thus, the measured natural frequencies of the specimens subjected to tensile load are lower than those of the perfectly clamped

specimen. The degree of divergence of the boundary conditions is greater when the specimen is loaded with higher in-plane load. As a result, the slope of the trend line of ω^{*2} vs. N_x is lower than expected and the intersection of the trend line with N_x -axis is further away from the origin than it should be. Therefore the buckling load obtained from VCT using vibration data in the tensile loading region is higher than the theoretical one.

In conclusion, specimens used in this study are supported with either a clamped support or free boundary condition. The clamped boundary conditions on the loaded edges as well as the free boundary conditions on the unloaded edges were very well set up. Imperfection of the clamped boundary condition on the unloaded edge was minimized if the boundary condition on the other edge was free boundary condition. The imperfection of the support was also decreased on an aluminum specimen because of the lower plate's stiffness. With these remarks, only CCCC stainless steel plates were not well supported with an intended clamped boundary condition. This observation clarifies the fact that the measured buckling loads of these specimens from VCT are diverged from the numerical solutions. Buckling loads of other sets of specimens are accurately indicated using the proposed technique.

4.2.1 Derivation the buckling load

Although the average percent differences of the measured buckling loads from the numerical solutions are very low for most of the experiments with properly-prepared boundary conditions. The standard deviations of the percent differences for each group of the specimens are, on the other hand, fairly high. The standard deviation for specimens with the same material and boundary condition is shown in the last row of Table 2 and 3. Unlike an average of the percent discrepancy, the standard deviations in each case of the experiments are not noticeably different. For CCCC and CCCF specimens, the standard

deviations of the percent difference are varied from 4% to 6.5% for both materials. The standard deviations of CFCF specimens are 3.38% and 3.76 % for aluminum and stainless steel plates, respectively. These deviations are moderately less than those of the specimens with CCCC and CCCF boundary conditions. The standard derivation of the percent difference indicates the precision or repeatability of the measurements. In the experiment, to obtain a buckling load, a specimen was clamped by tightening machine screws and tested for natural frequencies under an increasing tensile loading. Then, the supports on the specimen was loosened and retightened again for the next experiment. So, it is noticed that boundary conditions of the specimen for each measurement are not identical. Additional tests were conducted by repeating the experiment without loosening the machine screws, i.e. the same boundary conditions were maintained. The measured buckling loads were not significantly different. Therefore, a measured buckling load of one experiment deviates from those of other experiments because of the nonidentical boundary condition between each experiment. It is also notice that the boundary condition on the unloaded edges of a CFCF specimen is free or unsupported. So, the boundary condition on these edges is identical for all experiments. Accordingly, the boundary conditions of CFCF specimens are deviated from an experiment to another experiment less than those of specimens with other boundary condition. So, the standard deviations of percent difference of CFCF specimens are fairly less than those of the specimens with other boundary conditions.

The distribution of the percent differences of the experiments with proper-setting boundary conditions is presented as a histogram shown in Fig. 12. The experimental results of CCCC stainless steel plates are not included in the plot because of their ill-defined boundary conditions. There are a total of 580 comparisons between the measured and numerical buckling loads. It is seen that the histogram assemble a very symmetric

bell curve with the tip of the curve right around 0%. The average percent difference from 580 comparisons is -0.18% with the standard deviation of 5.05%. A total of 397 comparisons, or approximately 68%, have percent difference between measured and numerical buckling loads within ±5%. In conclusion, the accuracy of using VCT with vibration data in the tensile loading region to identify a buckling load of plates is very well demonstrated. The precision or repeatability of the technique is fairly acceptable, given the fact that the boundary conditions of the specimen for each experiment in this study are not exactly identical. In practice, the precision of using the VCT can be kept at maximum if the boundary conditions of the specimen are suitably arranged. The advantage of using VCT is that the technique is applicable for specimens with any boundary conditions. As long as the specimen is supported in the vibration test in the same manner as that of in the buckling problem, the buckling load obtained from the VCT should be accurate and precise without knowing the boundary conditions of the specimen.

5. Conclusions

The relationship between the natural frequency and the buckling load of a rectangular thin plate is developed in this study. It is shown that the square of natural frequency of a loaded plate is linearly varied with the in-plane load. By comparing the governing equations of both problems, the natural frequency of the plate decreases to be zero when the applied in-plane load approaches the buckling load of plate. The derived relationship is utilized as a technique to identify the buckling load and buckling mode of the structure. Due to a premature curvature which usually develops before buckling, the use of vibration data in the tensile-loading range, where the premature curvature is negligible, is proposed in this study. To verify the accuracy of the technique, the experiment was performed on a test frame in which the specimen was loaded and tested

for natural frequencies. Both aluminum and stainless steel specimen with CCCC, CCCF and CFCF boundary conditions are included in the specimen. The measured vibration data is plotted against the in-plane load to determine the buckling load and buckling mode. Square of the measured natural frequency is linearly varied with the applied load as expected. The experimental results show that all buckling modes obtained from VCT agree with numerical solutions very well, while most of the measured buckling loads conform to the numerical solutions. Buckling loads of CCCC stainless steel specimens were not well indicated using the proposed technique. The imperfection of boundary conditions of this group of specimens is believed to be a considerable factor in the high percentage difference between the measured and numerical buckling loads. If the experiments of stainless steel specimens with CCCC boundary condition are excluded, the average of the percent difference between measured buckling loads and numerical solutions is -0.18% with the standard deviation of 5.05%. The obtained percent difference assembles a bell-shape normal distribution. The standard deviation of the percent difference is fairly high because of the variation of the boundary conditions from one experiment to another experiment. In conclusion, the experimental study demonstrates the accuracy and reliability of using vibration data in the tensile-loading range to determine the buckling load. Boundary conditions of the specimen have a considerable effect on the precision of the measured buckling load. The proposed technique of identifying buckling load of plate has an advantage over the static methods for the fact that this method does not need human's judgment to draw two lines in the pre- and post- buckling regions. However, the boundary conditions of the specimen must be carefully set to get an accurate and precise measurement. The measured natural frequency of the specimen is sensitive to the boundary conditions and, hence, is a critical parameter in applying VCT to buckling of plate problem.

ACKNOWLEDGEMENTS

This research is supported by the Thailand Research Fund under project grant No. RMU4880021.

REFERENCES

- [1] Singer J, Arbocz J, Weller, T. Buckling experiments: experimental methods in buckling of thin-walled structures Vol. 1. Chichester, UK: John Wiley & Sons, 1992.
- [2] Chai GB, Banks WM, Rhodes J. An experimental study on laminated panels in compression. Composite Structures 1991;19(1):67-87.
- [3] Tuttle M, Singhatanadgid P, Hinds G. Buckling of composite panels subjected to biaxial loading. Experimental Mechanics 1999;39(3):191-201.
- [4] Lurie H, Monica S. Lateral vibrations as related to structural stability. Journal of Applied Mechanics1952;19:195-204.
- [5] Chailleux A, Hans Y, Verchery G. Experimental study of the buckling of laminated composite columns and plates. International Journal of Mechanical Sciences 1975;17:489-498.
- [6] Segall A, Springer GS. A dynamic method for measuring the critical loads of elastic flat plates. Experimental Mechanics 1986;26(4):354-359.
- [7] Souza MA, Assaid LMB. A new technique for the prediction of buckling loads from nondestructive vibration tests. Experimental Mechanics 1991;31(2):93-97.
- [8] Go CG, Lin YS, Khor EH. Experimental determination of the buckling load of a straight structural member by using dynamic parameters. Journal of Sound and Vibration 1997;205(3):257-264.

- [9] Go CG, Liou CD. Experimental determination of the buckling load of a flat plate by the use of dynamic parameters. Structural Engineering and Mechanics 2000;9(5):483-490.
- [10] Ding Z. Natural frequencies of rectangular plates using a set of static beam functions in Rayleigh-Ritz method. Journal of Sound and Vibration 1996;189(1):81-87.
- [11] Rajalingham C, Bhat RB, Xistris GD. Vibration of rectangular plates using plate characteristic functions as shape functions in the Rayleigh-Ritz method. Journal of Sound and Vibration 1996;193(2):497-509.
- [12] Lee JM, Chung JH, Chung TY. Free vibration analysis of symmetrically laminated composite rectangular plates. Journal of Sound and Vibration 1997;199(1):71-85.
- [13] Wang G, Wereley NM, Chang DC. Analysis of bending vibration of rectangular plates using two-dimensional plate modes. Journal of Aircraft 2005;42(2):542-550.
- [14] Timarci T, Aydogdu M. Buckling of symmetric cross-ply square plates with various boundary conditions. Composite Structures 2005;68(4):381-389.
- [15] Ni QQ, Xie J, and Iwamoto M. Buckling analysis of laminated composite plates with arbitrary edge supports. Composite Structures 2005;69(2):209-217.
- [16] Avitabile P, Experimental Modal Analysis: A Simple Non-Mathematical Presentation. Sound and Vibration 2001;35(1):20-31.

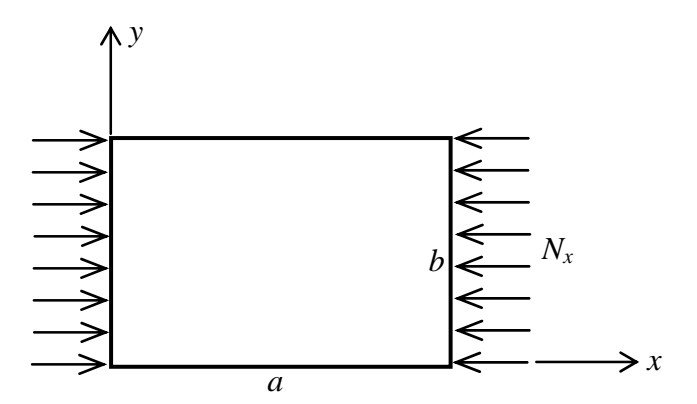


Figure 1. A rectangular plate subjected to a uniaxial in-plane load N_x

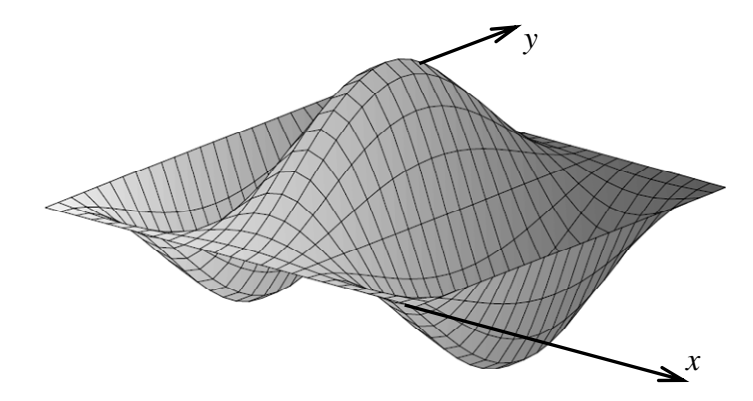


Figure 2. Buckling mode determined from the buckling problem

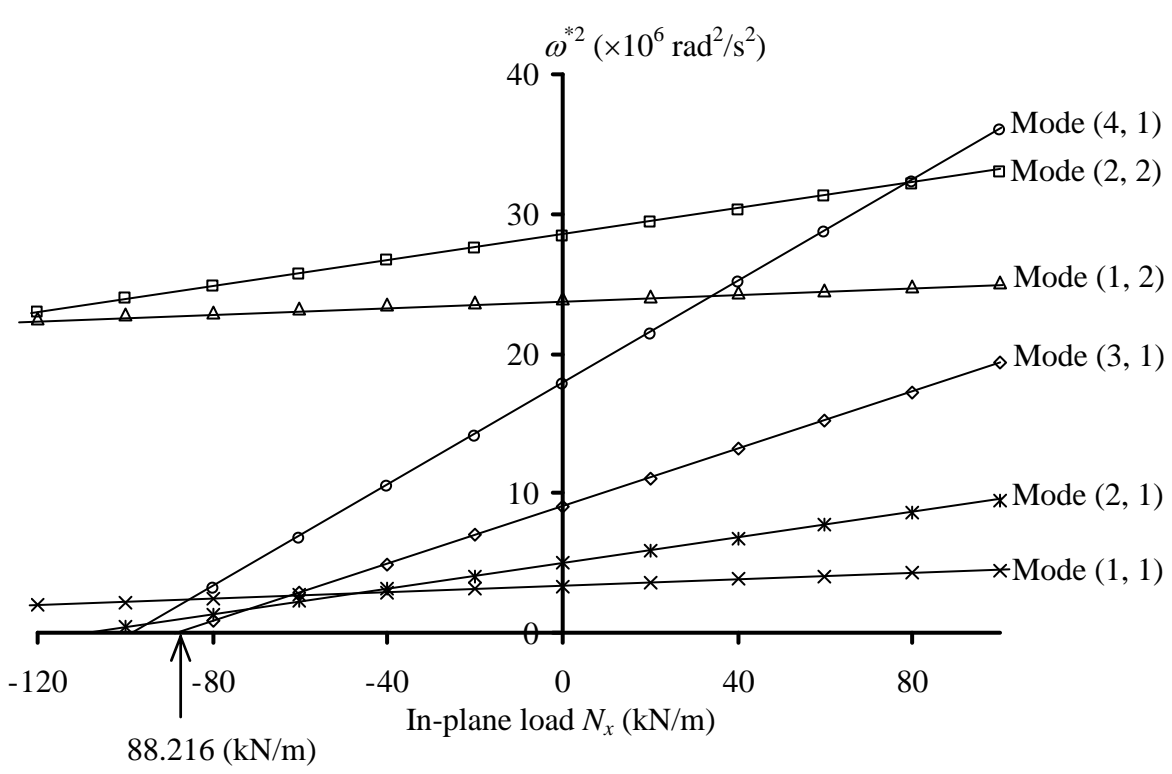


Figure 3. Square of the natural frequencies of an aluminum plate vs. applied loading.

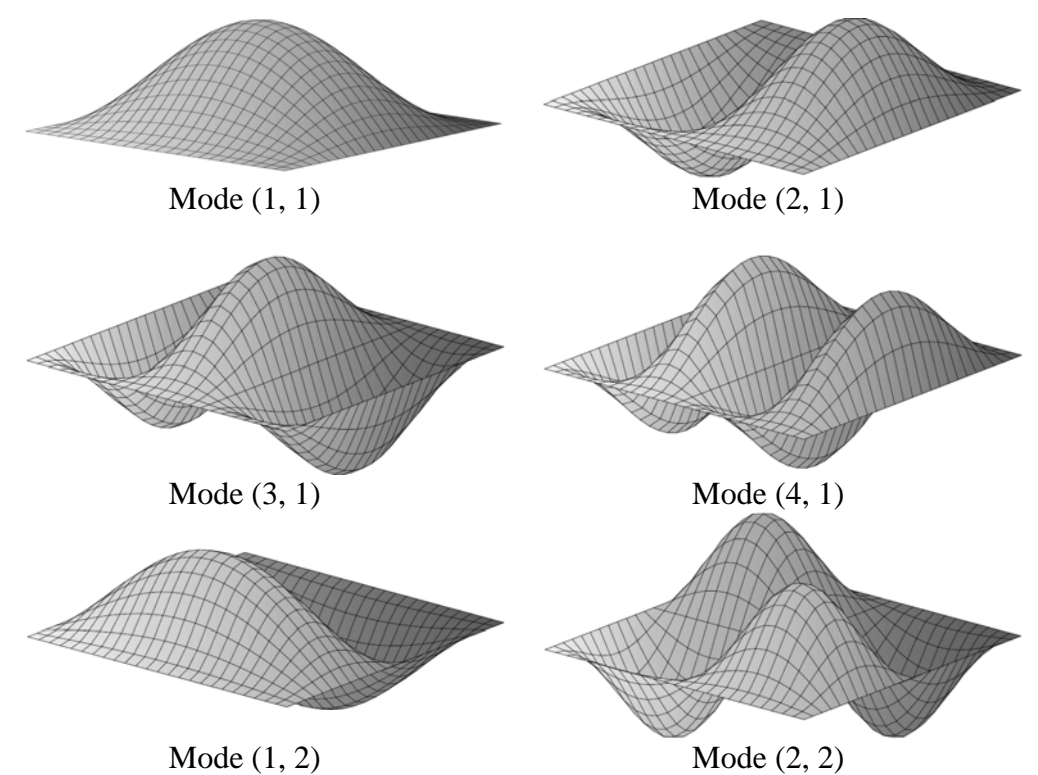


Figure 4. Vibration mode shapes of the first six vibration mode.

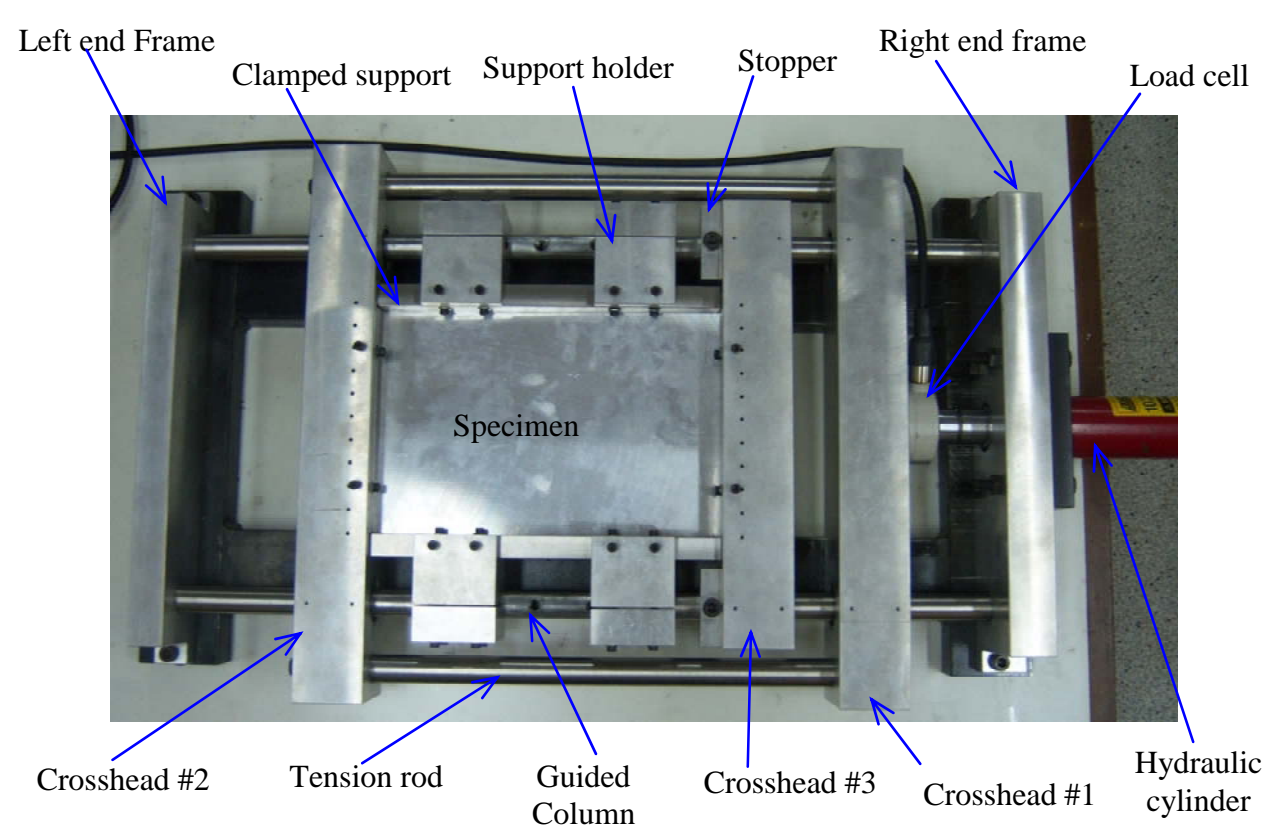


Figure 5. Experimental setup of a specimen with CCCC boundary condition subjected to tensile loading.

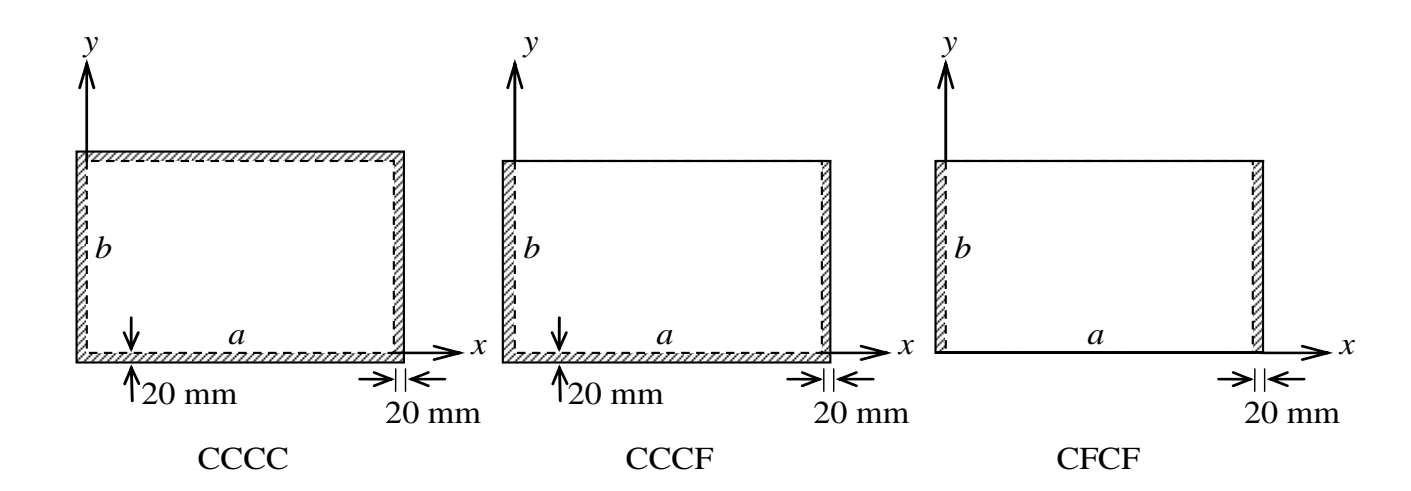


Figure 6. Nominal and actual dimensions of the specimens.

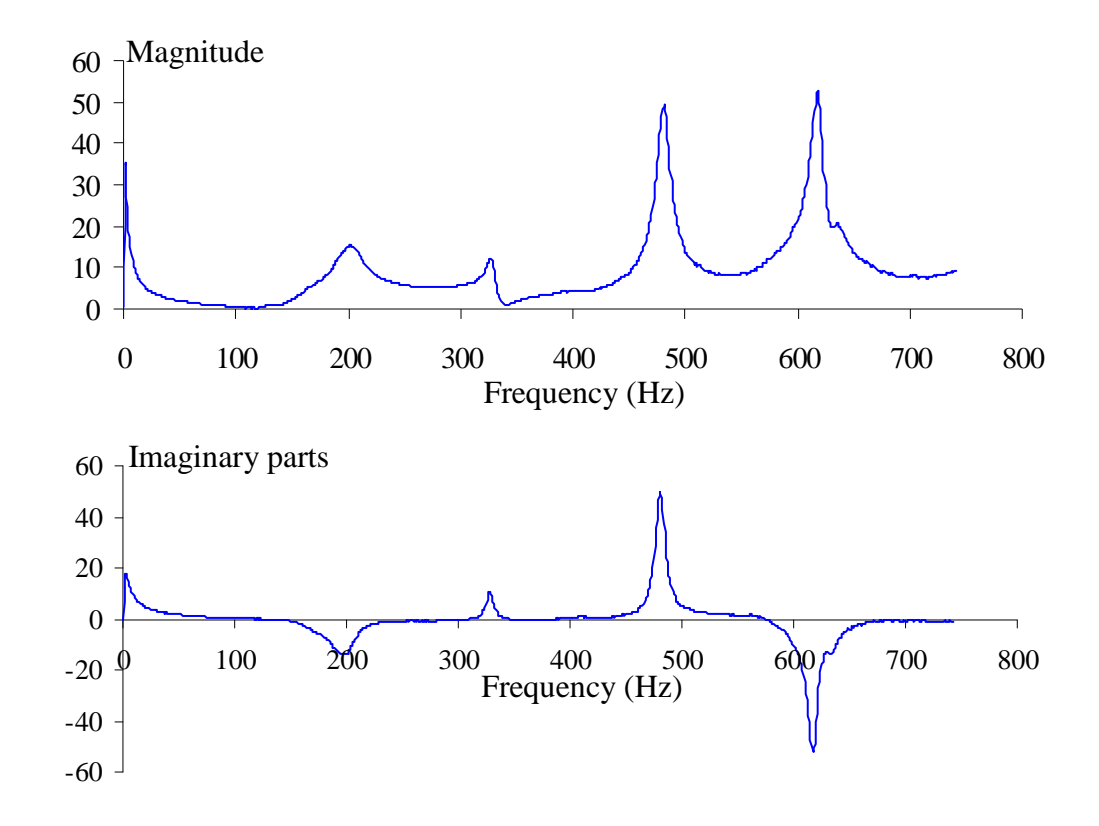


Figure 7. Magnitude and imaginary parts of the frequency response of the CCCC stainless specimen No. 2 without an in-plane load.

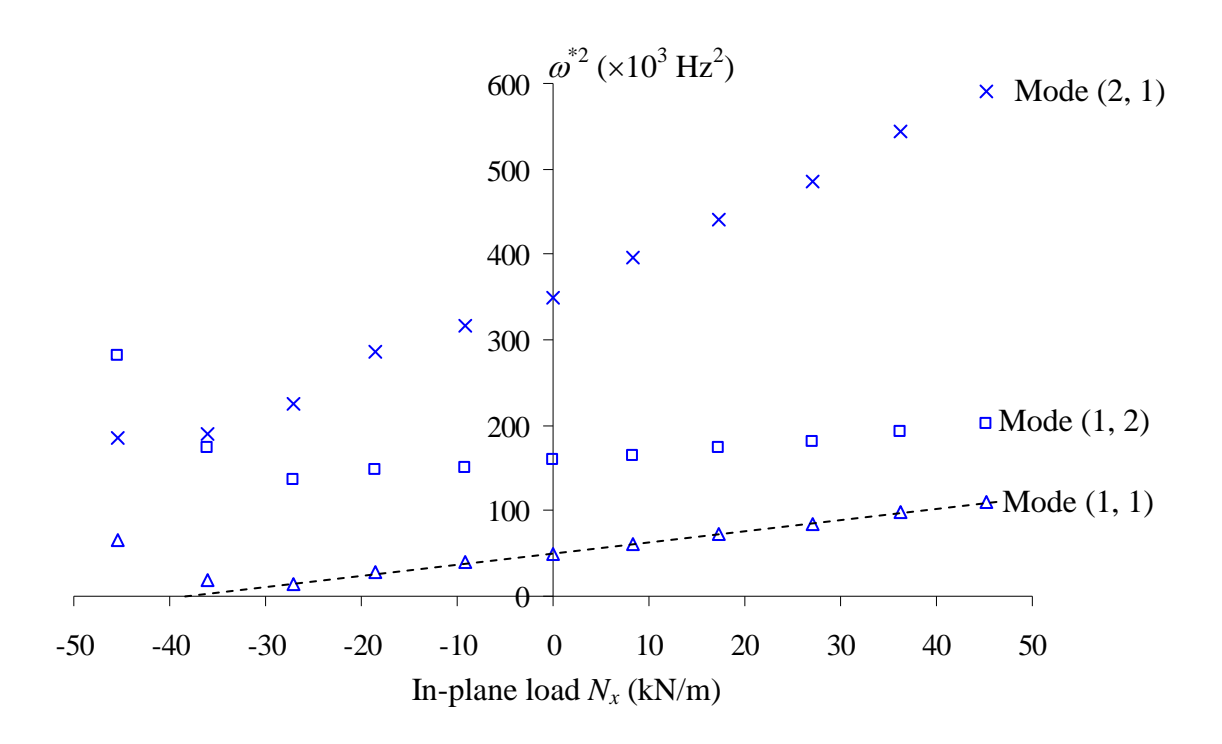


Figure 8. Plot of ω^{*2} vs. N_x of the aluminum specimen No.3 with CCCF boundary condition.

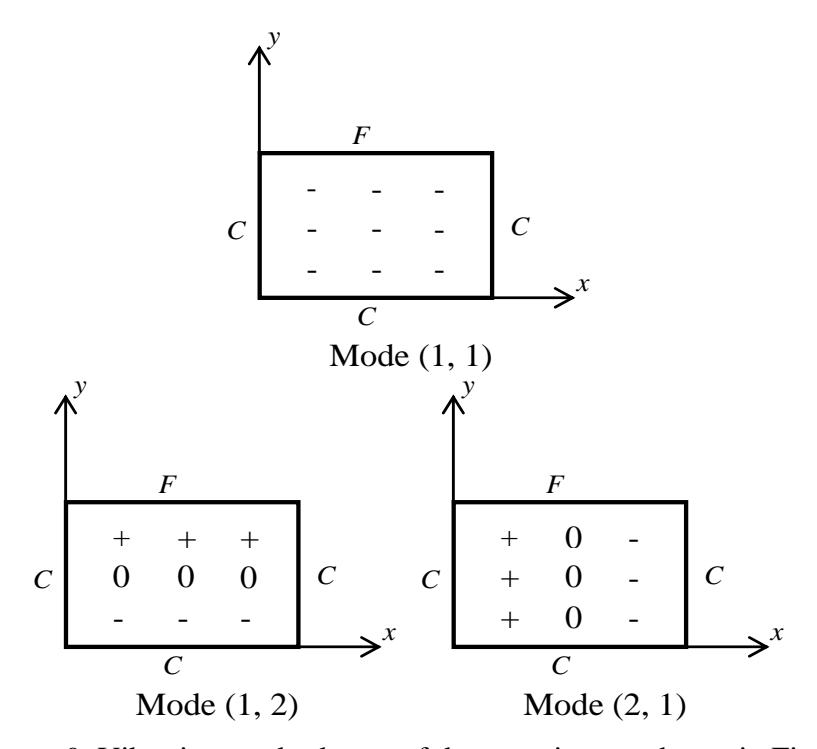


Figure 9. Vibration mode shapes of the experiments shown in Fig. 8.

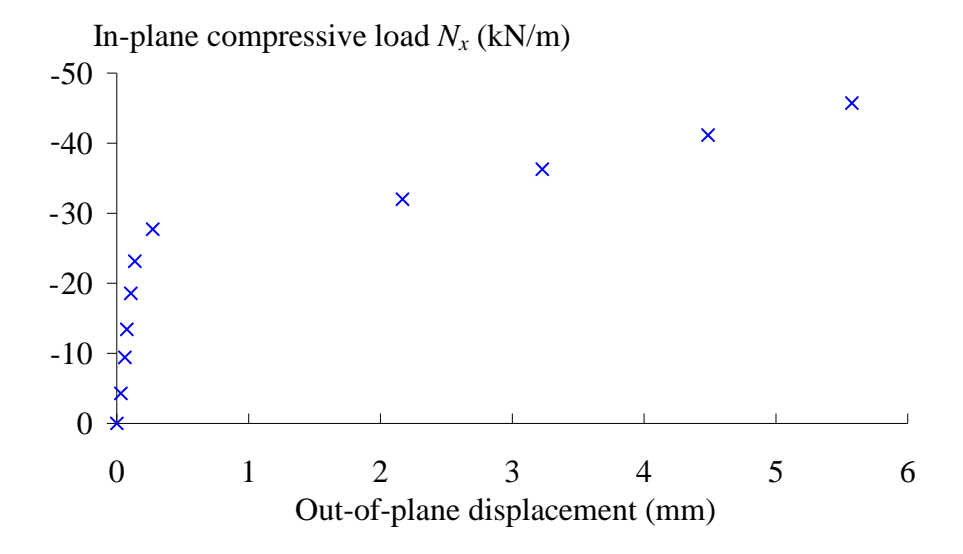


Figure 10. Plot of applied load vs. out-of-plane displacement of the experimental results shown in Fig. 8.

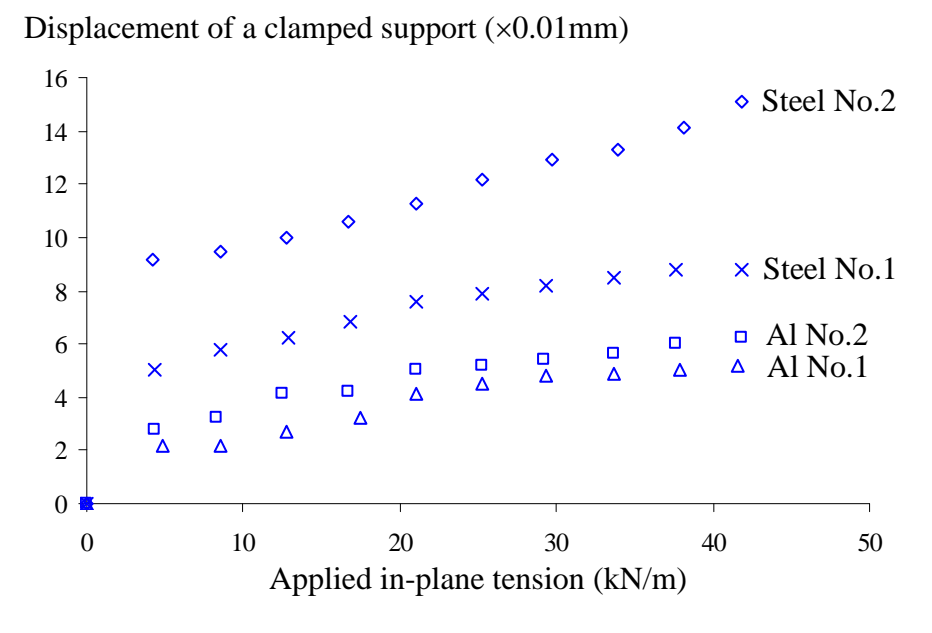


Figure 11. Plot of support displacement vs. in-plane tension of CCCC specimens

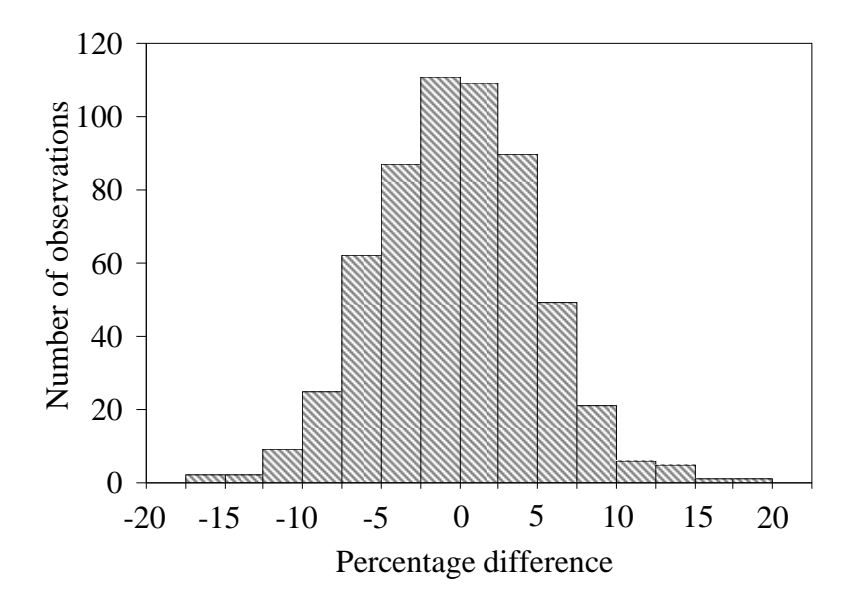


Figure 12. Histogram of the percentage difference between measured and predicted buckling loads of the experiment except CCCC of stainless steel

Table 1. Properties of materials used in the experiments.

Material	Modulus of Elasticity, E (GPa)	Poisson ratio, v	Density, ρ (kg/m ³)
Aluminum 6061-T6	70	0.33	2700
Stainless steel AISI 304	193	0.30	8000

Table 2. Buckling load in kN/m of aluminum specimens compared to numerical solutions.

				CCCC			CCCF			CFCF	
Specimen No.	Dimension $(a \times b) \text{ mm}^2$	Thickness, mm	Numerical	Exp.	%	Numerical	Exp.	%	Numerical	Exp.	%
140.	$(a \wedge b)$ min	111111	Solution	Measurement	Diff	Solution	Measurement	Diff	Solution	Measurement	Diff
1	300 x 200	2.032	113.198	115.7014	2.21	34.01854	34.84576	2.43	23.52831	24.09362	2.40
2	300 x 200	2.298	163.727	165.6002	1.14	49.20334	46.57304	-5.35	34.03061	34.19524	0.48
3	200 x 200	1.765	89.483	89.01088	-0.53	40.72324	38.30099	-5.95	34.89764	33.70079	-3.43
4	200 x 200	1.955	121.604	125.1282	2.90	55.34119	54.84334	-0.90	47.42444	46.76728	-1.39
5	150 x 200	1.745	100.1397	101.0814	0.94	65.48127	64.8182	-1.01	60.17814	57.05806	-5.18
6	150 x 200	1.976	145.4055	146.4931	0.75	95.08054	98.98151	4.10	87.38025	84.51399	-3.28
			Av	erage	1.24			-1.11			-1.73
			Standar	d deviation	4.44			6.30			3.38

Table 3. Buckling load in kN/m of stainless steel specimens compared to numerical solutions.

Specimen	Dimension	Thickness,		CCCC			CCCF			CFCF	
No.	$(a \times b) \text{ mm}^2$	mm	Numerical	Exp.	%	Numerical	Exp.	%	Numerical	Exp.	%
140.	$(a \wedge b)$ mm	111111	Solution	Measurement	Diff	Solution	Measurement	Diff	Solution	Measurement	Diff
1	300 x 200	1.173	58.79079	62.52427	6.35	18.04255	18.9684477	5.13	12.27434	12.044275	-1.87
2	300 x 200	1.389	97.61622	112.625	15.38	29.67785	28.4294318	-4.21	20.38031	20.558505	0.87
3	200 x 200	1.110	60.0928	64.64974	7.58	27.517	28.3914568	3.18	23.51676	23.63024	0.48
4	200 x 200	1.389	117.748	133.5815	13.45	53.91863	55.1761545	2.33	46.0803	46.689305	1.32
5	150 x 200	1.124	72.25424	79.15339	9.55	47.4231	48.327375	1.91	43.54222	44.1669325	1.43
6	150 x 200	1.406	141.423	164.2616	16.15	92.82115	87.3316045	-5.91	85.22511	N/A	N/A
			Av	erage	11.41			0.40			0.45
			Standar	d deviation	6.23			5.95			3.76

Reprint

Singhatanadgid, P. and Na Songkhla, A., "An experimental investigation into the use of scaling laws for predicting vibration responses of rectangular thin plates," Journal of Sound and Vibration 2008;311:314–327.





Journal of Sound and Vibration 311 (2008) 314-327



www.elsevier.com/locate/jsvi

An experimental investigation into the use of scaling laws for predicting vibration responses of rectangular thin plates

Pairod Singhatanadgid*, Anawat Na Songkhla

Department of Mechanical Engineering, Faculty of Engineering, Chulalongkorn University, Bangkok 10330, Thailand

Received 4 January 2007; received in revised form 5 September 2007; accepted 11 September 2007 Available online 22 October 2007

Abstract

A scaling law for the vibration response of rectangular plates along with a similarity requirement was derived and validated with the experimental results in this study. The scaling law was derived from the governing equation of the problem and was found to be exact after verifying with a closed-form solution. An experimental investigation was conducted on several model and prototype specimens using an impact test method. The natural frequencies of the models were substituted into the scaling law to obtain the scaling natural frequencies of the prototypes, which were then compared with the measured natural frequencies. In the first part of the study, a total of nine aluminum rectangular plates with various boundary conditions were tested for natural frequencies to determine the size effect on the accuracy of the scaling law. From a total of 108 comparisons, the average percentage discrepancy of the scaling natural frequencies was 4.90% with a standard deviation of 6.45%. Therefore, the scaling law is satisfactorily accurate for a pair of models and prototypes of the same material but of different size. The other part of the study involved the investigation of the material's effect on the accuracy of the scaling law. The experimental results showed that, unlike theoretical verification, using model and prototype systems with different materials resulted in an erroneous scaling natural frequency. The predicted natural frequency was inaccurate in this case because the boundary conditions enforced by the supports on the models and prototypes of different materials were significantly different. Consequently, the similarity requirement between the model and prototype is violated in the case of this study. With an additional experiment, the scaling law was found to be practically accurate for model-prototype pairs of different materials if their similitude requirements were fulfilled. The possible sources of discrepancy of the scaling natural frequency include uncertainties of the experiment, incomplete similarity of plate configurations and non-identical boundary conditions between the prototype and its model. © 2007 Elsevier Ltd. All rights reserved.

1. Introduction

The similitude concept has been utilized in many engineering applications. The principle provides a powerful tool for engineers and scientists to replicate the behavior of the prototype using an appropriate scaled model. Similitude theory can be stated as [1]; "the sufficient and necessary condition of similitude between two systems is that the mathematical model of the one be related by a bi-unique transformation to that of the other." For a prototype of interest, a scaled replica can be built to duplicate the behavior of the

^{*}Corresponding author. Tel.: +66 2 218 6595; fax: +66 2 252 2889. E-mail address: Pairod.S@chula.ac.th (P. Singhatanadgid).

full-scale system. The experimental results on the model can be utilized to predict the behavior of the prototype. The similitude concept is thus very useful, especially, for problems with either a complex domain or complicated boundary conditions for which numerical solutions are not sufficiently accurate, if possible. If the prototype is perfectly replicated, the experiment result on the model can be scaled to predict the behavior of the prototype with sufficient accuracy.

The similitude theory has been applied to many problems in the field of structural engineering, including vibration and buckling problems of plates. Simitses [2] applied similitude transformation to the bending, buckling, and vibration of laminated plates. The derived scaling laws were successfully employed to the problem with appropriate similarity requirements between model and prototype systems. Rezaeepazhand et al. [3] demonstrated a procedure for deriving a scaling law for the frequency response of laminated plates. Both Simitses and Rezaeepazhand derived scaling laws from the closed-form solutions of the problems. Alternatively, scaling laws can be derived directly from the governing equation of the problems. In Refs. [4–6], the authors derived the scaling laws for the vibration and buckling behavior of laminated rectangular plates. In those studies, similitude transformation was applied to the governing equations of the problems directly. Besides the scaling law, the similarity requirements were also obtained. An advantage of this approach is that a solution of the governing equations is not required. The obtained scaling laws were verified with the theoretical solution and found to be exact for complete similitude cases. Partial similitude cases were also investigated and recommended. It was also found that the scaling laws were independent of boundary conditions. This implies that, for a problem with complicated boundary conditions, the behavior of the prototype can be predicted from the experimental results of the corresponding scaled model given that the boundary conditions of both systems are identical. This concept is especially beneficial for problems where the boundary conditions cannot be numerically modeled in the numerical solutions but can be built in the scaled model.

In addition to a simple-supported rectangular thin plate, the similitude theory was moreover applied to the elastically restrained flat plates subjected to dynamic loads by Wu [7]. The author showed that the geometric, kinematic and dynamic similarities must be satisfied to assure the complete similitude. A similar concept was also applied to the dynamic analysis of rectangular plates under a moving load line [8]. Both complete and partial similitude cases were presented. An agreement between the theoretical vibration response of the full-scale prototype and the prediction from the solution of the scale model was obtained. Wu et al. [9] employed the similitude concept with a more complex structure where a scale model and the scaling law were utilized to determine the vibration characteristics of a full-size crane structure.

In past studies, the scaling laws were usually verified using analytical or numerical solutions. An exact agreement between the scaled solutions and theoretical solutions is always achieved for complete similitude cases. This so-called numerical experiment demonstrates that the derived scaling laws are accurate theoretically. However, its accuracy is not necessarily guaranteed when it is applied to practical engineering problems. In the present study, the scaling law for the vibration response of thin isotropic plates was therefore verified using experimental results of the model and prototype systems. The scaling law for the natural frequency of rectangular aluminum plates was derived and used to predict the natural frequency of the prototype system utilizing the experimental results of the model system. The accuracy of the scaling law was determined by comparing the scaled natural frequencies with the measured ones. The limitations of employing the scaling law for the vibration of thin plate problems are given along with some precautions in setting up the experiment on the model system.

2. Natural frequency of rectangular plates

The classical differential governing equation for the vibration of isotropic rectangular thin plates can be written as [10]

$$\frac{\partial^4 W(x,y,t)}{\partial x^4} + 2 \frac{\partial^4 W(x,y,t)}{\partial x^2 \partial y^2} + \frac{\partial^4 W(x,y,t)}{\partial y^4} + \frac{\rho}{D} \frac{\partial^2 W(x,y,t)}{\partial t^2} = 0, \tag{1}$$

where W is the displacement in the out-of-plane direction, ρ is the mass density per unit area of the specimen, and D is the flexural rigidity of the plate. Assuming that the out-of-plane displacement is separable as a

function of position and time, i.e. W(x, y, t) = w(x, y)T(t), the governing equation is reduced to

$$\frac{\partial^4 w}{\partial x^4} + 2 \frac{\partial^4 w}{\partial x^2 \partial y^2} + \frac{\partial^4 w}{\partial y^4} - \frac{\omega^2 \rho}{D} w = 0, \tag{2}$$

where w is function of x and y only and ω is the natural frequency of the vibration.

With given boundary conditions, the vibration governing equation, Eq. (2), can be solved using either an analytical or numerical method. For simple-supported plates, the analytical closed-form solution is possible by assuming the out-of-plane displacement of the vibrated plate in the form of

$$w(x,y) = w_{mn} \sin \frac{m\pi x}{a} \sin \frac{n\pi y}{b},\tag{3}$$

where a and b are the dimensions of plate in the x and y directions, respectively. By substituting the assumed displacement function w(x,y) into the governing equation, the natural frequency of the plate is obtained and written as

$$\omega_{mn} = \frac{\pi}{2a^2} \sqrt{\frac{D}{\rho}} \left(m^2 + \frac{a^2}{b^2} n^2 \right),\tag{4}$$

where ω_{mn} are the natural frequencies of the plate in Hz, m and n are positive integers. It should be noted that, for plates with other boundary conditions, the natural frequencies are not available in the form of exact analytical expression. The numerical or finite element methods are required for specimens with clamped or free boundary conditions.

3. Scaling law for the vibration of plate

Although the natural frequencies of thin plates with combinations of simple support, clamped support or free boundary conditions are available, they may not be practically appropriate for engineering structures where accurate natural frequencies are required. The boundary conditions of practical structures are usually non-classical ones such as elastically restrained or imperfect boundary conditions, which are not easily modeled because the level of restraining is unknown. This is where the scaling law can be utilized to determine the vibration behavior of the structure or prototype of interest using the experimental results of the scaled model. The scaled model is either a scaled-down or scaled-up test specimen having complete similarity with the real structure. Although the boundary conditions of the prototype are not exactly known, they can be modeled in the scaled model using similar supports. Thus, the experimental results from the corresponding test specimen along with the scaling law can be used to predict the vibration behavior of the prototype. The derivation of the scaling law for vibration behavior is briefly derived in this section.

The scaling law for the vibration of rectangular isotropic plates is derived from the governing equation, Eq. (2), by comparing the governing equations of the model with that of the prototype. From both equations, the similitude invariant term, which leads to the scaling law, is obtained. Let the variables of the prototype and their corresponding model variables be related to each other as follows:

$$x_p = C_x x_m$$
, $y_p = C_y y_m$, $w_p = C_w w_m$, $D_p = C_D D_m$, $\omega_p = C_\omega \omega_m$, and $\rho_p = C_\rho \rho_m$,

where subscripted p refers to the prototype system and subscripted m refers to the model system, and C_i are the scaling factors of the i parameters. To derive the similitude invariant, the governing equations of the model and prototype are written as the following:

$$\frac{\partial^4 w_m}{\partial x_m^4} + 2 \frac{\partial^4 w_m}{\partial x_m^2 \partial y_m^2} + \frac{\partial^4 w_m}{\partial y_m^4} - \frac{\omega_m^2 \rho_m}{D_m} w_m = 0, \tag{5}$$

$$\frac{C_{w}}{C_{x}^{4}} \frac{\partial^{4} w_{m}}{\partial x_{m}^{4}} + 2 \frac{C_{w}}{C_{x}^{2} C_{v}^{2}} \frac{\partial^{4} w_{m}}{\partial x_{m}^{2} \partial y_{m}^{2}} + \frac{C_{w}}{C_{v}^{4}} \frac{\partial^{4} w_{m}}{\partial y_{m}^{4}} - \frac{C_{\omega}^{2} C_{\rho} C_{w}}{C_{D}} \frac{\omega_{m}^{2} \rho_{m}}{D_{m}} w_{m} = 0.$$
 (6)

It should be noted that Eq. (6) can be written in the same form as Eq. (5) with subscript "p" instead of subscript "m." However, the scaling factors are utilized so that the governing equations of both systems can be compared and simplified. Comparing both equations, the vibration behavior of the model and of the prototype are similar if groups of the scaling factors in Eq. (6) are all equal. This implies that Eq. (6) can be reduced to Eq. (5) when the scaling factor groups are canceled out. Thus, the similitude requirement is obtained as

$$\frac{1}{C_{v}^{4}} = \frac{1}{C_{v}^{2}C_{v}^{2}} = \frac{1}{C_{v}^{4}} = \frac{C_{\omega}^{2}C_{\rho}}{C_{D}}.$$
(7)

By assuming that the model and prototype have a geometric similarity ($C_x = C_y = C_a = C_b$), the similarity requirement is simplified to

$$\frac{C_{\omega}^2 C_{\rho} C_b^4}{C_D} = 1. \tag{8}$$

Eq. (8) is the similitude invariant of the vibration behavior of rectangular plates. This invariant can be reduced to the scaling law of plate natural frequency as

$$\omega_p^2 = \omega_m^2 C_D \frac{b_m^4 \rho_m}{b_p^4 \rho_p}. \tag{9}$$

This scaling law relates the natural frequencies of the model to that of the corresponding prototype. The derived scaling law is valid for a model–prototype pair with complete geometric similarity, i.e. $C_a = C_b$ or both systems having the same aspect ratio. The scaling law can be verified with the theoretical solution shown in the previous section. As shown in Table 1, rectangular aluminum plates with b = 250 mm and an aspect ratio, a/b, of 1–3.5 are selected as models and used to predict the natural frequencies of the stainless steel prototypes with a width b of 200 and 300 mm, respectively. The model plates are assumed to be Al6061-T6 with E = 68.9 GPa, v = 0.35, density = 2.71×10^3 kg/m³, and plate thickness h = 2 mm, while the prototypes are stainless steel with E = 193 GPa, v = 0.27, density = 7.86×10^3 kg/m³, and plate thickness h = 2 mm. The fundamental natural frequencies of the models determined from the analytical solution, Eq. (4), are shown in column 2. These natural frequencies are substituted into the scaling law to predict the scaling natural frequencies of the prototypes, as presented in the " ω_{Scaling} " columns. The scaling frequencies are verified by the theoretical solutions shown in column 3 and 5. The data confirms that the natural frequencies determined from the scaling law and those from the closed-form solutions are identical.

Therefore, the scaling law for the natural frequency of rectangular plate is verified, theoretically. The derived scaling law is applicable to a model and prototype pair with the same aspect ratio, although they are made of different materials. However, it is not assured that the scaling law will be accurate in real applications. The objective of the present study was therefore to validate the scaling law with the experiment results. Thus, vibration experiment was performed to determine the natural frequencies of the model and prototype

Table 1
The fundamental natural frequencies in Hz for Al6061-T6 specimens

Aspect ratio (a/b)	Aluminum model	Stainless steel	Stainless steel prototype								
	$b = 250 \mathrm{mm}$	$b = 200 \mathrm{mm}$		$b = 300 \mathrm{mm}$							
		$\omega_{ m Theory}$	$\omega_{ ext{Scaling}}$	$\omega_{ m Theory}$	$\omega_{ ext{Scaling}}$						
1.0	156.2	233.4	233.3	103.7	103.7						
1.5	112.8	168.5	168.5	74.9	74.9						
2.0	97.6	145.9	145.8	64.8	64.8						
2.5	90.6	135.4	135.4	60.2	60.2						
3.0	86.8	129.6	129.6	57.6	57.6						
3.5	84.5	126.2	126.2	56.1	56.1						

specimens. The measured natural frequencies of the models were then substituted into the scaling law to predict the natural frequencies of the prototypes. Subsequently, the scaling frequencies of the prototype were compared with the measured ones to determine the accuracy of the derived scaling law.

4. Experimental setup

Several samples of thin rectangular plates were tested to determine their first three natural frequencies. The specimens were composed of aluminum, structural steel and stainless steel rectangular thin plates. The boundary conditions of the test panels were a combination of the knife-edge support and free boundary conditions. The knife-edge support was employed to simulate the theoretically simple-supported boundary condition. Schematic drawings of the specimens' dimensions and boundary conditions are shown in Fig. 1. The boundary of specimen supported by the knife-edge constraint is designated as "S," while the free supported edge is represented by "F." The boundary conditions of the specimens used in this study were SSSS, SFSS, SFSF, and SSFF, as shown in the figure. The first and second letters represent the boundary condition on the y = 0 and b edges, respectively. Similarly, the last two letters symbolize the boundary conditions on the other edges. The specimens were mounted in the test setup and equipped with an impact hammer and an accelerometer as shown in Fig. 2. The knife-edge support replicating the simply supported boundary condition was enforced by two stainless steel bars coupled on the specimen. The steel bars were machined in an inclined direction to form a knife-edge. With this support, the specimens were intentionally allowed to freely rotate but any out-of-plane displacement was restrained. The knife-edge supports were fixed with steel boxes with a number of machine screws. Additional machine screws were also used to push the knife-edge supports against the specimen surface. The assembly of steel boxes and knife-edge supports was also tested for natural frequency to confirm that their natural frequencies were not in the range of those of the specimens.

The vibration test for natural frequency was performed using an impact test [11,12]. Briefly, the specimens were excited by an impact hammer while the applied impulse was monitored by a dynamic signal analyzer. An accelerometer was placed on the specimen at a selected location to measure the plate response in terms of acceleration. It is recommended that the accelerometer should not be set on the node line of the vibration to avoid a low response signal. If the node line is unknown or uncertain, more than one measurement is recommended. In the present study, several pretests were conducted to determine a suitable location of the accelerometer. Besides the applied impulse from the impact hammer, the acceleration responses from the accelerometer were collected by a dynamic signal analyzer. The accelerations were recorded five times from five excitations of the impact hammer. These five sets of the acceleration data measured in the time domain were processed by a fast Fourier transform (FFT) algorithm using the dynamic signal analyzer to obtain the response in the frequency domain. From the vibration response in the frequency domain, the natural

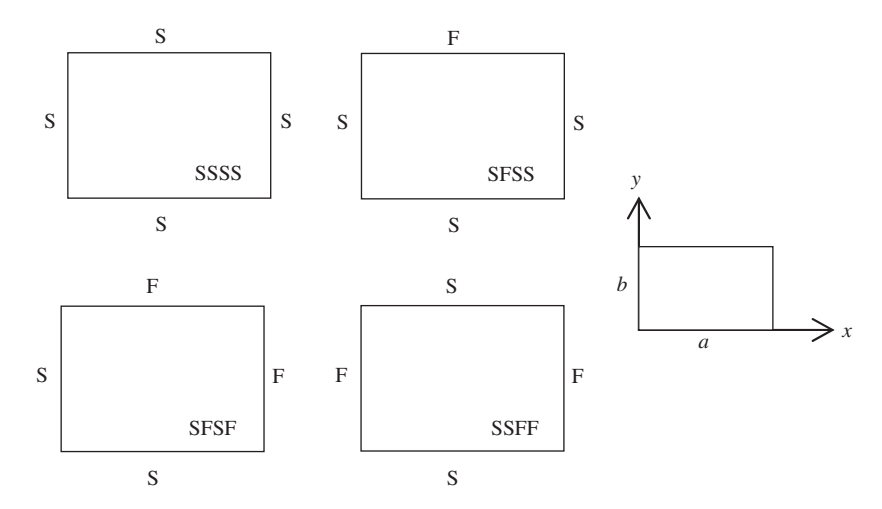


Fig. 1. Schematic drawings of the rectangular test specimens.

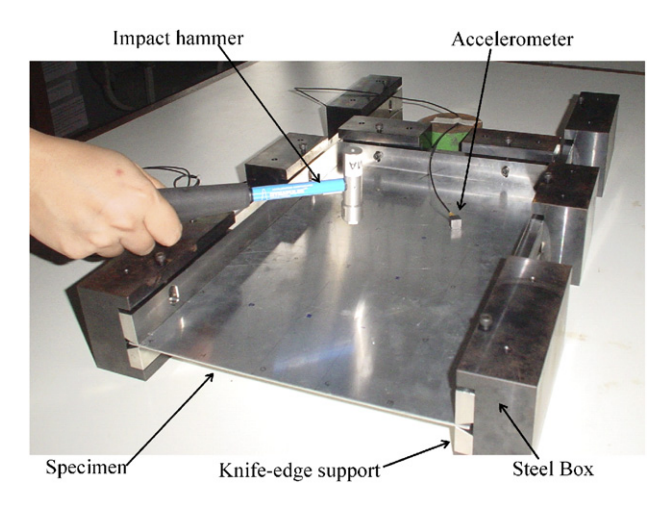


Fig. 2. Experimental setup with accelerometer and impact hammer.

frequencies of the specimen were identified from the peak of the response. Theoretically, there are infinite numbers of natural frequency; however, only the first three modes are of interest in this study. Fig. 3 shows examples of the vibration response measured in the frequency domain obtained from the dynamic signal analyzer for a $300 \times 300 \, \text{mm}^2$ aluminum plate with various boundary conditions. The measured natural frequencies in Hz for the first three modes of the specimen with SSSS boundary conditions are 149.0, 293.5, and 322.5 Hz, respectively. A response similar to those of shown in Fig. 3 can be obtained from experiments with excitation and accelerometer located at various positions. Ideally, the measured natural frequencies are independent of the location of either excitation or accelerometer. From the experiments, varying the position of excitation and the location of the response measurement has a minimal effect on the measured natural frequencies. In this study, a minimum of 5 experiments were performed for each specimen and the experimental natural frequency was determined from the average of each measurement.

5. Experimental results

Two sets of the experiment were conducted in this study to determine the accuracy of the scaling law using experimental measurements in two cases, i.e. (a) aluminum model and prototype of different sizes and (b) equal-size model-prototype pairs composed of different materials. The former part of the study was designed to investigate the size effect, while the material effect was studied in the latter part. To examine the size effect, the test specimens were nine aluminum plates with aspect ratios (a/b) of 1, 1.5, and 2 and a specimen nominal width b of 200, 250, and 300 mm, respectively. The natural frequencies of all the specimens with four combinations of boundary conditions were experimentally determined and used to validate the scaling law. The other set of experiments involved tests on four groups of specimens, i.e. two groups of aluminum, a group of structural steel and a group of stainless steel. The dimensions of the specimens in this set of experiments were $300 \times 200 \,\mathrm{mm}^2$ and $375 \times 250 \,\mathrm{mm}^2$.

5.1. Size effect

For the first part of the experiment, the measured natural frequencies for the SSSS aluminum plates with nine different dimensions are presented in Table 2. In the table, the test specimens are classified into three groups: rectangular plates with aspect ratios of 1, 1.5, and 2. The experimental data showed that the natural frequencies decreased with plate size. Similar experimental results were obtained for aluminum specimens with other boundary conditions but are not presented here. The specimens shown in Table 2 were assumed to be a model or a prototype and used to validate the scaling law, as shown in Table 3. From the three specimens with an aspect ratio of 1, three pairs of models and prototypes were assigned to the test specimens. As shown in

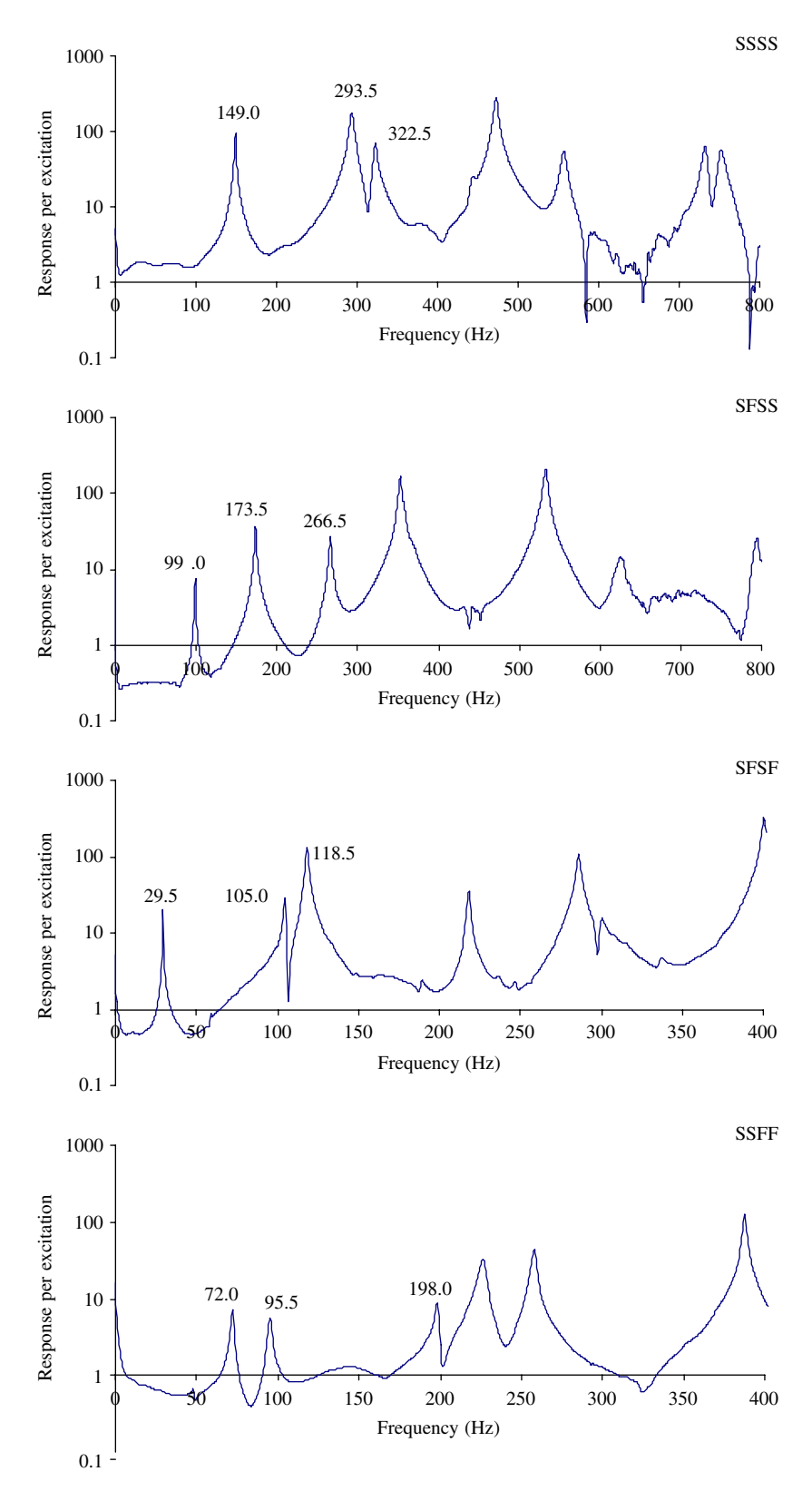


Fig. 3. Vibration response in frequency domain of $300 \times 300 \,\mathrm{mm}^2$ aluminum plate.

Table 2
Measured natural frequencies of the SSSS aluminum specimens

Aspect ratio	Specimen size, $a \times b$	Natural frequency (Hz)							
	(mm ²)	1st mode	2nd mode	3rd mode					
1	200 × 200	309.8	676.9	729.6					
	250×250	196.7	409.0	444.6					
	300×300	148.8	293.2	321.8					
1.5	300×200	221.2	376.3	580.7					
	375×250	150.5	255.4	376.6					
	450×300	99.6	171.4	257.4					
2	400×200	199.6	256.2	425.2					
	500×250	132.4	173.6	275.5					
	600×300	90.1	117.8	193.4					

Table 3
The measured and scaling natural frequencies for the SSSS aluminum specimens

Aspect ratio	Model	Prototype	Mode	Model	Prototype		
					ω_{Exp}	$\omega_{ ext{Scaling}}$	%Dis
1	200 × 200	300 × 300	1	309.8	148.8	137.7	-7.47
			2	676.9	293.2	300.8	2.61
			3	729.6	321.8	324.3	0.77
	250×250	200×200	1	196.7	309.8	307.3	-0.79
			2	409.0	676.9	639.1	-5.59
			3	444.6	729.6	694.7	-4.79
	300×300	250×250	1	148.8	196.7	214.3	8.93
			2	293.2	409.0	422.2	3.23
			3	321.8	444.6	463.4	4.23
1.5	300×200	450×300	1	221.2	99.6	98.3	-1.29
			2	376.3	171.4	167.2	-2.42
			3	580.7	257.4	258.1	0.27
	375×250	300×200	1	150.5	221.2	235.2	6.31
			2	255.4	376.3	399.1	6.05
			3	376.6	580.7	588.4	1.33
	450×300	375×250	1	99.6	150.5	143.4	-4.70
			2	171.4	255.4	246.8	-3.36
			3	257.4	376.6	370.7	-1.58
2	400×200	600×300	1	199.6	90.1	88.7	-1.54
			2	256.2	117.8	113.9	-3.34
			3	425.2	193.4	189.0	-2.29
	500×250	400×200	1	132.4	199.6	206.9	3.64
			2	173.6	256.2	271.3	5.87
			3	275.5	425.2	430.5	1.24
	600×300	500×250	1	90.1	132.4	129.7	-2.01
			2	117.8	173.6	169.6	-2.29
			3	193.4	275.5	278.5	1.09

column 2 and 3 of Table 3, a $200 \times 200 \text{ mm}^2$ specimen was set as a model and used to model the $300 \times 300 \text{ mm}^2$ prototype specimen. The other two model–prototype pairs were a $250 \times 250 \text{ mm}^2$ model with $200 \times 200 \text{ mm}^2$ prototype and a $300 \times 300 \text{ mm}^2$ model with $250 \times 250 \text{ mm}^2$ prototype. Specimens with aspect ratios of 1.5 and 2 were also assigned as models or prototypes in the same approach. In Table 3, columns 5 and 6 are the

measured natural frequencies of the model and prototype, respectively. The next column labeled as " ω_{Scaling} " presents the scaling natural frequencies of the prototypes. These scaling natural frequencies were determined from the scaling law shown in Eq. (9) using the measured natural frequencies of the model in column 5. The experimental and scaling natural frequencies shown in columns 6 and 7, respectively, were compared with each other. The percentage discrepancy of the scaling natural frequency shown in the last column was determined according to

$$\% \text{Dis} = \frac{\omega_{\text{Scaling}} - \omega_{\text{Exp}}}{\omega_{\text{Exp}}} \times 100\%. \tag{10}$$

Most of the comparisons show a good agreement between the scaling and measured natural frequency. The average of the absolute values of percentage discrepancy for experiment on all 27 model-prototype pairs is 3.30% with a standard deviation of 4.05%. The minimum and maximum percentage discrepancies are -7.47% and +8.93%, respectively, while more than half of the comparisons have a percentage discrepancy within $\pm 3\%$. There was no significant difference in percentage discrepancy for each vibration mode or plate aspect ratio. The causes of discrepancy between the scaling and measured natural frequencies are probably related to the imperfections of the boundary conditions and specimens. As described in the previous section, knife-edge supports of the test setup were controlled by several machine screws. In the experiments, the machine screws were tightened until the gaps between the specimen and support were invisible. Although it was desired to obtain identical boundary conditions for the model and its prototype, it was expected that the boundary conditions for each experiment would not be perfectly identical. Besides the imperfect boundary conditions, imperfections of specimens such as non-uniform thickness and the existence of plate curvature might be the cause of discrepancy between the scaling and measured behaviors. These two causes of error are classified as an experimental uncertainty, which is typical in experimental study and is very difficult to completely eliminate.

Another three comparable studies were performed on the same test specimens with boundary conditions of SFSS, SFSF, and SSFF. An inconsistency between the scaling and measured natural frequencies of all comparisons in terms of percentage discrepancy is shown in Table 4. The last two rows of the table show the average of absolute values of percentage discrepancy and the standard deviation of the percentage discrepancy, respectively. The overall average and standard deviations of the percentage discrepancy were 4.90% and 6.46%, respectively. The histogram in Fig. 4 represents the frequency distribution of the percentage discrepancy, which revealed that the distribution of the percentage discrepancy closely resembles a normal distribution and the percentage discrepancies of 95 from 108 comparisons were in the range of $\pm 10\%$. However, percentage errors for some pairs of model and prototype were slightly higher, especially for the experiments on the SFSF specimens. Eight values of percentage discrepancy from the experiments on this

Table 4
Percentage discrepancy between scaling and measured natural frequencies

Aspect	Model	Prototype	SSSS			SFSS		SFSS				SSFF		
ratio			Model	Mode2	Mode3	Model	Mode2	Mode3	Model	Mode2	Mode3	Model	Mode2	Mode3
1	200 × 200	300 × 300	-7.47	2.61	0.77	-0.86	3.75	0.06	-5.56	-2.12	-4.52	3.55	2.80	2.05
	250×250	200×200	-0.79	-5.59	-4.79	2.91	-2.62	2.19	1.37	0.45	-0.58	0.89	-4.90	-0.19
	300×300	250×250	8.93	3.23	4.23	-1.98	-1.03	-2.20	4.46	1.72	5.35	-4.28	2.30	-1.83
1.5	300 × 200	450 × 300	-1.29	-2.42	0.27	7.26	2.83	6.84	-17.74	-10.07	-10.96	-9.00	-15.54	-0.86
	375×250	300×200	6.31	6.05	1.33	-11.91	-8.50	-5.50	13.41	6.00	5.41	7.06	5.42	3.15
	450×300	375×250	-4.70	-3.36	-1.58	5.84	6.28	-0.95	7.19	4.90	6.54	2.64	12.31	-2.21
2	400 × 200	600×300	-1.54	-3.34	-2.29	3.94	2.75	2.57	-11.22	-14.29	-9.69	-6.24	-12.66	-6.07
	500×250	400×200	3.64	5.87	1.24	2.06	1.00	-0.46	-6.78	-1.55	2.48	-3.51	8.36	5.92
	600×300	500×250	-2.01	-2.29	1.09	-5.73	-3.64	-2.06	20.84	18.51	8.06	10.54	5.67	0.52
Average	•			3.30			3.62			7.47			5.20	
Standar	d deviation	L		4.05			4.63			9.46			6.64	

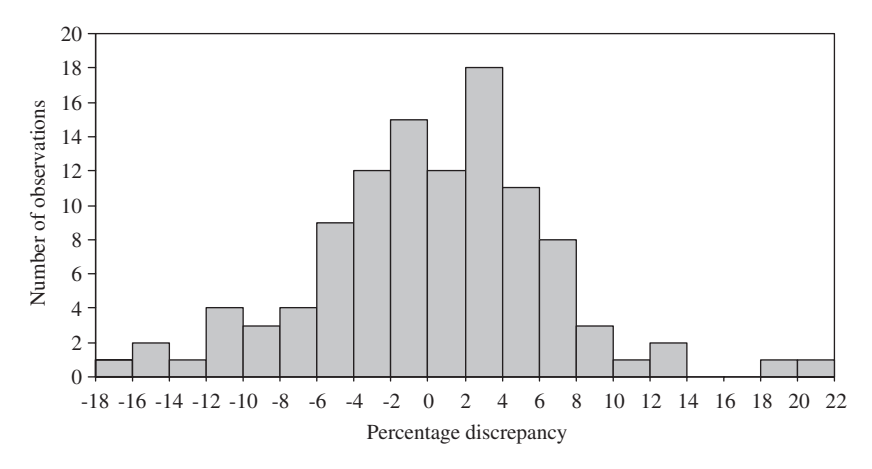


Fig. 4. Histogram of the percentage discrepancy between scaling and measured natural frequencies.

boundary condition resulted in a percentage discrepancy higher than $\pm 10\%$, compared with only four values and one value for SSFF and SFSS cases, respectively. The average of the absolute percentage discrepancy for SFSF specimens was 7.47%, which is higher than those of other boundary conditions. The higher percentage discrepancy of the scaling law observed in specimens with SFSF boundary conditions was probably caused by the particular characteristics of these boundary conditions. For SFSF specimens, the free boundary condition was imposed on two adjacent edges of the plate, i.e. two adjacent edges were free to move, as shown in Fig. 1. As a result, the specimen with this combination of boundary conditions tended to be slightly curved at the free corner because of its own weight. The degree of non-flatness of the test specimens was probably different for specimens with different dimensions, that is, the size effect had an influence on the accuracy of the scaling law in this case. So, the model and prototype with these boundary conditions did not have a complete similarity, resulting in a slightly higher percentage discrepancy for these specific boundary conditions.

Therefore, from the experimental study in the first part, the scaling law provided reasonable accuracy for modeling a prototype using a model with different dimensions. Uncertainties of the experiments in boundary condition and thickness are believed to be the sources of the discrepancy. To obtain a decent prediction from the scaling law, the experiment on the model specimen should be carefully performed to assure near-complete, if not perfectly complete, similarity with the prototype. The specimen size might slightly affect the precision of the scaling law in case of SFSF specimens because the flatness of the model and prototype cannot be maintained.

5.2. Material effect

The second part of the study was to determine the applicability of using a model with one type of material to predict the vibration behavior of the prototype made from another type of material. Four types of specimen including two types of aluminum specimen; called herein Aluminum-A and Aluminum-B, and the other two groups of steel and stainless steel specimens were tested. All specimens are commercially available in form of sheet metal. They were prepared and machined to the nominal dimensions of $300 \times 200 \, \text{mm}^2$ and $375 \times 250 \, \text{mm}^2$. The physical and mechanical properties of all the materials were experimentally determined and are presented in Table 5. It should be noted that the mechanical properties of Aluminum-A and Aluminum-B are more or less comparable and so are the properties of steel and stainless steel. Therefore, a total of eight thin plates were tested in this part of the study. Since material effect was investigated in this study, only specimens of the same size were assigned as a model–prototype pair. All specimens with four different boundary conditions were tested for the first three natural frequencies. The test results were then assigned as experimental natural frequencies of the model or the prototype. The accuracy of the scaling law was determined by comparing the scaling and experimental natural frequencies in the same manner as the previous study. Lists of the percentage discrepancies between both natural frequencies are shown in Table 6.

Table 5
Properties of materials used in the second part of the experiments

Material	Thickness (mm)	Mass density per area (kg/m²)	Modulus of elasticity (GPa)	Poisson ratio
Aluminum-A	1.81	5.10	62.3	0.316
Aluminum-B	1.42	3.63	58.0	0.320
Steel	1.95	15.29	197.0	0.346
Stainless steel	1.48	11.23	200.0	0.327

Table 6
Percentage discrepancies between scaling and measured natural frequencies demonstrating the material effect

Model	Prototype	Specimen size,	SSSS			SFSS			SFSF			SSFF			Avg.
		$a \times b \text{ (mm}^2\text{)}$	Model	el Mode2 Mode3	Mode3	Model	Mode2	Mode3	Model	1 Mode2	Mode3	Model	Mode2	Mode3	
Al-A	Al-B	300 × 200	-11.61	-4.67	-5.15	14.40	6.51	6.67	-11.72	6.12	-1.85	4.55	1.51	5.36	6.68
		375×250	-12.39	-1.71	-3.65	3.74	-4.28	-2.67	-8.44	-7.61	5.06	0.62	2.82	-1.77	4.56
	Steel	300×200	19.58	16.51	19.94	36.13	23.16	25.86	12.02	7.30	12.12	24.56	14.97	19.69	19.32
		375×250	26.84	27.68	18.63	21.57	14.04	18.60	19.94	7.45	16.24	33.47	20.87	23.96	20.77
	Stainless steel	300×200	22.11	23.80	22.48	34.08	27.18	29.63	12.37	11.87	19.42	33.50	22.67	29.91	24.09
		375×250	27.03	32.71	24.02	23.71	20.23	22.16	17.06	13.24	24.82	34.32	28.02	21.06	24.03
Al-B	Steel	300×200	35.29	22.22	26.45	18.99	15.63	17.99	26.89	1.12	14.23	19.14	13.26	13.61	18.74
		375×250	44.77	29.90	23.13	17.19	19.14	21.85	30.99	16.30	10.64	32.65	17.55	26.20	24.19
	Stainless steel	300×200	38.15	29.87	29.13	17.20	19.41	21.52	27.28	5.42	21.67	27.69	20.84	23.30	23.46
		375×250	44.99	35.01	28.72	19.25	25.61	25.51	27.85	22.56	18.81	33.49	24.51	23.24	27.46
Steel	Stainless steel	300 × 200	2.11	6.26	2.12	-1.51	3.26	2.99	0.31	4.26	6.51	7.18	6.69	8.53	4.31
		375×250	0.15	3.94	4.54	1.76	5.43	3.00	-2.40	5.39	7.38	0.64	5.92	-2.34	3.57

The first two columns of the table are materials of the model and prototype, respectively, with the specimen dimensions shown in column 3. The next twelve columns indicate the percentage discrepancies between the scaling and measured natural frequencies. The last column shows the averages of absolute percentage discrepancy for each pair of model and prototype. Clearly, the degree of discrepancy was separated into two groups; the lower one and the higher one. The scaling natural frequencies were well correlated with the measured ones for model-prototype pairs with the same type of material, i.e. a pair of Aluminum-A and Aluminum-B or a pair of steel and stainless steel. The averages of absolute percentage discrepancy for these model-prototype pairs were in the range of 3.57-6.68%. On the contrary, the scaling natural frequencies did not match the corresponding experimental results well for a pair of model and prototype with different types of material, for example, the Aluminum-A model and steel prototype or the Aluminum-B model and stainless steel prototype. The average percentage discrepancies varied from 18.74% to 27.46%. These fairly high percentage discrepancies are contradictory to the theoretical validation of the scaling law, shown in Table 1. It is proved that the scaling law is theoretically precise although both model and prototype are composed of different materials. These high percentage discrepancies can be explained by considering the boundary conditions provided by the experimental setup. Although aluminum or steel plates were restrained by the same knife-edge supports, they were probably not subjected to similar boundary conditions because of the difference between the stiffness of the knife-edge supports and the stiffness of the test specimens. The knifeedge supports which were used to simulate the simply supported boundary condition were made of stainless steel with an elastic modulus of about 200 GPa. Because of the comparable stiffness, when steel or stainless steel specimens were mounted on the knife-edge support, an approximate simple support was achieved, supposedly. On the other hand, it would seem that a near-clamped support was obtained for the experiments of the aluminum plates due to the mismatch in stiffness between the specimen and the support. This hypothesis

can be tested by comparing the experimental results of the SSS specimens with the theoretical solutions, as shown in Fig. 5. The experimental natural frequencies of all eight specimens with knife-edge supports on all edges, i.e. SSSS specimens, were plotted and compared with the theoretical solutions. In the figure, the experimental natural frequencies of the first three vibration modes of both $300 \times 200 \,\mathrm{mm}^2$ and $375 \times 250 \,\mathrm{mm}^2$ specimens with different materials are shown, labeled as "Exp". The theoretical natural frequencies of the specimens with all edges simple supported and all edges clamped were also plotted, labeled as "Theory (SSSS)" and "Theory (CCCC)," respectively. Obviously, all of the experimental natural frequencies of the aluminum specimens (both Aluminum-A and Aluminum-B) were close to the theoretical solutions of the CCCC specimens. In contrast, the experimental results of the steel and stainless steel specimens closely approximated to the theoretical solutions of the SSSS specimens. Because of the greater stiffness of the support, the aluminum specimens were probably not allowed to rotate as much as the steel specimens were, although they were constrained by the same supports. Therefore, the boundary condition provided by the experimental setup, which was supposed to be simple support, was a fairly clamped boundary condition for the aluminum specimens. For the steel specimens, the near simply supported boundary condition was successfully obtained as intended. That is, the very same knife-edge support provided quite different boundary conditions for the aluminum and steel specimens because the kinetic conditions of both types of material were different. The high percentage discrepancy in this case was not caused by experimental uncertainty as of those in Section 5.1, but was the result of the dissimilar boundary conditions which violated the similarity requirements. It is concluded that, in practice, the type of material of the model indirectly affects the accuracy of the scaling law because specimens with different types of material may be supported differently by the same support.

To confirm that the derived scaling law is applicable for a model and prototype composed of different materials if their boundary conditions are sufficiently comparable, an additional set of experiments was performed. The supplementary tests were similar to the experiments shown in Table 6 but boundary conditions for the specimens were free boundary condition on all edges (FFFF). The specimens used in the experiment included all four groups of materials with plate dimensions of $300 \times 200 \,\mathrm{mm^2}$ and $375 \times 250 \,\mathrm{mm^2}$. The FFFF boundary condition was set up by hanging the test specimen using a small rope. With this test setup, the specimens were allowed to freely vibrate in an out-of-plane direction when excited by the impact hammer. The first three natural frequencies were experimentally determined and assigned as a model or a prototype similar to the study shown in Table 6. The percentage discrepancies between the scaling and measuring natural frequencies for the experiment with FFFF boundary conditions are presented in Table 7.

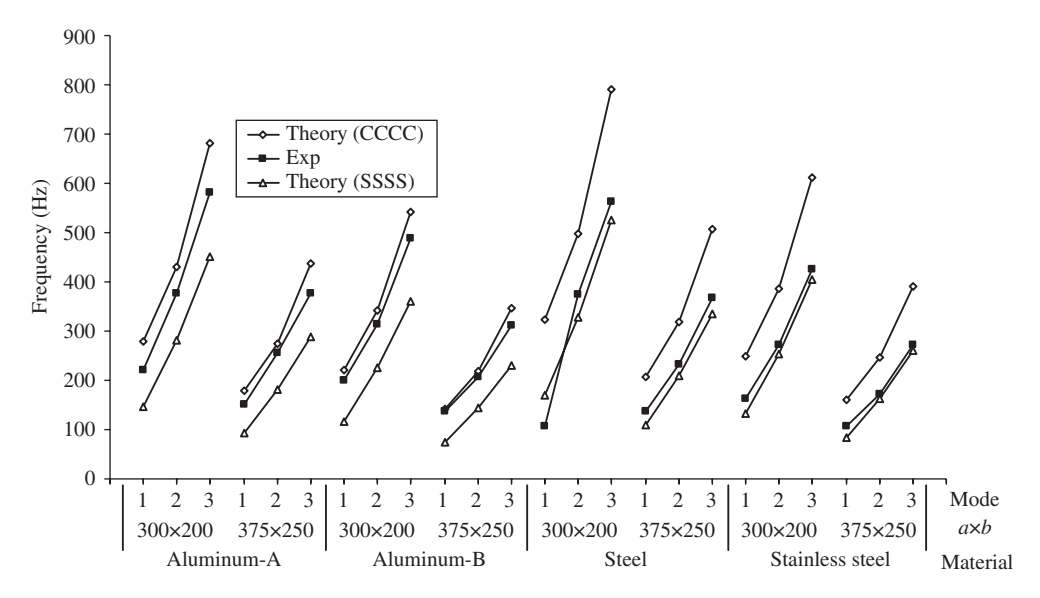


Fig. 5. Experimental and theoretical natural frequencies of the SSSS specimens.

Table 7
Percentage discrepancies between scaling and measured natural frequencies of FFFF specimens

Model	Prototype	Specimen size, $a \times b \text{ (mm}^2\text{)}$	FFFF			Avg.
		$u \wedge v$ (IIIIII)	Mode1	Mode2	Mode3	
Al-A	Al-B	300 × 200	10.47	-2.39	9.59	7.48
		375×250	14.15	3.53	7.11	8.26
	Steel	300×200	2.86	9.71	4.06	5.54
		375×250	5.71	-3.17	-7.84	5.57
	Stainless steel	300×200	2.28	6.98	9.13	6.13
		375×250	14.66	1.15	-1.53	5.78
Al-B	Steel	300×200	-6.89	12.39	-5.05	8.11
		375×250	-7.40	-6.47	-13.95	9.27
	Stainless steel	300×200	-7.42	9.59	-0.42	5.81
		375×250	0.45	-2.30	-8.06	3.60
Steel	Stainless steel	300×200	-0.57	-2.49	4.87	2.64
		375×250	8.47	4.46	6.84	6.59

The scaling law was able to predict the natural frequency of the prototype fairly well. From 36 comparisons, only 5 model–prototype pairs had a percentage error higher than $\pm 10\%$. The averages of absolute percentage discrepancy for each pair of model and prototype ranged from 2.64% to 9.27%. Unlike the experiments shown in Table 6, there is no significant difference in percentage error between specimens of the same and different types of materials. Experimental results from either aluminum or steel models were able to predict the behavior of the prototypes with comparable accuracy. A good prediction by scaling law is achieved in the experiment with FFFF boundary conditions because of the similarity of the boundary conditions of the model and prototype are similar, geometrically and kinetically. Thus, the scaling law is applicable for a model and prototype composed of different materials if the boundary conditions of both systems have sufficient similarity. The boundary conditions of two systems are said to be identical if they have geometric and kinetic similarities. The same set of supports may not provide identical boundary conditions for each specimen because of the mismatch of material properties between specimen and support causing kinetic dissimilarity.

6. Conclusions

This study derives the scaling law and similitude requirements for vibration response of rectangular thin plates. The scaling law was theoretically verified and found to be exact for a pair of models and prototypes with complete similarities. To determine the accuracy of the scaling law in practice, an experimental setup was prepared to accommodate the vibration experiment. The specimen was excited by an impact hammer and measured for vibration response using an accelerometer. The natural frequencies could be identified from the peaks of the response in the frequency domain. In the first part of the experiment, the scaling law was applied to a pair of models and prototypes with the same material. From 108 comparisons, the average percentage error between the scaling and experimental natural frequencies was 4.90%. This fairly low percentage discrepancy confirms that scaling law is accurate and practical in engineering applications. The experimental uncertainty in term of imperfect boundary conditions and specimens is probably the cause of this slight discrepancy. However, it is noticed that the scaling natural frequency for some cases of SFSF plates did not correspond well with the measured data. The sources of this error were not only caused by the experiment uncertainty but also caused by the fairly high degree of dissimilarity between the model and prototype specimens, i.e. curvature of the test specimens due to two adjacent edges having no support. For specimens with a combination of these particular boundary conditions, the size effect influenced the accuracy of the scaling law because of the dissimilarity in plate configuration of the model and prototype. In the second part of the study, natural frequencies of the prototypes were predicted using model specimens of different materials. The data shows that the scaling natural frequencies were not very well matched to the experimental ones if the model and prototype were composed of different types of materials. In comparison with the theoretical solutions, it is believed that the boundary conditions of the model and prototype are different, resulting in a very high percentage discrepancy of the scaling natural frequency. This suggests that boundary conditions on the test specimens are not only dependent on the geometry of the support but also on the kinetic conditions of the support. Additional experiments were performed on specimens made of different materials using FFFF boundary condition to validate the scaling law for model and prototype with identical boundary conditions and composed of different materials. Without a support, the boundary conditions of the model and prototype are identical, thus, the accuracy of the scaling law is achieved as expected.

In conclusion, the derived scaling law is practical to employ in engineering applications. From this study, the discrepancy of the scaling solutions might develop from the uncertainty of the experiment, curvature of the specimens due to two adjacent free edges, and dissimilar boundary conditions due to a mismatch in the material properties of the specimen and support. Errors from the uncertainty of the experiment are fewer than those from other sources and can be kept minimal by carefully setting up the experimental conditions on the model to match those of the prototype. This type of error is typical in the experimental investigation and impossible to completely eliminate in practice. Errors from the latter two sources, on the other hand, are the result of the incomplete similarity conditions between the model and prototype. These causes of error could be eliminated by ensuring that the plate configurations and boundary conditions of both systems are completely identical. To utilize the scaling law, precautions should be taken for a specimen with some particular combinations of boundary conditions where plate configurations might be effected by the size of the test specimen. Moreover, without a procedure to obtain a complete similarity of boundary conditions of the model and prototype with different materials, it is strongly recommended that the model is prepared from the same material as the prototype. It is also worthwhile to further study the possibility of overcoming the difficulties in utilizing the support on different materials as well as the chance of deriving a scaling law for a model-prototype pair with different boundary conditions.

Acknowledgments

This research is supported by the Commission on Higher Education and Thailand Research Fund under project Grant No. RMU4880021.

References

- [1] E. Szucs, Similitude and Modelling, Elsevier Scientific Publishing Co., New York, 1980.
- [2] G.J. Simitses, Structural similitude for flat laminated surfaces, Composite Structures 51 (2001) 191-194.
- [3] J. Rezaeepazhand, G.J. Simitses, J.H. Starnes Jr., Use of scaled-down models for predicting vibration response of laminated plates, *Composite Structures* 30 (1995) 419–426.
- [4] P. Singhatanadgid, V. Ungbhakorn, Buckling similitude invariants of symmetrically laminated plates subjected to biaxial loading, SEM Annual Conference and Exposition, Milwaukee, WI, USA, June, 2002.
- [5] P. Singhatanadgid, V. Ungbhakorn, Scaling laws for vibration response of anti-symmetrically laminated plates, *Structural Engineering and Mechanics* 14 (2002) 345–364.
- [6] V. Ungbhakorn, P. Singhatanadgid, Similitude invariants and scaling laws for buckling experiments on anti-symmetrically laminated plates subjected to biaxial loading, *Composite Structures* 59 (2003) 455–465.
- [7] J.J. Wu (Ed.), Letter to the editor: the complete-similitude scale models for predicting the vibration characteristics of the elastically restrained flat plates subjected to dynamic loads, *Journal of Sound and Vibration* 268 (2003) 1041–1053.
- [8] J.J. Wu, Dynamic analysis of a rectangular plate under a moving line load using scale beams and scaling laws, *Computers and Structures* 83 (2005) 1646–1658.
- [9] J.J. Wu, M.P. Cartmell, A.R. Whittaker, Prediction of the vibration characteristics of a full-size structure from those of a scale model, *Computers and Structures* 80 (2002) 1461–1472.
- [10] D.J. Gorman, Free Vibration Analysis of Rectangular Plates, Elsevier, New York, 1982.
- [11] J.P. Lecointea, R. Romarya, J.F. Brudnya, T. Czaplab, Five methods of stator natural frequency determination: case of induction and switched reluctance machines, *Mechanical Systems and Signal Processing* 18 (2004) 1133–1159.
- [12] G.P. Zou, M. Naghipour, F. Taheri, A nondestructive method for evaluating natural frequency of glued-laminated beams reinforced with GRP, *Nondestructive Testing and Evaluation* 19 (2003) 53–65.

Reprint

Singhatanadgid, P. and Sukajit, P., "Determination of buckling load of rectangular plates using measured vibration data." International Conference on Experimental Mechanics (ICEM2008), Nanjing, China, 8-11 November 2008.

Determination of buckling load of rectangular plates using measured vibration data

Pairod Singhatanadgid*, Padol Sukajit Department of Mechanical Engineering, Chulalongkorn University, Bangkok 10330, Thailand

ABSTRACT

In this study, the vibration correlation technique was introduced to determine the buckling load of rectangular thin plates. It is theoretically shown that the natural frequency approaches zero when the applied compressive load approaches the buckling load of the plate. To avoid the effects of premature out-of-plane deformation, it is proposed in this study that the buckling load is to be identified using the natural frequencies of plates under tensile loading. A set of aluminum plates was tested for natural frequencies using an impact test method. Specimens with two types of boundary conditions, i.e., CCCC and CCCF, were included in the experiment. The square of the measured natural frequency was plotted against the applied load and extrapolated to determine the predicted buckling load. The buckling loads from vibration data compare closely with numerical solutions. The average percentage differences between the measured buckling loads and the numerical solutions are 1.24 % and -1.14 % for specimens with CCCC and CCCF boundary conditions, respectively. In conclusion, the buckling load of rectangular thin plates can be experimentally identified with acceptable accuracy using vibration data. This approach is very useful especially for structures with unknown or imperfect boundary conditions where analytical or numerical solutions to the problem are not available.

Keywords: Buckling load, vibration, natural frequency, thin plate, experiment

1. INTRODUCTION

Buckling load is one of the important parameters which should be considered in the design of thin, plate-like structures subjected to compressive loading. The stability of plates has been investigated using theoretical, numerical and experimental approaches. For experimental studies, identification of the buckling point is an important process, since it directly affects the accuracy of the measured buckling load. In an experiment, the buckling load of plates can be identified using various kinds of plots, for example: 1) a plot of in-plane loads vs. out-of-plane displacement; 2) a plot of in-plane loads vs. end-shortening; 3) a plot of in-plane loads vs. difference of surface strains; and 4) a plot of the ratio of out-of-plane displacement to in-plane load vs. out-of-plane displacement [1]. Chai et al. [2] compared the experimental buckling load of composite plates with theoretical solutions. The discrepancies between the experimental and theoretical solutions ranged between -7 % and +11 %. Tuttle et al. [3] determined buckling loads from plots of applied in-plane load vs. out-of-plane displacement of composite panels, and compared the experimental results to numerical predictions obtained using a Galerkin method. Although the average percentage error between the measured and predicted buckling loads is low, the standard deviation of the percentage error is as high as 15%. The difficulties of identifying the buckling load using a static test method were documented. In particular, drawing two lines in the pre-buckling and post-buckling regions to identify the buckling point depended on personal judgment, and could be a cause of error.

There is a need for an alternative approach to experimentally identify the buckling load of a plate. In this paper, the vibration correlation technique (VCT) is explored. Lurie and Monica [4] showed that the square of the frequency of the lateral vibration of a thin plate with simple supports on all edges is linearly related to the end load. They also conducted some experiments on elastically restrained columns, rigid-joint trusses, and thin flat plates. The authors reported that VCT was successfully employed to predict the buckling load of only columns and trusses. For flat plates, because of the initial curvature, the buckling load cannot be predicted by the proposed method. However, Chailleux et al. [5] later showed that with a carefully designed experimental setting, VCT can be used to determine the buckling load with satisfactory accuracy.

*Pairod.s@chula.ac.th; phone 66 2 218-6595; fax 66 2 252-2889

In this research, the relationship between buckling and vibration behavior of thin plates is investigated. The relationship between applied in-plane load and the natural frequency of plates is derived from the differential governing equations of both problems. The derived relationship, which is applicable to thin plates with any boundary conditions, is verified using a numerical method. Because of premature curvature, which is usually detected even before the specimen has buckled, it is proposed in this study that the buckling load be determined from the vibration of a plate subjected to tensile loading. A test frame, capable of applying tensile and compressive loading to a specimen, was prepared. A series of vibration tests was performed to determine the natural frequencies of the plates. The vibration data, along with the derived relationship, are used to predict the buckling load. Experimental buckling loads are compared to the numerical solutions to verify the proposed technique.

2. RELATIONSHIP BETWEEN VIBRATION AND BUCKLING BEHAVIORS

Vibration and buckling behaviors of a thin plate are investigated and their relationship is derived in this section. A rectangular plate with a dimension of $a \times b$ is subjected to a uniform uniaxial loading N_x , as shown in Fig. 1. The buckling load of a plate-represented by \overline{N}_x - is the in-plane compressive load N_x at which buckling occurs. For vibration behavior, the natural frequencies of a plate can be determined for a specimen with a given N_x . It should be noted that \overline{N}_x and N_x refer to the same in-plane load; however, \overline{N}_x is the buckling load which must be a compressive load (negative value), while N_x is the applied in-plane load which can be either tension or compression. The governing equations for buckling and vibration of a thin isotropic plate are:

$$\frac{\partial^4 w}{\partial x^4} + 2 \frac{\partial^4 w}{\partial x^2 \partial y^2} + \frac{\partial^4 w}{\partial y^4} - \frac{\overline{N}_x}{D} \frac{\partial^2 w}{\partial x^2} = 0 \tag{1}$$

and

$$\frac{\partial^4 w}{\partial x^4} + 2 \frac{\partial^4 w}{\partial x^2 \partial y^2} + \frac{\partial^4 w}{\partial y^4} - \frac{N_x}{D} \frac{\partial^2 w}{\partial x^2} - \frac{\omega^{*2} \rho}{D} w = 0,$$
 (2)

respectively. The relationship between natural frequency and applied in-plane load N_x can be determined by considering the governing equations, Eqs. (1) and (2). For a given plate with particular boundary conditions, it is widely known that the buckling mode is identical to one of the vibration modes. Specifically, the out-of-plane displacement of the buckled plate is the same as the out-of-plane displacement of one of the vibration modes. So, the governing of the buckling problem can be rewritten as:

$$L_1(w) - \overline{N}_x L_2(w) = 0$$
, (3)

where
$$L_1(w) = \frac{\partial^4 w}{\partial x^4} + 2 \frac{\partial^4 w}{\partial x^2 \partial y^2} + \frac{\partial^4 w}{\partial y^4}$$
 and $L_2(w) = \frac{1}{D} \frac{\partial^2 w}{\partial x^2}$.

Similarly, the governing equation of the vibration of loaded plates is written as:

$$L_{1}(w) - N_{x}L_{2}(w) - \omega^{*2}L_{3}(w) = 0$$
(4)

where $L_3(w) = \frac{\rho w}{D}$.

It should be noted that the terms containing derivatives of w are the same for both problems because the buckling mode and vibration mode are identical. From Eq. (3), the buckling load of a plate can be written as:

$$\overline{N}_{x} = \frac{L_{1}\left(w\right)}{L_{2}\left(w\right)}.\tag{5}$$

Similarly, the natural frequency of a plate, with and without the applied in-plane load N_x can be written as:

$$\omega^{*2} = \frac{L_1(w) - N_x L_2(w)}{L_3(w)} \tag{6}$$

and
$$\omega^2 = \frac{L_1(w)}{L_3(w)},\tag{7}$$

respectively, where ω^* is the natural frequency of a plate with applied load N_x , and ω is the natural frequency of a plate without an applied load. From Eqs. (5), (6) and (7), the ratio of the square of the natural frequency of a loaded plate to that of an unloaded plate is written as:

$$\left(\frac{\omega^*}{\omega}\right)^2 = 1 - \frac{N_x}{\bar{N}_x} \,. \tag{8}$$

The buckling load \overline{N}_x and the natural frequency of an unloaded plate ω in Eq. (8) are constant for a specific specimen. The variables in that equation are the natural frequency of the loaded plate ω^* and the applied in-plane load N_x . Thus, the square of the natural frequency (ω^{*2}) varies linearly with the applied load N_x . With the buckling load being a negative value, it is observed that the natural frequency of the plate increases with the applied tensile load. On the other hand, it decreases with the applied compression. Moreover, if the applied load N_x equals the buckling load of the plate, the natural frequency ω^* theoretically equals zero. With this observation, the natural frequencies of the loaded plate can be utilized to predict its buckling load by plotting ω^{*2} versus the in-plane load N_x . The buckling load can be determined from the applied load N_x at which the natural frequency approaches zero. Since this relationship is derived from the governing equations, it is applicable to specimens with any boundary conditions.

To verify the derived relationship in Eq. (8), a numerical study of the vibration and buckling of a plate was performed. A 200x200 mm² aluminum plate with 2 mm thickness was chosen as a specimen. The plate was assumed to be simply supported on the loading edges and clamp supported on the other two edges. The buckling load of this specimen was numerically determined using the Ritz method, and found to be -97.323 kN/m with buckling mode 2. Similarly, the Ritz method was employed to solve for natural frequencies of the plate subjected to in-plane loads. The square of the natural frequencies for the first three modes was plotted versus applied load, as shown in Fig. 2. The relationship between ω^{*2} and N_x is linear, as expected according to the derived relationship. The predicted buckling load can be determined by extrapolating the vibration data to the in-plane load at which the square of the natural frequency approaches zero. Trend lines of each vibration mode intercept the N_x axis at a different load level. The lowest compressive load is the buckling load, and its corresponding vibration mode shape is the predicted buckling mode. From the simulation, the predicted buckling is -97.322 kN/m and the buckling mode is (2, 1). The buckling behaviors determined from the vibration data compare closely with the numerical solution. The buckling mode is also similar to the corresponding vibration mode shape. Thus, the derived relationship shown in Eq. (8) is theoretically verified.

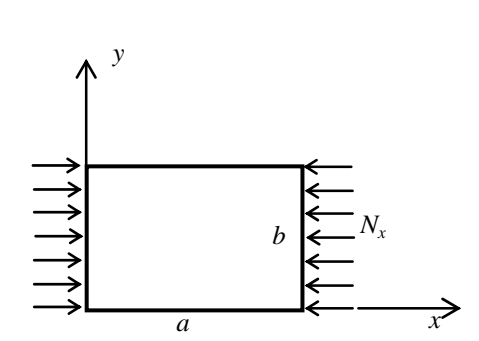


Fig. 1. A rectangular plate subjected to a uniaxial in-plane load N_x

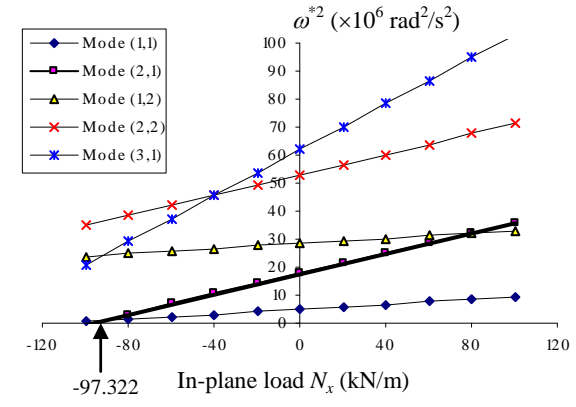


Fig. 2. Square of the natural frequencies of an aluminum plate vs. applied loading.

3. EXPERIMENTAL STUDY

A series of experiments was performed to determine the accuracy and reliability of the proposed technique. A set of aluminum plates was used; each plate was uniaxially loaded and tested for natural frequencies. The measured natural frequencies and applied loading were plotted, with results similar to those shown in Fig. 2. The predicted buckling load was identified using natural frequency data in the tensile-loading range.

3.1 Test frame

The test setup, shown in Fig. 3, was specifically designed to accommodate the loading configuration and vibration testing. The test frame is capable of applying CCCC and CCCF boundary conditions to the test specimens. Both tensile and compressive loads can be applied on the specimens. In-plane loads are applied horizontally using a hydraulic cylinder pressurized with a hand pump. The hydraulic cylinder is mounted on the right end frame, which is fixed to the left end frame using two guided columns. For a tension test configuration, the ram of the hydraulic cylinder applies a compressive force against crosshead #1. Loads are monitored using a load cell mounted between crosshead #1 and the hydraulic cylinder. Two linear bearings are embedded within the crossheads such that they can move linearly along two guided columns. The applied loading is transferred through two tension rods to crosshead #2. A rectangular thin plate is mounted with clamp support between crosshead #2 and crosshead #3. For a tension test configuration, crosshead #3 is blocked by two stoppers mounted on the guided columns, as shown in Fig. 3. In the case of a compression test, these stoppers are placed next to crosshead #2 to prevent horizontal motion of the crosshead. Crosshead #1 and tension rods are removed in a tension test configuration. The unloaded edges of the specimens are clamped by rigid stainless steel bars, denoted in Fig. 3 as "clamp support." These supports are mounted on the support holders, which are tightly clamped to the guided columns. Machine screws are used to push the steel supports against the specimen surface. In the experiments, the machine screws are finger-tightened until the gaps between the specimen and support are invisible. The clamp support on one of the unloaded edges of the specimen is removed so that a free edge is formed for CCCF boundary conditions.

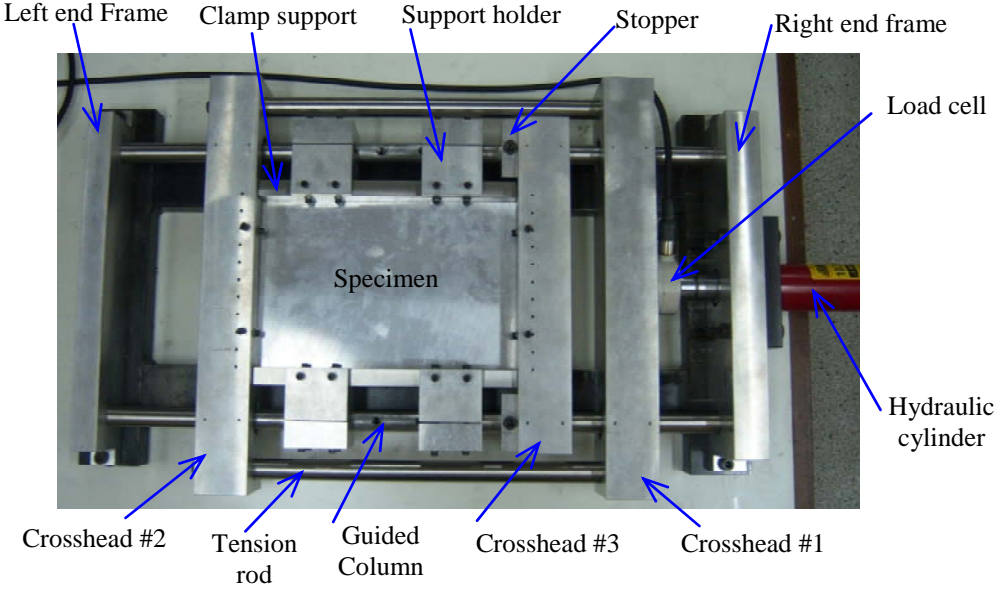


Fig. 3. Experimental setup of a specimen with CCCC boundary condition.

3.2 Specimens

The test specimens consisted of six thin plates with nominal dimensions $a \times b$ of 300x200, 200x200, and 150x200 mm². For each plate size, there were two specimens with different thicknesses. The specimens were prepared from 6061-T6 aluminum alloy, with mechanical properties of E = 70 Gpa and v = 0.33. The boundary conditions of the specimens included both CCCC and CCCF boundary conditions. The specimen's dimensions are summarized in the first three columns of Table 1.

3.3 Experimental procedures and results

In this study, the natural frequencies of a loaded plate are required data in order to predict the buckling behavior of the plate. Vibration testing was performed using an impact test, in which the specimen is excited by an impact hammer while the applied impulse is monitored by a dynamic signal analyzer. Acceleration response of the specimen was measured by an accelerometer placed on the specimen at a selected location. Acceleration data measured in the time domain were processed by a Fast Fourier Transform algorithm using the dynamic signal analyzer to obtain the frequency response function (FRF). From the vibration response in the frequency domain, the natural frequencies of the specimen were identified from the peak of the response. Vibration mode shape was also obtained from an imaginary part of the response function.

Natural frequencies of the specimen under unloaded, tensile-loaded and compressive-loaded conditions were determined, respectively. The square of the natural frequency was plotted against applied in-plane load. A typical relationship between ω^{*2} and N_x is presented in Fig. 4. Natural frequencies of vibration modes (1, 1), (1, 2) and (1, 3) are included. From the plot, the buckling mode of the specimen was determined to be mode (1, 1), since the trend line of this mode intersects the N_x axis at the lowest value. It is observed that ω^{*2} varies linearly with the applied load in the tensile-loading range, as expected. The relationship between both parameters in the compressive-loading range is not as linear as that in the tensile-loading range, which is contradicted by the result from the numerical simulation shown in Fig. 2. This observation regarding compressive-loading was also reported by Lurie and Monica [4]. It is speculated that the nonlinear behavior is a result of a premature curvature which develops before buckling. For this reason, the buckling load was determined using only vibration data of the specimen subjected to tensile loading. To determine the buckling load, a specimen was reloaded under increased levels of tensile loading. At each load level, a vibration test was performed to determine the natural frequency of the loaded plate. Only the natural frequencies of the relevant mode shape, the buckling mode, were collected. A plot of ω^{*2} versus N_x in the tensile-loading range was generated and extrapolated to determine the measured buckling load. Because the measurement of natural frequency is very sensitive to boundary conditions, the experiment was repeated 20 times by loosening and re-tightening the machine screws on the clamp supports. An average of the measured buckling load is reported as the buckling load obtained from vibration data, as shown in columns 5 and 8 of Table 1.

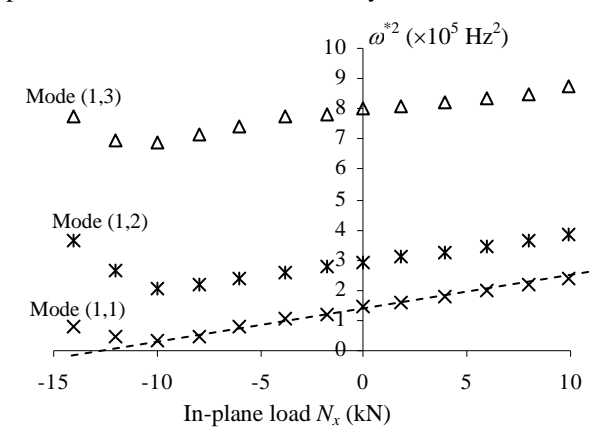
Specimen	Dimension	Thickness,		CCCC			CCCF	
No.	$(a \times b) \text{ mm}^2$	mm	Numerical Solution	Exp. Measurement	% Diff	Numerical Solution	Exp. Measurement	% Diff
1	200 200	2.022			2.21			2.42
1	300 x 200	2.032	27.17	27.77	2.21	7.48	7.67	2.43
2	300 x 200	2.298	39.29	39.74	1.14	10.82	10.23	-5.52
3	200 x 200	1.765	21.48	21.36	-0.53	8.96	8.43	-5.95
4	200 x 200	1.955	29.18	30.03	2.90	12.18	12.07	-0.90
5	150 x 200	1.745	24.03	24.26	0.94	14.41	14.26	-1.01
6	150 x 200	1.976	34.90	35.16	0.75	20.92	21.78	4.10

Table 1. Buckling load in kN of CCCC and CCCF specimens compared to numerical solutions.

3.4 Data reduction and discussion

The experimental buckling loads determined from a plot of natural frequencies of a loaded plate are compared with the numerical solutions in Table 1. Numerical buckling load and buckling mode are determined using the Ritz method, using beam functions as the assumed displacement functions. Buckling modes determined from the experiment correspond very well to the numerical solutions. Discrepancies between the experimental buckling load and the numerical solution are reported as a percentage difference. As seen in Table 1, the absolute percentage differences are as low as 0.53% and as high as 5.95%, with average percentage differences of 1.24% and -1.14% for CCCC and CCCF specimens, respectively. It should be noted that each percentage difference shown in Table 1 is an average value from 20 experiments. The discrepancy of the measured buckling load using vibration data is minimal compared to the experimental results using static methods [2, 3]. However, the standard deviation of all 240 measurements is found to be 5.57%. The distribution of percentage differences from all measurements is plotted as a histogram, and shown in Fig. 5. Although the overall average percentage difference is 0.05%, some measured buckling loads deviate from the numerical

solutions by a percentage difference as high as \pm 15%. This deviation of the measured buckling is probably a result of imperfect and non-identical boundary conditions.



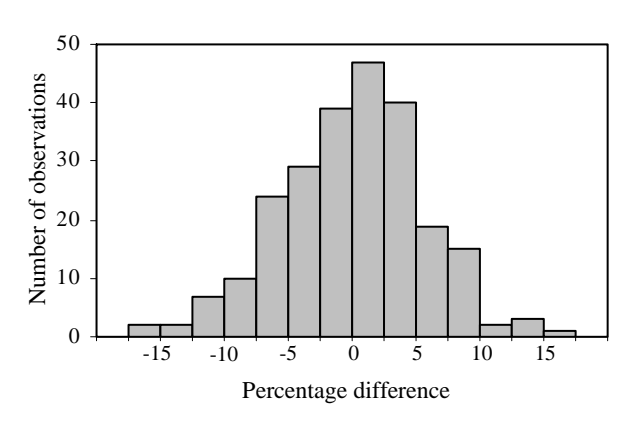


Fig. 4. Plot of the square of natural frequency vs. applied load of the 150x200 mm² specimen with CCCF boundary condition.

Fig. 5. Histogram of the percentage difference between measured and predicted buckling loads

4. CONCLUSIONS

The relationship between the natural frequency and the buckling load of a rectangular thin plate is investigated in this study. The derived relationship is utilized as a technique to identify the buckling load and buckling mode of the structure. Due to a premature curvature which usually develops before buckling, the use of vibration data in the tensile-loading range, where the premature curvature is negligible, is proposed in this study. To verify the accuracy of the technique, the experiment was performed on a test frame where the specimen was loaded and tested for natural frequencies. The measured vibration data were plotted against the in-plane load to determine the buckling load and buckling mode. The experimental results show that most of the measured buckling loads agree well with numerical solutions. Boundary conditions are believed to be a considerable factor in the high percentage difference between the measured and numerical buckling loads. In conclusion, the preliminary study demonstrates the accuracy and reliability of using vibration data in the tensile-loading range to determine the buckling load. Boundary conditions of the specimen have a considerable effect on the precision of the measured buckling load. Additional experiments should be performed on specimens made of different materials to obtain more concrete conclusions about the technique.

ACKNOWLEDGEMENTS

This research is supported by the Thailand Research Fund under project grant No. RMU4880021.

REFERENCES

- [1] Singer, J., Arbocz, J. and Weller, T., "Buckling experiments: experimental methods in buckling of thin-walled structures, Vol. 1," John Wiley & Sons, Chichester, UK (1992).
- [2] Chai, G.B., Banks, W.M. and Rhodes, J., "An experimental study on laminated panels in compression," Composite Structures 19(1), 67-87 (1991).
- [3] Tuttle, M., Singhatanadgid, P. and Hinds, G., "Buckling of composite panels subjected to biaxial loading," Experimental Mechanics 39(3), 191-201 (1999).
- [4] Lurie, H. and Monica, S., "Lateral vibrations as related to structural stability," J Appl Mech 195-204 (1952).
- [5] Chailleux, A., Hans, Y. and Verchery, G., "Experimental study of the buckling of laminated composite columns and plates," J Mech Sci 17, 489-498 (1975).

Reprint

Sukajit, P. and Singhatanadgid, P. "Identification of buckling load of thin plate using the vibration correlation technique," Proceedings of the 21st Conference of the Mechanical Engineering Network of Thailand (ME-NETT 21), Chonburi, Thailand, 17-19 October 2007, code AMM10.

The 21st Conference of Mechanical Engineering Network of Thailand 17-19 October 2007, Chonburi, Thailand

Identification of buckling load of thin plate using the vibration correlation technique

Padol Sukajit and Pairod Singhatanadgid*

Department of Mechanical Engineering, Chulalongkorn University, Bangkok 10330 Thailand Tel. 0-2218-6595, Fax 0-2252-2889, *Email: Pairod.S@chula.ac.th

Abstract

Stability is one of the important failure modes of thin-walled structures subjected to compressive loading. Besides theoretical and numerical studies, buckling of plate problem has been experimentally investigated. In this paper, the vibration correlation technique (VCT) is introduced as an alternative method to determine the buckling load. The relationship between applied in-plane load and the natural frequency of plates are derived from the differential governing equations of both problems. In this technique, square of the natural frequency of flexural vibration of plate is plotted against the applied in-plane load. It is shown that when the applied load approaches the buckling load of plate, the natural frequency of plate approaches zero. The square of the natural frequency is also linearly related to the applied load. Thus, the buckling load can be determined by extrapolating the data to the applied load at which natural frequency approaches zero. The vibration correlation technique is numerically verified by plotting square of natural frequency of loaded plate with applied in-plane load. The obtained buckling load from the plot is successfully compared with the buckling load determined by direct numerical method. The Ritz method along with the beam functions is employed to determine the natural frequency and the buckling load of rectangular isotropic plate with combined boundary conditions. Besides buckling load, buckling mode can also be determined from vibration mode. The specimens used in this study are rectangular isotropic plates with simple-clamped-simple-clamped (S-C-S-C) and simple-clamped-simple-free (S-C-S-F) boundary conditions.

Keywords: Buckling, Vibration, Plate, Vibration correlation technique, Ritz method.

1. Introduction

Stability is one of the important factors that should be

considered in design of thin-walled structures subjected to compressive loading. Besides buckling of columns and shells, buckling of plates is a problem that has been in the interest of many structural engineers and researchers. Studies in this field include theoretical, numerical, and experimental investigations. Identification of the buckling point of isotropic rectangular plates with simple support on all edges has been studied by Supasak [1]. In that study, buckling loads of aluminum plates were identified from the experiment using four different methods; i.e. 1) a plot of in-plane loads vs. out-of-plane displacement, 2) a plot of in-plane loads vs. end-shortening, 3) a plot of inplane loads vs. difference of surface strains, and 4) a plot of the ratio of out-of-plane displacement to in-plane load vs. out-of-plane displacement. Experimental buckling loads determined from the first three methods have a fairly high percent error compared with the theoretical solutions. The last identification method gave the value of buckling loads with percent error as high as 69% compared with the theoretical solutions. The author also indicated the difficulty in identifying the buckling load from the plots of measured data. Chai et. al. [2] compared experimental buckling load of composite plates with the theoretical solutions. The discrepancy between the experimental and theoretical solutions was ranged between -7 % and +11 %. Tuttle et. al. [3] determined buckling loads from plots of applied in-plane load vs. out-of-plane displacement of composite panels and compared the experiment results to numerical predictions obtained from Galerkin method. Although the average percent error between the measured and predicted buckling loads is very low, the standard deviation of the percent error is as high as 15%. This high deviation reflects the accuracy of the measurements. Thus, it is difficult to experimentally determine the buckling load of plates using static test method, since even the smallest amount of imperfection of the specimen, loading

apparatus, or boundary conditions can have an apparent impact on the buckling behavior. Moreover, in the static approach, there is a need to draw two lines in the prebuckling and post-buckling regions which may be a cause of error.

There is a need for an alternative approach to experimentally identify the buckling load of plate. In this paper, the vibration correlation technique (VCT) which is a dynamic approach is explored. Lurie and Monica [4] shown that square of the frequency of the lateral vibration of thin plate with simple supports on all edges is linearly related to the end load. They also conducted some experiments on elastically restrained columns, rigid-joint trusses, and thin flat plates. The authors reported that VCT was successfully employed to predict buckling load of only columns and truss. For flat plates, because of the initial curvature, the buckling load cannot be predicted by the proposed method. However, Chailleux et. al. [5] showed later that with a careful experiment setting, VCT can be used to determine the buckling load with satisfied

In this research, the relationship between buckling and vibration behavior of thin plate is investigated. The relationship between applied in-plane load and the natural frequency of plates are derived from the differential governing equations of both problems. The derived relationship is verified using a numerical method. This relationship also implies that buckling load of plate can be obtained from the vibration data of the loaded plates. So, an alternative method for buckling load identification using dynamic approach is proposed.

2. Relationship between vibration and buckling behaviors

In this study, the vibration and buckling behaviors of a rectangular isotropic plate as shown in Fig.1 are investigated. The buckling load of plate represented by \overline{N}_x is the in-plane load N_x at which buckling occurs. For vibration behavior, the natural frequencies of plate can be determined for a specimen with a given tensile or compressive load N_x .

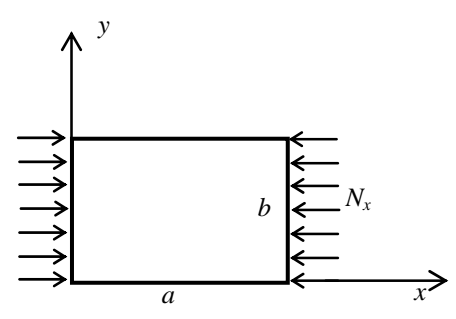


Figure. 1 A rectangular plate subjected to a uniaxial inplane load

The governing equation for buckling and vibration of thin isotropic plate can be written as;

$$\frac{\partial^4 w}{\partial x^4} + 2 \frac{\partial^4 w}{\partial x^2 \partial y^2} + \frac{\partial^4 w}{\partial y^4} - \frac{\overline{N}_x}{D} \frac{\partial^2 w}{\partial x^2} = 0$$
 (1)

$$\frac{\partial^4 w}{\partial x^4} + 2 \frac{\partial^4 w}{\partial x^2 \partial y^2} + \frac{\partial^4 w}{\partial y^4} - \frac{N_x}{D} \frac{\partial^2 w}{\partial x^2} - \frac{\omega^{*2} \rho}{D} w = 0, \qquad (2)$$

respectively.

w = out-of-plane displacementwhere

 ρ = mass of plate per unit area

$$D = \frac{Et^3}{12(1-v^2)}$$
 (Plate flexural rigidity)

 \overline{N}_r = buckling load

 N_x = applied in-plane load

 ω^* = natural frequency of the plate with applied in-plane load N_r

It should be noted that \overline{N}_x and N_x refer to the same inplane load, however, \bar{N}_x is the buckling load which must be a compressive load (negative value), while N_x is the applied in-plane load which can be either tension or compression.

For a given rectangular plate, the relationship between the natural frequency and an applied in-plane load N_x can be determined by considering the governing equations, Eq.(1 and 2). For a specimen with a given boundary conditions, it is widely known that buckling mode and vibration mode of the plates are identical. Specifically, the out-of-plane displacement of the buckled plate is identical to the out-of-plane displacement of one of the vibration mode. So, for a given specimen, the governing of the buckling problem can be rewritten as.

$$L_{1}(w) - \bar{N}_{x}L_{2}(w) = 0 \tag{3}$$

where
$$L_1(w) = \frac{\partial^4 w}{\partial x^4} + 2 \frac{\partial^4 w}{\partial x^2 \partial y^2} + \frac{\partial^4 w}{\partial y^4}$$

$$L_2(w) = \frac{1}{D} \frac{\partial^2 w}{\partial x^2}$$

Similarly, the governing of the vibration of loaded plates is written as:

$$L_{1}(w) - N_{x}L_{2}(w) - \omega^{*2}L_{3}(w) = 0$$
 (4)

where
$$L_3(w) = \frac{\rho w}{D}$$

It should be noted that the terms contained derivatives of w for both problems are the same because the buckling mode and vibration mode are identical. From Eq.(3), the buckling load of plate can be written as;

$$\bar{N}_{x} = \frac{L_{1}(w)}{L_{2}(w)} \tag{5}$$

Similarly, the natural frequency of plate with and without the applied in-plane load can be written as;

$$\omega^{*2} = \frac{L_1(w) - N_x L_2(w)}{L_3(w)}$$
 (6)

and

$$\omega^2 = \frac{L_1(w)}{L_2(w)} \tag{7}$$

where

 ω^* is natural frequency of a plate with applied load N_x ω is natural frequency of a plate without applied load

From Eq.(5-7), ratio of the square of natural frequency of the loaded plate to that of the unloaded plate is written as;

$$\left(\frac{\omega^*}{\omega}\right)^2 = 1 - \frac{N_x}{\bar{N}_x} \tag{8}$$

Since buckling load \overline{N}_x and natural frequency of the unloaded plate ω is constant for a given specimen, it is concluded that square of the natural frequency of the loaded plate ω^{*2} is linearly varied with the applied load N_x . Since this relationship is derived from the governing, it is independent of boundary conditions.

From the linear relationship between ω^{*2} and N_x shown in Eq.(8), with the buckling load being a negative value, it is notice that the natural frequency of the plate increases with the applied tensile load. On the other hand, it is decreased with the applied compression. Moreover, if the applied load N_x equals the buckling load of the plate, the natural frequency ω^* theoretically equals zero. With this observation, ones can utilize the natural frequencies of the loaded plate to predict the buckling load of plate by plotting ω^{*2} versus the in-plane load N_x . The buckling load could be determined from the applied load N_x at which the natural frequency approaches zero.

3. Numerical investigation

To verify the relationship between the natural frequency and buckling load of plate, natural frequencies of the loaded plate and buckling load of plate are determined. The vibration mode and buckling load are also investigated. Since the closed form solutions are available for all edges simple support (SSSS) specimen only, the numerical method is used in this study. Both vibration and buckling problems are solved using the Ritz method [6]. The total potential energy for the vibration of loaded plate can be written as;

$$\Pi = \frac{1}{2} \iint \left[D \left(\frac{\partial^2 w}{\partial x^2} + \frac{\partial^2 w}{\partial y^2} \right)^2 - 2(1 - v) D \left(\frac{\partial^2 w}{\partial x^2} \frac{\partial^2 w}{\partial y^2} - \left(\frac{\partial^2 w}{\partial x \partial y} \right)^2 \right) + N_x \left(\frac{\partial w}{\partial x} \right)^2 - \rho \omega^{*2} w^2 \right] dx dy$$

$$(9)$$

and the total energy for the buckling problem is represent by:

$$\Pi = \frac{1}{2} \iiint \left[D \left(\frac{\partial^2 w}{\partial x^2} + \frac{\partial^2 w}{\partial y^2} \right)^2 - 2(1 - v) D \left(\frac{\partial^2 w}{\partial x^2} \frac{\partial^2 w}{\partial y^2} - \left(\frac{\partial^2 w}{\partial x \partial y} \right)^2 \right) + \overline{N}_x \left(\frac{\partial w}{\partial x} \right)^2 \right] dx dy$$

$$(10)$$

To determine the natural frequency of the loaded plate, Eq.(9) is considered by treating N_x as a applied load which is known and ω^* is the unknown to be determined. For buckling behavior, the total energy in Eq.(10) is used with an unknown variables \overline{N}_x . To solve both problems, the out-of-plane displacement w is assumed to be;

$$w(x, y) = \sum_{m=1}^{M} \sum_{n=1}^{N} A_{mn} X_{m}(x) Y_{n}(y)$$
 (11)

 A_{mn} are the unknown coefficients representing vibration mode or buckling mode. $X_m(x)$ and $Y_n(y)$ are the basis

functions satisfied the boundary conditions at x = 0, x = a and y = 0, y = b, respectively. In this study, beam function is chosen as basis functions. For simple support on both ends, the function is represented by a well-known double sine series. For other boundary conditions, the beam functions can be written in form of; [7]

$$\varphi_{m}(r) = \gamma_{m} \cos\left(\frac{\lambda_{m} r}{L}\right) - \gamma_{m} \cosh\left(\frac{\lambda_{m} r}{L}\right) + \sin\left(\frac{\lambda_{m} r}{L}\right) - \sinh\left(\frac{\lambda_{m} r}{L}\right)$$
(12)

where φ is either X or Y, and r can be x or y. The values of γ_m and λ_m depend on the boundary condition of the plate. For case of clamp boundary condition on both ends, λ_m can be determined from roots of;

$$\cos \lambda_m \cosh \lambda_m = 1,$$

and γ_m is determined from:

$$\gamma_m = \frac{\cos \lambda_m - \cosh \lambda_m}{\sin \lambda_m + \sinh \lambda_m}.$$

For clamp-free boundary condition where one end is clamped and one end has no support, λ_m is determined from roots of;

$$\cos \lambda_m \cosh \lambda_m = -1$$

and γ_m is determined from;

$$\gamma_m = \frac{\cos \lambda_m + \cosh \lambda_m}{\sin \lambda_m - \sinh \lambda_m}.$$

The basis functions for the first four modes for the cases of clamp-clamp boundary condition and clamp-free boundary conditions are plotted as examples in Fig.(1)

To solve for the natural frequency and buckling load, the total potential energy is determined for each problem by substituting the approximate displacement functions Eq.(11) into the total potential energy Eq.(9,10), respectively. The displacement functions must be selected according to the boundary conditions of the plate. After performing integrations, the total potential energy is written in term of the undetermined coefficients $A_{\scriptscriptstyle \rm mm}$ and the natural frequency ω^* or buckling load \bar{N}_x for vibration and buckling problems, respectively. According to the principle of minimum total potential energy, the total potential energy is minimized with respect to the unknown coefficients $A_{\scriptscriptstyle mm}$ according to;

$$\frac{\partial \Pi}{\partial A_{mn}} = 0 \tag{13}$$

Eq.(13) is a system of $M \times N$ linear equations, which can be rearranged as a matrix form of generalized eigenvalue problems as:

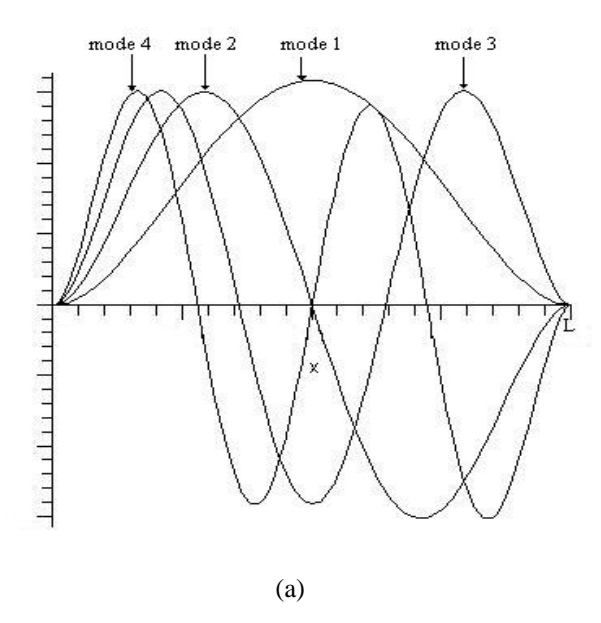
$$[A][C] - \omega^{*2}[B][C] = 0$$
, for vibration problem, and (14a)

$$[A][C] + \overline{N}_x[B][C] = 0$$
, for buckling problem. (14b)

where [A] and [B] are square matrices whose elements are determined from the plate properties. [C] is a column matrix of eigenvector A_{mn} . ω^{*2} and \overline{N}_x are the eigenvalues representing square of natural frequency and buckling load of plate, respectively. A number of eigenvalues will

be obtained after the generalized eigenvalue problem equation, Eq.(14), is solved. For vibration problem, each eigenvalue is square of the natural frequency of plates. However, only the lowest eigenvalue of Eq.(14b) is the buckling load which is of interest in buckling problem. The corresponding eigenvectors of each is used to determine the vibration mode or buckling mode by substituting into the displacement function Eq.(11).

Before implementing the Ritz method, convergence studies was performed to ensure that the number of term used in the displacement function is enough to give a converged solution. An aluminum rectangular plate is used in the convergence study. The mechanical properties of aluminum are assumed to be E=70 GPa, v=0.3, and $\rho=2707$ kg/m³ with plate thickness of 2 mm. The convergence of a rectangular plates with a=b=200 mm, and all edge clamp boundary condition is shown in Fig 2. It is observed that the buckling load converges when the value of m and n in the displacement function equals 5. The value of m and n used in this study is 12, i.e. there are 144 terms in the displacement function.



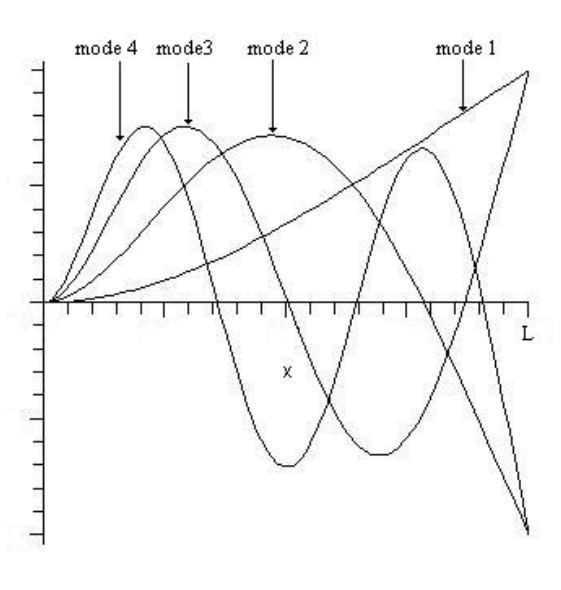


Figure 1. Displacement functions for (a) clamp-clamp boundary condition and (b) clamp-free boundary conditions.

(b)

4. Numerical results

In this study, three cases of aluminum plates are investigated using a numerical method outlined in the previous section. Dimensions, boundary conditions, and theoretical bucking load of plate are summarized in Table 1. The buckling loads are determined from the solution of generalized eigenvalue problem, Eq.(14b). This buckling load is considered herein as the "theoretical solution." Specimens with two different combinations of boundary condition are investigated. For SCSC boundary condition, the first letter S and third letter S represent the boundary condition on the x = 0 and x = a edges, respectively. Similarly, the second and fourth letters represent the boundary condition on the y = 0, and y = b edges, respectively. To verify the relationship shown in Eq.(8), the natural frequency of the loaded plate is determined for different applied in-plane loads N_x . The in-plane load can be either tension, compression, or no load. A generalized eigenvalue problem shown in Eq(14a) is set for the specimens with a particular applied load N_x . This applied load is treated as a known and constant value. The obtained square of natural frequency for each vibration mode is plotted against the applied in-plane load as shown in Fig. 3-5, for all specimens, respectively.

Table 1. Dimensions and boundary conditions of the specimen

вреч			
Specimen	Dimension	Boundary	Buckling load
No.	$a \times b \text{ (mm}^2)$	Condition	\overline{N}_x , (kN/m)
1	200 × 200	SCSC	-97.323
2	400 × 200	SCSC	-88.215
3	200×200	SCSF	-21.019

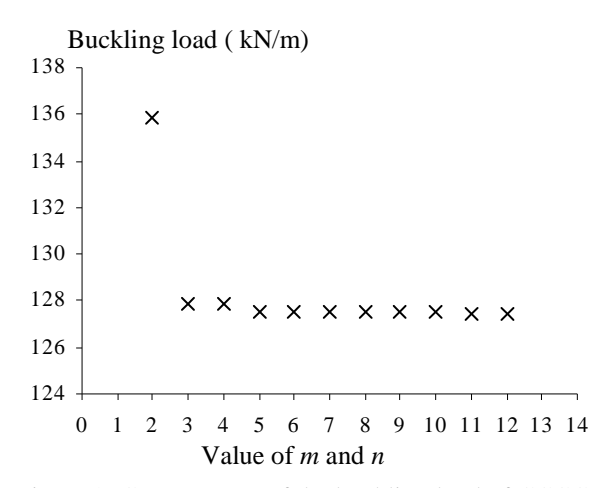


Figure 2. Convergence of the buckling load of CCCC aluminum plates

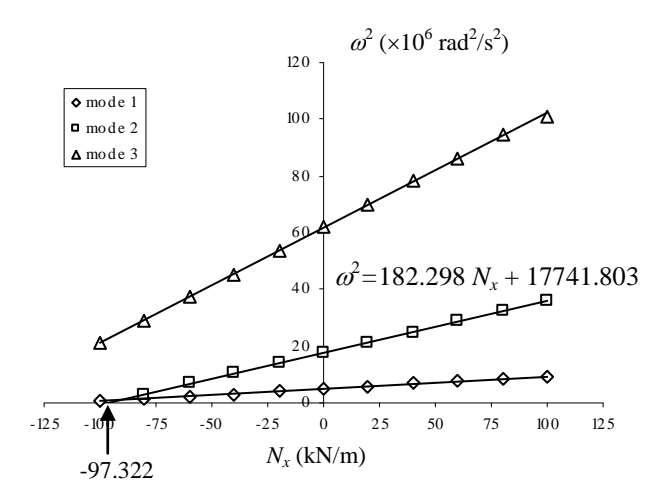


Figure 3. Plot of ω^{*2} and N_x of specimen No. 1

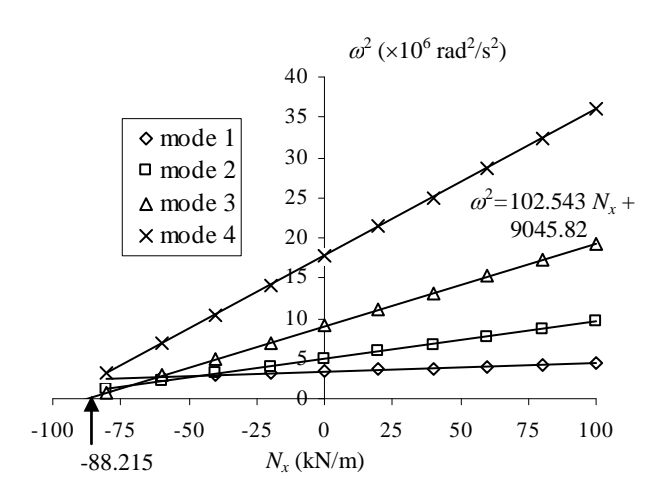


Figure 4. Plot of ω^{*2} and N_x of specimen No. 2

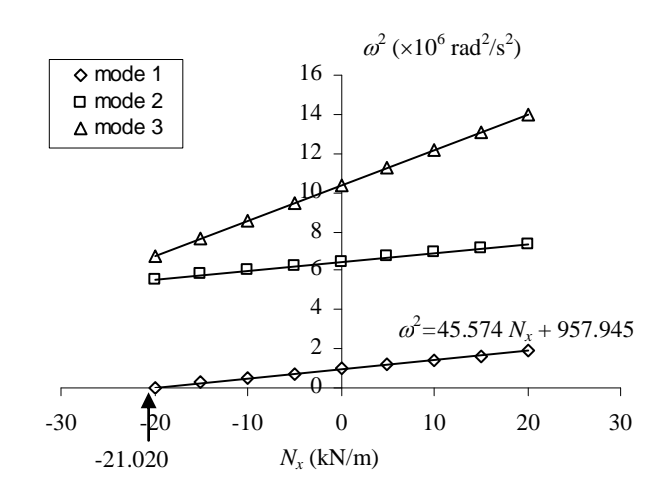


Figure 5. Plot of ω^{*2} and N_x of specimen No. 3

From Fig 3-5, the relationship between ω^{*2} and N_x is linear as expected. It is also shown that the natural frequency is increased as the in-plane load becomes higher in the tensile direction (positive N_x). On the other hand, the natural frequency approaches zero when the applied load is amplified in the compressive direction (negative N_x). The plots of ω^{*2} vs. N_x can be used to verified the relationship shown in Eq.(8) by extrapolating the value of N_x at which the natural frequency becomes zero. The extrapolation can be systematically performed by determined the equation representing the relationship between ω^{*2} and N_r for each mode of vibration and solved for N_r for zero natural frequency. The obtained N_r at zero natural frequency of each vibration mode are compared with each other. The lowest value of N_x at zero natural frequency shown in the figures is the predicted buckling load. In the figure, only the equation of ω^{*2} and N_x of the vibration mode with the lowest value of N_x at zero natural frequency is presented.

For the SCSC specimens with aspect ratios of 1 and 2, it is found that the predicted buckling loads are -97.322 and -88.215 kN/m, respectively, which are practically identical to the theoretical ones. The buckling mode for specimen No. 1 is mode 2 since the plot of mode 2 vibration intersects the applied load axis before other modes. With different aspect ratio, the predicted buckling mode for specimen No. 2 is mode 3. Predicted buckling modes for both cases are agreed with the solutions obtained from the buckling problem. Fig.6 shows the vibration mode corresponding to the vibration data shown in Fig.4. The theoretical buckling mode for specimen No.2 which is mode 3 is presents in Fig.7. Clearly, the predicted bucking mode using vibration data matches the theoretical solution very well. Besides specimen with SCSC boundary conditions, a SCSF specimen is also investigated. It is found that the derived relationship between ω^{*2} and N_x can be used to predicted the buckling load with very good accuracy. The predicted buckling load for the case of SCSF specimen is -21.020 kN/m compared with the theoretical solution of -21.019 kN/m. The buckling mode is also very well predicted.

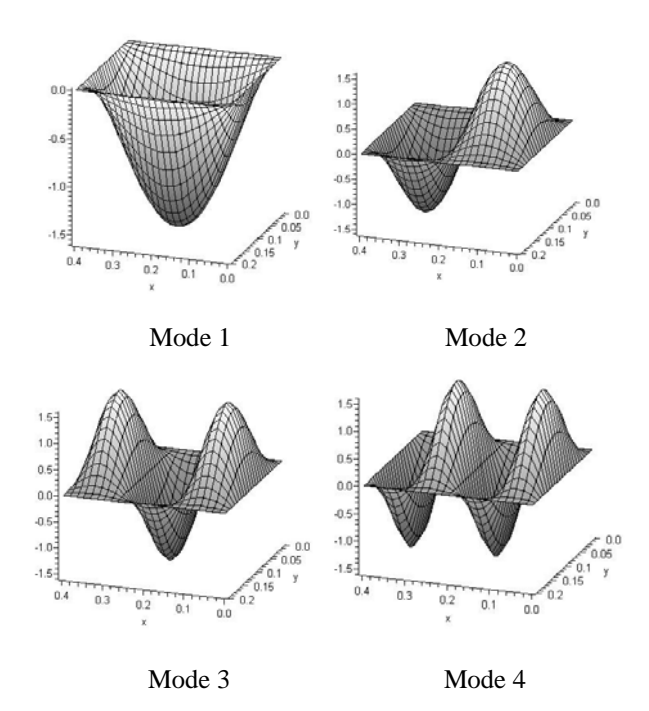


Figure 6. Vibration mode shapes of specimen No.2

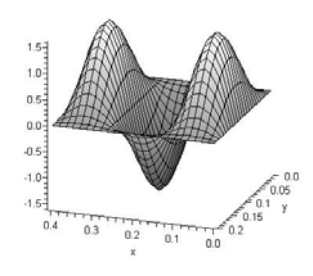


Figure 7. Buckling mode of specimen No.2

5. Conclusion

This research investigates the vibration response of isotropic rectangular plates subjected to uniform in-plane load. By considering the governing equations of the vibration and buckling problems, it is shown that square of the natural frequency of the loaded plate is linearly varied with the applied load. The natural frequency is increased with the tensile load and decrease with the compressive load. This relationship is determined without a need to solve the differential governing equations, so it is applicable for plates with any boundary conditions. It is also shown that the square of the nature frequency approaches zero when the in-plane load approaches the

buckling load. The derived relationship is verified by theoretically solving the vibration and buckling problems of specimens with combinations of boundary conditions. The Ritz method is employed to determine natural frequency of the loaded plate and buckling load of plate. In the process, vibration mode shape and buckling mode are also obtained. From the study, the predicted buckling load and mode from the vibration data are corresponded to the theoretical solution very well.

The derived relationship between square of the natural frequency and the applied load can be used as an alternative method of identifying the buckling load experimentally. The advantage of dynamic approach over the static approach is that, in the dynamic approach, there is no need to drawn lines in the pre-buckling and post-buckling region. So, the error from human judgment can be eliminated. For future study, the derived relationship should be verified with the measurement data.

Acknowledgments

This research is supported by the Thailand Research Fund under project grant No. RMU4880021.

References

- [1] Supasak, C., 2005. Conparison of buckling loads of thin plates by experiment method. Master Thesis, Mechanical Engineering Department, Chulalongkorn University, Bangkok, Thailand.
- [2] Chai, G.B., Banks, W.M., and Rhodes, J., 1991. An experiment study on laminated panels in compression. Composite Structures, Vol. 19, No. 1, pp. 67-87.
- [3] Tuttle, M., Singhatanadgid, P., and Hinds, G., 1999.3 Buckling of composite panels subjected to biaxial loading. Experiment Mechanics, Vol. 39, No. 3, pp. 191-201
- [4] Lurie, H. and Monica, S., 1952. Lateral vibrations as related to structural stability. Journal of Applied Mechanics, pp. 195-204.
- [5] Chailleux, A., Hans, Y., and Verchery, G. 1975. Experimental study of the buckling of laminated composite columns and plates. Journal of Mechanical Sciences, Vol. 17, pp. 489-498.
- [6] Pannok, C. and Singhatanadgid, P., 2006 Buckling analysis of composite laminate skew plates with various edge support conditions Proceedings of the 20th Conference of the Mechanical Engineering Network of Thailand (ME-NETT 20), Nakhon Ratchasima, Thailand. 18-20 October 2006.
- [7] Weaver Jr., W., Timoshenko, S.P., and Young, D.H. 1990. Vibration problems in engineering. Wiley, New York, USA.